

Extracting topological orders of generalized Pauli stabilizer codes in two dimensions

Zijian Liang (梁子健)^{1,2,*} Yijia Xu (许逸葭)^{3,4,*} Joseph T. Iosue,³ and Yu-An Chen (陳昱安)^{1,†}

¹*International Center for Quantum Materials, School of Physics, Peking University, Beijing 100871, China*

²*School of Physics, Shandong University, Jinan 250100, China*

³*Joint Quantum Institute and Joint Center for Quantum Information and Computer Science,
NIST/University of Maryland, College Park, Maryland 20742, USA*

⁴*Institute for Physical Science and Technology, University of Maryland, College Park, Maryland 20742, USA*

(Dated: December 19, 2023)

In this paper, we introduce an algorithm for extracting topological data from translation invariant generalized Pauli stabilizer codes in two-dimensional systems, focusing on the analysis of anyon excitations and string operators. The algorithm applies to \mathbb{Z}_d qudits, including instances where d is a nonprime number. This capability allows the identification of topological orders that may differ from \mathbb{Z}_d toric codes, thereby extending the scope beyond the established theorem that Pauli stabilizer codes of \mathbb{Z}_p qudits (with p being a prime) are equivalent to finite copies of \mathbb{Z}_p toric codes and trivial stabilizers. The algorithm is designed to determine all anyons and their string operators, enabling the computation of their fusion rules, topological spins, and braiding statistics. The method converts the identification of topological orders into computational tasks, including Gaussian elimination, the Hermite normal form, and the Smith normal form of truncated Laurent polynomials. Furthermore, the algorithm provides a systematic approach for studying quantum error-correcting codes. We apply it to various codes, such as self-dual CSS quantum codes modified from the color code and non-CSS quantum codes that contain the double semion topological order or the six-semion topological order.

CONTENTS

I. Introduction	2	D. Topological spins from the T-junction process	17
II. Physical intuitions	3	V. Algorithm for extracting topological data	17
III. Formulating translation invariant Pauli stabilizer models	6	A. Extracting string operators from translation invariant Pauli stabilizers	17
A. Review of the Laurent Polynomial method on a square lattice	6	B. Extracting topological spins of anyons	18
B. Examples	9	C. Rearranging the basis anyons	19
1. Trivial model $H_0 = -\sum_e X_e$	9	VI. Applications on various quantum codes	19
2. Standard \mathbb{Z}_d toric code	9	A. Modified color code	20
3. Two copies of \mathbb{Z}_d toric codes	9	B. CSS codes induced from double semion	21
4. Double semion	10	C. Six-semion stabilizer code	23
C. Shifted double semion	10	Acknowledgment	23
IV. Computational Method	11	References	24
A. Prime-dimensional qudit \mathbb{F}_p	12	A. Relation between braiding statistics and topological spins	26
1. Topological order condition	12	B. The Hermite normal form and the Smith normal form	27
2. Solving the anyon equation	13	C. String operators of various examples	28
3. Equivalence relations between anyons	13	1. Color code and modified color codes	28
B. Nonprime-dimensional qudit \mathbb{Z}_d	13	2. CSS code induced from double semion code	28
1. Topological order condition	15	3. Double semion code	28
2. Solving the anyon equation	16	4. Six-semion code	28
3. Equivalence relations between anyons	16		
C. Fusion rules from the Smith normal form	16		

* equal contribution.

† E-mail: yuanchen@pku.edu.cn

I. INTRODUCTION

The topological phases of matter in gapped systems are conceptualized as equivalence classes of physical systems. These systems are considered equivalent if they can be continuously transformed into each other while maintaining an energy gap above the ground state subspace. A defining characteristic of a topological phase is its stability against local perturbation. As a result, research in this field focuses on identifying topological invariants under continuous transformations and building models that exhibit various invariants. To this end, numerous intricate models have been studied and partially classified across different spatial dimensions, both with and without symmetries, in both condensed matter physics [1–10] and quantum information [11–19]. Despite these advances, the complete classification and comprehensive characterization of topological phases remain areas of ongoing research.

A notable subset of lattice models includes generalized Pauli stabilizer codes, characterized by Hamiltonian terms composed of commuting products of generalized Pauli operators for \mathbb{Z}_d qudits.¹ Bombin’s investigation into translation invariant topological stabilizer codes in two-dimensional lattices with qubit ($d = 2$) degrees of freedom provided foundational insights [20]. He demonstrated that any non-chiral topological stabilizer code, under locality-preserving automorphisms of the operator algebra, can be expressed as a direct sum of toric code stabilizers and trivial stabilizers (corresponding to product states). A widely believed conjecture [14, 21, 22] states that all commuting projector Hamiltonians are non-chiral, suggesting that the classification of translation invariant Pauli stabilizer codes for two-dimensional qubit systems is essentially complete. Extending this framework, Haah applied these principles to prime-dimensional qudits² [23]. Given that any translation invariant topological general Pauli stabilizer code on such qudit systems must include a nontrivial “boson” [24], it is inferred that all two-dimensional topological generalized Pauli stabilizer codes for prime-dimensional qudits can be transformed into a direct sum of finite copies of toric code stabilizers and trivial stabilizers using finite-depth Clifford circuits. However, the classification of generalized Pauli stabilizer models with nonprime-dimensional qudits remains an unresolved challenge. It is conjectured that such systems may be equivalent to a direct sum of finite copies of trivial stabilizers and condensation descendants of the \mathbb{Z}_d toric code stabilizers [19].

The study of stabilizer codes is also crucial from the quantum code perspective, particularly in the context of error correction. In these codes, anyons and their string operators correlate directly with the logical qubits and logical operators within the code space. Recently, there has been notable progress in the experimental implementation of surface codes on various quantum computing platforms [25–28]. Prominent examples of surface codes, including the toric code and color code, have been individually designed and analyzed. This raises a pertinent question: Is there a systematic method for extracting topological information from a wide range of quantum codes? For example, taking inspiration from the color code, one can design numerous novel quantum codes, as illustrated in Fig. 1. A critical question is how to quickly determine the potential utility of these quantum codes for error correction. From a practical perspective, benefiting from the development of digital quantum computers and simulators, various topological phases have been realized on digital quantum devices [26, 29–33]. Given the progress of experimental implementations, analysis and characteristics of those topological phases is a challenging and vital topic. Various characterizations or experimental protocols for wavefunctions are proposed [34–51]. On the other hand, given the rich structure of stabilizer codes, characterizing and searching novel stabilizer Hamiltonian is less investigated, and it would be beneficial for searching models that can be implemented in near-term devices. This paper addresses this question by introducing an algorithm that efficiently identifies the topological data of various quantum codes. This algorithm aims to streamline the study of the topological properties of generalized Pauli stabilizer codes with the assistance of classical computers.

In summary, we provide an algorithm to determine the topological order of generalized Pauli stabilizer codes with \mathbb{Z}_d qudits in two dimensions, which applies to both prime and non-prime d . Our method checks whether a generalized Pauli stabilizer code satisfies the topological order condition. Upon confirmation, the algorithm outputs the topological data of the input quantum code, the abelian anyon theory (unitary modular tensor category). This includes identifying anyon types (simple objects), their fusion rules, explicit string operators, self-statistics (topological spins), and braiding statistics. The functions of our algorithm are shown in Fig. 2.

The paper is organized as follows: In Sec. II, we review the Pauli stabilizer codes of qudits and the theory of abelian anyons to motivate the development of our work. In Sec. III, we review the Laurent polynomial formulation of translation invariant Pauli stabilizer codes with examples and the definition of topological data in the Laurent polynomial framework. In Sect. IV, we provide details of individual techniques used in the algorithm for extracting topological order, including the procedure to check the topological order condition, solve the anyon equation, and obtain topological spins for given anyons. In Sec. V, we discussed the workflow of the algorithm. In Sec. VI, we apply our algorithm to various stabilizer

¹ A **generalized Pauli stabilizer** Hamiltonian $H = -\sum_i S_i$ consists of stabilizers S_i such that each S_i is a product of generalized Pauli matrices and commutes with each other $[S_i, S_j] = 0$. The mathematical expression of generalized Pauli matrices will be shown explicitly in the next section. The group formed by S_i (and their products) is the **stabilizer group**.

² A **prime-dimensional qudit** refers to a \mathbb{Z}_d qudit where the qudit dimension d is a prime number.

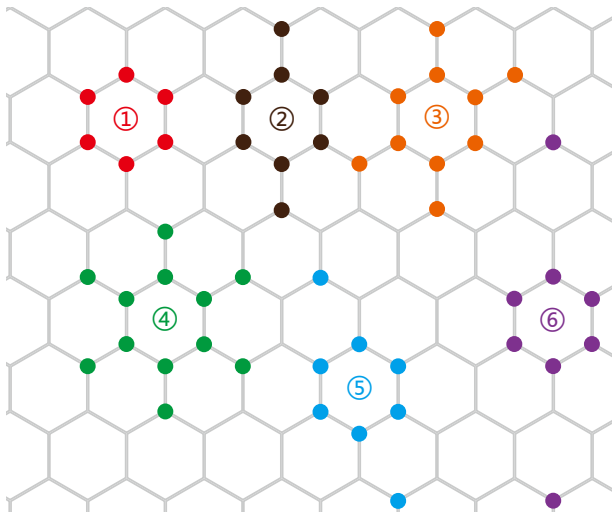


FIG. 1. Six examples of self-dual CSS codes in the 2d honeycomb lattice, where each vertex hosts one qubit. The first is the color code [15], with stabilizers composed of all Pauli X (or Z) operators on red vertices and their translations. The remaining five codes are similar but include additional vertices in each stabilizer term. While it is established that the color code is equivalent to two copies of toric codes [52], the broader analysis of 2d translation invariant Pauli stabilizer models remains less clear. Our work introduces an algorithm capable of detecting topological orders in these models and extracting crucial information such as anyon string operators, fusion rules, topological spins, and braiding statistics.

codes defined on qubits or nonprime-dimensional qudits and show the effectiveness of this algorithm on extracting anyon string operators, fusion rules, topological spins, and braiding statistics.

II. PHYSICAL INTUITIONS

This section provides a pedagogical overview of generalized Pauli operators and abelian anyon theories in the stabilizer formalism with the microscopic picture. Then, we outline the workflow of our algorithm.

First, recall standard definitions of $d \times d$ **generalized Pauli matrices** for a \mathbb{Z}_d qudit:

$$X = \sum_{j \in \mathbb{Z}_d} |j+1\rangle\langle j|, \quad Z = \sum_{j \in \mathbb{Z}_d} \omega^j |j\rangle\langle j|. \quad (1)$$

where ω is defined as $\omega := \exp(\frac{2\pi i}{d})$. More explicitly,

$$X = \begin{bmatrix} 0 & 0 & \cdots & 0 & 1 \\ 1 & 0 & \cdots & 0 & 0 \\ 0 & 1 & \cdots & 0 & 0 \\ \vdots & \vdots & \ddots & \vdots & \vdots \\ 0 & 0 & \cdots & 1 & 0 \end{bmatrix}, \quad Z = \begin{bmatrix} 1 & 0 & 0 & \cdots & 0 \\ 0 & \omega & 0 & \cdots & 0 \\ 0 & 0 & \omega^2 & \cdots & 0 \\ \vdots & \vdots & \vdots & \ddots & \vdots \\ 0 & 0 & 0 & \cdots & \omega^{d-1} \end{bmatrix}, \quad (2)$$

X and Z satisfy the commutation relation

$$ZX = \omega XZ. \quad (3)$$

For the sake of simplicity, “Pauli” will be used as a shorthand for “generalized Pauli”.

We begin by considering a local³ Pauli stabilizer Hamiltonian on a two-dimensional lattice. Our initial step is to check whether this Hamiltonian fulfills the **topological order (TO) condition** [23, 53, 54]. The detailed mathematical formulation of this condition will be addressed in subsequent sections. Briefly, the TO condition requires that any local operator \mathcal{O} , which commutes with all stabilizers, must be a product of certain stabilizers, denoted as $\mathcal{O} = \prod_{i \in A} S_i$ for a set A . In other words, the TO condition implies that the stabilizer group is “saturated,” i.e., no more local operator can be added to the stabilizer group while commuting with all existing stabilizers. Fundamentally, this condition indicates the local indistinguishability of the ground state(s) in a local Pauli stabilizer code that satisfies this criterion. If the Hamiltonian exhibits a degeneracy in its ground state, these states cannot be differentiated by any local operator. An example is the toric code [13], which illustrates topological order with a 4-fold degeneracy on a torus. Thus, a local Pauli stabilizer code that meets the TO condition is referred to as **topological Pauli stabilizer code**, which suggests the presence of topological order in this code (which may be a trivial order).

Furthermore, given a topological Pauli stabilizer code, our interest then lies in identifying the specific type of “topological order” it exhibits. **Topological orders** in two dimensions are categorized by “unitary modular tensor categories” (UMTC) [55–59], which describe the properties of local excitations in the low-energy spectrum of the Hamiltonian. It is important to note that stabilizer models are restricted to generating abelian anyon theories, a subset within the broader scope of UMTCs. While UMTCs have a formal definition for general cases, this paper will focus only on abelian anyon theories pertaining to stabilizer formalism and provide a more streamlined description.

An **anyon** is a (local) violation of stabilizers on the lattice. Given a ground state $|\Psi_{\text{gs}}\rangle$, which is in the +1 eigenstate of all the stabilizers: $S_i |\Psi_{\text{gs}}\rangle = |\Psi_{\text{gs}}\rangle$. However, if a Pauli operator M is applied on the ground state, the perturbed state might not be in the +1 eigenspace of stabilizers: $S_i (M |\Psi_{\text{gs}}\rangle) = e^{i\phi_i} (M |\Psi_{\text{gs}}\rangle)$ with $\phi_i \in [0, 2\pi)$, where ϕ_i depends on the commutation relation between S_i and M . This perturbed state contains an anyon labeled as a list $\{\phi_1, \dots, \phi_N\}$ consisting $U(1)$ angles⁴. So far, an anyon is defined for a state, which is a global description. Next, the locality plays a crucial role. If the violated stabilizers ($\phi_i \neq 0$) are spatially far apart, e.g., created by a long string operator M that violates only a finite number of stabilizers near its two endpoints, we divide the stabilizers

³ “Local” refers to each operator, e.g., stabilizer S_i , having Pauli matrices supported on a finite area in the lattice.

⁴ Note that we record the angles ϕ for all the stabilizers and their translations.

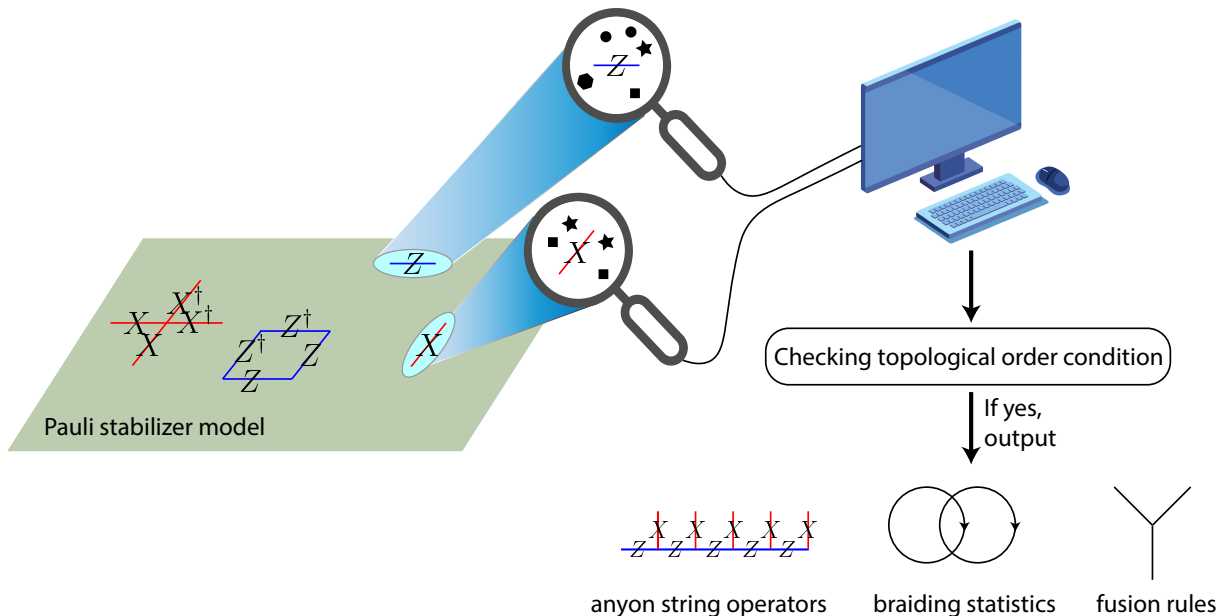


FIG. 2. Illustration of the algorithm. We want to determine whether a given Pauli stabilizer model presents a topological order. If it is a topological order, what are anyon string operators, braiding statistics, and fusion rules? In the first step, we record the syndrome pattern of a single Pauli operator, which is indicated by circles, stars, squares, or hexagons representing the violations of different stabilizers. Next, we convert syndrome patterns into the Laurent polynomial rings. Then, we use our algorithm to check whether the Pauli stabilizer code satisfies the topological order condition. If satisfied, this algorithm can obtain the topological data of the given model, including anyon string operators, fusion rules, topological spins, and braiding statistics.

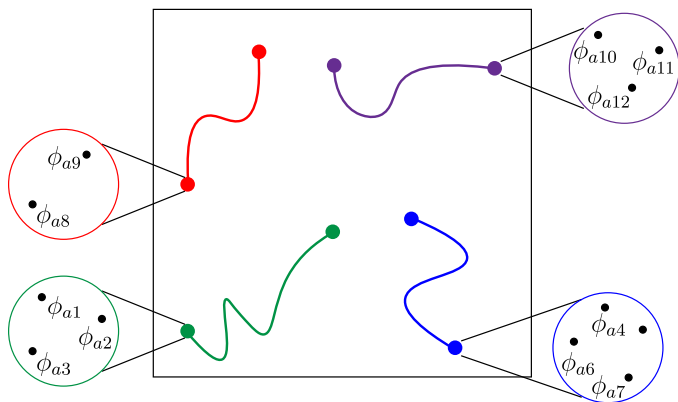


FIG. 3. The black dots label the locations where stabilizers act as $e^{i\phi}$ (with $\phi \neq 0$) on the state. These stabilizers are labeled as S_{a_1} , S_{a_2} , and so on... If these violated stabilizers are spatially far apart, we group $\{S_{a_i}\}$ into different patches and treat each patch as a local anyon. In topological stabilizer codes, any anyon is generated by a string operator, i.e., a product of Pauli matrices along the string that only fails to commute with a finite number of stabilizers near its endpoints.

with $\phi_i \neq 0$ into local patches, as the physical picture shown in Fig. 3. Each patch can be viewed as a local anyon, which $\{\phi_i\}$ is referred to as the **syndrome pattern**. Another way to visualize this local anyon is

to extend M into a semi-infinite⁵ string, which only violates stabilizers around one endpoint, where the anyon is located. In two-dimensional topological Pauli stabilizer codes, each instance of local violations is attributable to string operators. Nonetheless, this property ceases to be applicable in higher-dimensional models, primarily due to the fracton phases of matter [60–64]. Our method is adaptable to higher-dimensional topological Pauli stabilizer codes with string operators; however, our focus is predominantly on two-dimensional applications for the remainder of this study.

Now, anyon types (or superselection sectors) can be defined as equivalence classes under the equivalence relations between anyons v and v' :

$$v := \{\phi_i\} \sim v' := \{\phi'_i\}, \quad (4)$$

if and only if $\{\phi_i\}$ and $\{\phi'_i\}$ are differed by local Pauli operators. In other words, if the syndrome pattern v' can be achieved by applying local Pauli operators on the

⁵ There are subtleties about semi-infinite operators in the infinite plane since the algebra is only well-defined for finite operators. In practice, a clear way to define a local anyon a labeled by local ϕ_i is that for any arbitrary large R , there always exists some Pauli operator M such that it violates S_i the same as ϕ_i , while commutes with all other stabilizers within range R . Refs. [23, 54] demonstrate that M in a topological Pauli stabilizer code can always be chosen as a string operator that is extendable.

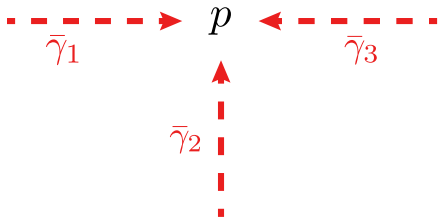


FIG. 4. The exchange statistics (topological spin) of anyon a can be computed using the formula in Eq. (6). $\bar{\gamma}_1$, $\bar{\gamma}_2$, and $\bar{\gamma}_3$ are oriented paths in the lattice incident at the same position p . The string operators W_1^a , $(W_2^a)^\dagger$ and W_3^a of anyon a along paths $\bar{\gamma}_1$, $-\bar{\gamma}_2$, and $\bar{\gamma}_3$ might not commute, giving the exchange statistics $\theta(a)$.

state with the syndrome pattern v , two syndrome patterns v and v' are identified to the same type. With the concept of anyon types, we can now discuss the fusion rules. The **fusion rules** of (abelian) anyons describe the process of bringing two anyons a and b closer to each other (via their string operators) and identifying the composite of them as a third anyon c under the equivalence relation (4). We express the fusion rule as

$$a \times b = c. \quad (5)$$

Also, the **topological spin** $\theta(a)$ can be computed for each anyon a , which determines the exchange statistics (by spin-statistics theorem), e.g., boson, fermion, and semion. The T-junction process that exchanges the positions of two particles can detect the topological spin [24, 65–68]. Let $\bar{\gamma}_1$, $\bar{\gamma}_2$, and $\bar{\gamma}_3$ be paths sharing a common endpoint p and ordered counter-clockwise around p , as in Fig. 4. Then, the topological spin $\theta(a)$ of anyon a is computed by the expression:

$$W_3^a (W_2^a)^\dagger W_1^a = \theta(a) W_1^a (W_2^a)^\dagger W_3^a, \quad (6)$$

where W_i^a is the string operator moving anyon a along the path $\bar{\gamma}_i$. Eq. (6) represents the exchange of two anyons⁶ a_1, a_2 can be seen as follows. Suppose that a_1 is initialized at the start $\bar{\gamma}_1(0)$ of $\bar{\gamma}_1$ and a_2 at the start $\bar{\gamma}_3(0)$ of $\bar{\gamma}_3$. Then $(W_3^a)^\dagger W_2^a (W_1^a)^\dagger W_3^a (W_2^a)^\dagger W_1^a$ takes a_1 from $\bar{\gamma}_1(0) \rightarrow p \rightarrow \bar{\gamma}_2(0)$, then takes a_2 from $\bar{\gamma}_3(0) \rightarrow p \rightarrow \bar{\gamma}_1(0)$, and then takes a_1 from $\bar{\gamma}_2(0) \rightarrow p \rightarrow \bar{\gamma}_3(0)$. Thus, in the end, we have exchanged the positions of a_1 and a_2 , while keeping all dynamical phases cancel out. By Eq. (6), this results in the phase $\theta(a)$. In abelian anyon theories, the **braiding statistics** (e.g., the phase factors arising from the Aharonov-Bohm effect) are completely determined by topological spins. More precisely, let $B_\theta(a, b)$ be the $U(1)$ phase of braiding anyon a around anyon b counterclockwise. It is related to the topological

spins of a , b and $a \times b$ by the relation

$$B_\theta(a, b) = \frac{\theta(a \times b)}{\theta(a)\theta(b)}. \quad (7)$$

In Appendix A, we derive Eq. (7) with the definition $W_i^{a \times b} := W_i^b W_i^a$ and the fact that $W_{1,2,3}^{a,b}$ are Pauli operators that anti-commute by a $U(1)$ phase. Therefore, the complete data for abelian anyon theories are anyon types, fusion rules, and topological spins.

In summary, the algorithm for extracting the topological order from a topological Pauli stabilizer code includes the following steps:

1. Enumerate string operators that create anyons around its endpoints.
2. Classify these anyons into different types by the equivalence relation (4).
3. Obtain the fusion rules of anyon types.
4. Compute topological spins (and braiding statistics) for anyons from its string operator.

The primary aim is to identify string operators for distinct anyon types. This task is inherently challenging, but locality and translation invariance can simplify this problem. We focus on a finite region, designated as A , where, due to the finite amount of anyon types in two dimensions and the assumption of translation invariance, all topological data are contained inside A (if A is large enough). Anyon string operators, fusion rules, topological spins, and braiding statistics, can be analyzed in this region A . As illustrated in Refs.[54, 69], the required size l_A of the region A should be upper bounded by at least $d \exp(r)$, where d is the qudit dimension and r is the range of stabilizers. Our method successfully retrieves all topological information for typical stabilizer codes with reasonable qudit dimensions and ranges of stabilizers.⁷ We obtain the syndrome pattern for each single Pauli error and combine them to form a string-like operator, shown in Fig. 5. The naive approach of listing all combinations of Pauli matrices will take an exponential time. The approach described later in this paper can achieve the discovery of string operators for all anyon types within polynomial time.

Note that our way of classifying topological Pauli stabilizer codes based on topological data is different from Refs. [20, 23], which utilize Clifford circuits to transform a topological Pauli stabilizer code into finite copies of the standard toric code stabilizers and trivial stabilizers. The equivalence of Pauli stabilizer codes by the Clifford

⁶ Anyon a_1 and a_2 are in the same anyon type. The subscript is a label to keep track of them.

⁷ Our algorithm has the time complexity $O(l_A^3 \log^2 d) = O(d^3 \log^2 d \exp(r))$, which is from the modified Gaussian elimination process discussed in Sec. IV B. However, for the exotic \mathbb{Z}_p toric code example constructed in Ref.[69], especially with a large prime p , such as $p = 1009$, the computational power required surpasses what a personal computer can provide.

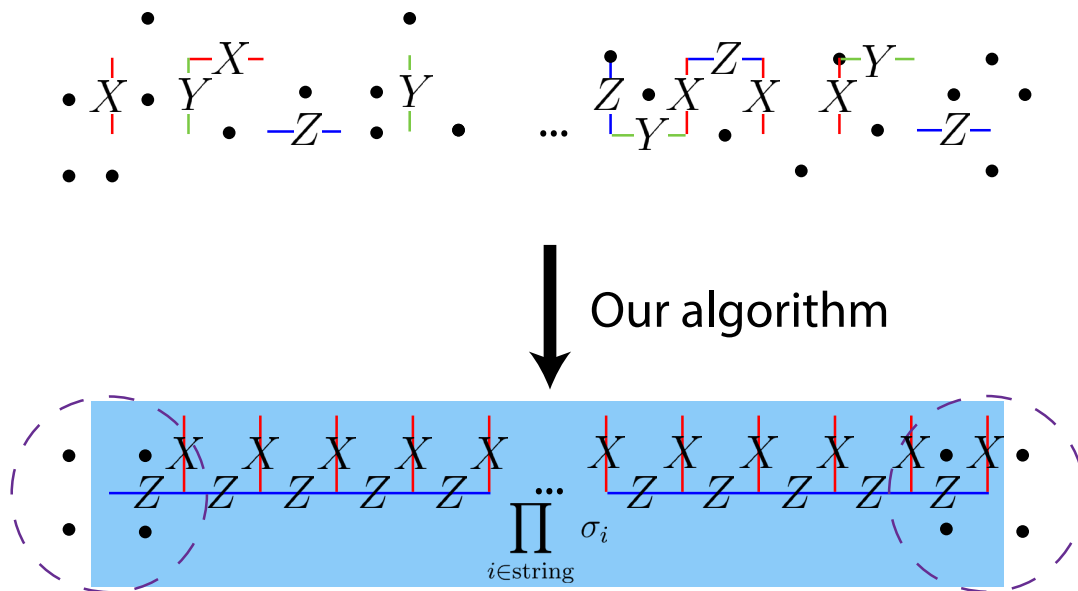


FIG. 5. Demo of our algorithm. Given the syndrome of each single Pauli matrix, we play the LEGO game to assemble them into a string operator such that stabilizers are only violated near its two endpoints.

circuit transformation is a stronger condition than the equivalence of their topological data. For example, consider \mathbb{Z}_4 Pauli stabilizer codes:

$$H_1 := - \sum_{i=1}^N Z_i, \quad H_2 := - \sum_{i=1}^N (X_i^2 + Z_i^2). \quad (8)$$

Both codes have trivial topological data since each one has the ground state as a product state $|0\rangle^{\otimes N}$ or $(\frac{|0\rangle+|2\rangle}{\sqrt{2}})^{\otimes N}$, but there is no Clifford circuit that transforms from H_1 to H_2 . Therefore, instead of using the equivalence of parent Hamiltonians under Clifford circuit transformations to classify Pauli stabilizer codes, our classification is based on topological data, which are properties of its low-energy excitations.

III. FORMULATING TRANSLATION INVARIANT PAULI STABILIZER MODELS

In this section, we first review the polynomial method to formulate translation invariant Pauli stabilizer models and demonstrate how to utilize it to derive the topological data in Sec. III A. In Sec. III B, we provide the polynomial representations of various known models.

A. Review of the Laurent Polynomial method on a square lattice

The Laurent polynomial has been demonstrated to be useful for searching 3d fracton phases [70] and error-correcting codes [71, 72], which serves as a basis for our algorithm. In this subsection, we will review the Laurent

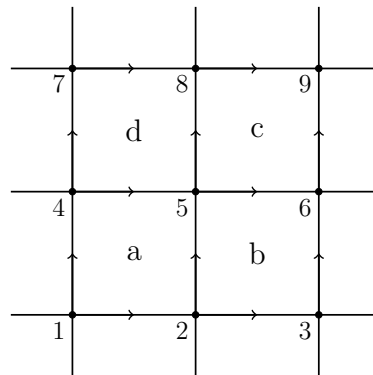


FIG. 6. We put Pauli matrices X_e , Y_e , and Z_e on each edge.

polynomial and how to use it to represent translation invariant stabilizer codes.

This section examines a scenario involving two \mathbb{Z}_d qudits in each unit cell, exemplified by a qudit at each edge of a square lattice. This setting is extendable to cases with k qudits per unit cell.

Our initial step is to demonstrate that any Pauli operator, constituted by a finite tensor product of Pauli matrices at different sites, can be represented (up to an overall factor) as a column vector over the polynomial ring $R = \mathbb{Z}_d[x, y, x^{-1}, y^{-1}]$ ⁸, as established in Ref. [54]. We assign column vectors over \mathbb{Z}_d to the (generalized)

⁸ This ring includes all polynomials in x, x^{-1}, y, y^{-1} , with coefficients in \mathbb{Z}_d .

Pauli matrices X_{12} , Z_{12} , X_{14} , and Z_{14} , depicted in Fig. 6:

$$\mathcal{X}_{12} = \begin{bmatrix} 1 \\ 0 \\ 0 \\ 0 \end{bmatrix}, \quad \mathcal{Z}_{12} = \begin{bmatrix} 0 \\ 0 \\ 1 \\ 0 \end{bmatrix}, \quad \mathcal{X}_{14} = \begin{bmatrix} 0 \\ 1 \\ 0 \\ 0 \end{bmatrix}, \quad \mathcal{Z}_{14} = \begin{bmatrix} 0 \\ 0 \\ 0 \\ 1 \end{bmatrix}, \quad (9)$$

where column vector representations of operators are indicated using curly letters. The coefficients in these vectors correspond to their powers:

$$\mathcal{P} = \begin{bmatrix} i \\ j \\ k \\ l \end{bmatrix} \Rightarrow \mathcal{P}^m = \begin{bmatrix} mi \\ mj \\ mk \\ ml \end{bmatrix} \quad \forall m \in \mathbb{Z}_d. \quad (10)$$

The translation of operators is achieved using polynomials of x and y to denote translations in the x and y directions, respectively. To illustrate, translating the operator on edge e_{12} to edge e_{78} (using the vector $(0, 2)$) or to edge e_{58} (using the vector $(1, 1)$) involves multiplying the column vector of the operator by y^2 or xy , respectively:

$$\mathcal{Z}_{78} = y^2 \mathcal{Z}_{12} = \begin{bmatrix} 0 \\ 0 \\ y^2 \\ 0 \end{bmatrix}, \quad \mathcal{X}_{58} = xy \mathcal{X}_{14} = \begin{bmatrix} 0 \\ xy \\ 0 \\ 0 \end{bmatrix}. \quad (11)$$

In conclusion, any Pauli operator can be decomposed as follows:

$$P = \eta X_{e_1}^{a_1} X_{e_2}^{a_2} \dots X_{e_n}^{a_n} Z_{e'_1}^{b_1} Z_{e'_2}^{b_2} \dots Z_{e'_m}^{b_m}, \quad (12)$$

where η represents a root of unity of order $2d$. After dropping the overall phase η , the corresponding column vector for this operator is a linear combination of individual Pauli matrices, expressed as

$$\mathcal{P} = a_1 \mathcal{X}_{e_1} + a_2 \mathcal{X}_{e_2} + \dots + a_n \mathcal{X}_{e_n} + b_1 \mathcal{Z}_{e'_1} + b_2 \mathcal{Z}_{e'_2} + \dots + b_m \mathcal{Z}_{e'_m}. \quad (13)$$

More examples are included in Fig. 7.

Next, we introduce the **antipode map** that is a \mathbb{Z}_d -linear map from R to R defined by

$$x^a y^b \rightarrow \overline{x^a y^b} := x^{-a} y^{-b}. \quad (14)$$

To determine whether two Pauli operators represented by vectors v_1 and v_2 commute or anti-commute, we define the dot product as

$$v_1 \cdot v_2 = \overline{v_1}^T \Lambda v_2, \quad (15)$$

where T is the transpose operation on a matrix and

$$\Lambda = \left[\begin{array}{cc|cc} 0 & 0 & 1 & 0 \\ 0 & 0 & 0 & 1 \\ \hline -1 & 0 & 0 & 0 \\ 0 & -1 & 0 & 0 \end{array} \right] \quad (16)$$

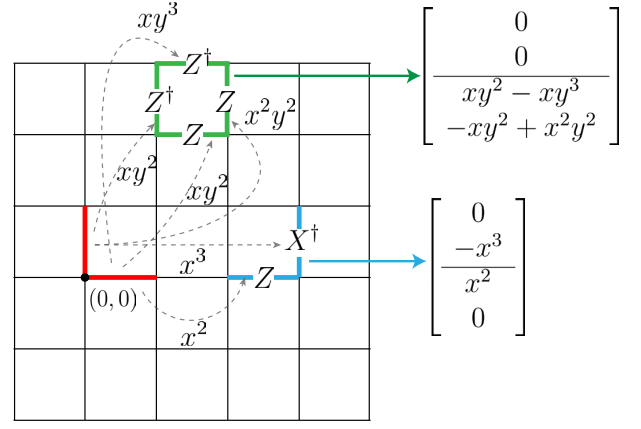


FIG. 7. Examples of polynomial expressions for Pauli strings. The flux term on a plaquette and the XZ term on edges are shown. The factors such as x^2y^2 and x^2 represent the locations of the operators relative to the origin.

is the matrix representation of the standard **symplectic bilinear form**. For simplicity, we denote $(\dots)^T$ as $(\dots)^\dagger$.

The two operators v_1 and v_2 commute if and only if the constant term of $v_1 \cdot v_2$ is zero. For example, we calculate the dot products

$$\mathcal{X}_{12} \cdot \mathcal{Z}_{12} = 1, \quad \mathcal{X}_{58} \cdot \mathcal{Z}_{14} = x^{-1}y^{-1}, \quad (17)$$

and, therefore, X_{12} and Z_{12} anti-commute, whereas X_{58} and Z_{14} commute (their dot product only has a non-constant term $x^{-1}y^{-1}$). Furthermore, the physical interpretation of $\mathcal{X}_{58} \cdot \mathcal{Z}_{14} = x^{-1}y^{-1}$ is that shifting of X_{58} in $-x$ and $-y$ directions by 1 step will anti-commute (by the factor of ω) with Z_{14} .

A translation invariant stabilizer code forms an R -submodule⁹ σ such that

$$v_1 \cdot v_2 = v_1^\dagger \Lambda v_2 = 0, \quad \forall v_1, v_2 \in \sigma, \quad (18)$$

i.e., a module of commuting Pauli operators. This σ is named the **stabilizer module**. The Hamiltonian could have two (or more) terms per square to have a unique ground state on a simply-connected manifold, denoted as $H = -\sum_{\text{cells}} (S_1 + S_2)$ with corresponding column vectors

$$S_1 = \begin{bmatrix} f_1(x, y) \\ f_2(x, y) \\ g_1(x, y) \\ g_2(x, y) \end{bmatrix}, \quad S_2 = \begin{bmatrix} h_1(x, y) \\ h_2(x, y) \\ k_1(x, y) \\ k_2(x, y) \end{bmatrix}. \quad (19)$$

⁹ The R -submodule is similar to a subspace of a vector space, but the entries of the vector are in the ring $R = \mathbb{Z}_d[x, y, x^{-1}, y^{-1}]$. In a ring, the inverse element may not exist. This is the distinction between a module and a vector space.

For example, the trivial phase $H_0 = -\sum_e X_e$ is

$$\mathcal{S}_1 = \begin{bmatrix} 1 \\ 0 \\ 0 \\ 0 \end{bmatrix}, \quad \mathcal{S}_2 = \begin{bmatrix} 0 \\ 1 \\ 0 \\ 0 \end{bmatrix}, \quad (20)$$

and the standard \mathbb{Z}_d toric code Hamiltonian

$$H_{\text{TC}} = -\sum_v \begin{array}{c} | \\ \color{blue}{X} \\ \color{blue}{X^\dagger} \color{black}{-} \color{black}{\color{blue}{v}} \color{black}{-} \color{black}{X} \\ | \end{array} - \sum_p \begin{array}{c} \color{blue}{Z^\dagger} \\ \color{black}{\left[\begin{array}{c} \color{blue}{Z^\dagger} \color{black}{-} \color{black}{p} \color{black}{-} \color{black}{Z} \\ \color{blue}{Z} \end{array} \right]} \\ \color{blue}{Z} \end{array}, \quad (21)$$

corresponds to

$$\mathcal{S}_1 = \begin{bmatrix} 1 - \bar{x} \\ 1 - \bar{y} \\ 0 \\ 0 \end{bmatrix}, \quad \mathcal{S}_2 = \begin{bmatrix} 0 \\ 0 \\ 1 - y \\ -1 + x \end{bmatrix}. \quad (22)$$

For general stabilizers \mathcal{S}_1 and \mathcal{S}_2 in Eq. (19), the commutation condition in Eq. (18) implies

$$\begin{cases} -\bar{g}_1 f_1 - \bar{g}_2 f_2 + \bar{f}_1 g_1 + \bar{f}_2 g_2 = 0, \\ -\bar{k}_1 h_1 - \bar{k}_2 h_2 + \bar{h}_1 k_1 + \bar{h}_2 k_2 = 0, \\ -\bar{k}_1 f_1 - \bar{k}_2 f_2 + \bar{h}_1 g_1 + \bar{h}_2 g_2 = 0. \end{cases} \quad (23)$$

One simple solution is $g_1 = g_2 = h_1 = h_2 = 0$ and $f_1 = -\bar{k}_2$ and $f_2 = \bar{k}_1$:

$$\mathcal{S}_1 = \begin{bmatrix} f_1 \\ f_2 \\ 0 \\ 0 \end{bmatrix}, \quad \mathcal{S}_2 = \begin{bmatrix} 0 \\ 0 \\ \bar{f}_2 \\ -\bar{f}_1 \end{bmatrix}, \quad (24)$$

where \mathcal{S}_1 only has X part and \mathcal{S}_2 only has Z part, representing translation invariant CSS codes on a square lattice.

Next, we define the **excitation map** for any Pauli operator \mathcal{P} (a column vector over R) as

$$\epsilon(\mathcal{P}) := [\mathcal{S}_1 \cdot \mathcal{P}, \mathcal{S}_2 \cdot \mathcal{P}], \quad (25)$$

which indicates how the Pauli operator violates stabilizers \mathcal{S}_1 and \mathcal{S}_2 . The error syndromes of a single Pauli matrix for the generic Hamiltonian (19) can be written as

$$\begin{aligned} \epsilon(\mathcal{X}_1) &= [\mathcal{S}_1 \cdot \mathcal{X}_{12}, \mathcal{S}_2 \cdot \mathcal{X}_{12}] = [-\bar{g}_1, -\bar{k}_1], \\ \epsilon(\mathcal{X}_2) &= [\mathcal{S}_1 \cdot \mathcal{X}_{14}, \mathcal{S}_2 \cdot \mathcal{X}_{14}] = [-\bar{g}_2, -\bar{k}_2], \\ \epsilon(\mathcal{Z}_1) &= [\mathcal{S}_1 \cdot \mathcal{Z}_{12}, \mathcal{S}_2 \cdot \mathcal{Z}_{12}] = [\bar{f}_1, \bar{h}_1], \\ \epsilon(\mathcal{Z}_2) &= [\mathcal{S}_1 \cdot \mathcal{Z}_{14}, \mathcal{S}_2 \cdot \mathcal{Z}_{14}] = [\bar{f}_2, \bar{h}_2]. \end{aligned} \quad (26)$$

Each syndrome is a row vector with two entries in $\mathbb{Z}_d[x, y, x^{-1}, y^{-1}]$. For a general case where the stabilizer group is generated by t stabilizers $\mathcal{S}_1, \mathcal{S}_2, \mathcal{S}_3, \dots, \mathcal{S}_t$, the syndrome would be a row vector with t entries in $\mathbb{Z}_d[x, y, x^{-1}, y^{-1}]$.

Given this excitation map ϵ , the **topological order (TO) condition** can be formulated as

$$\ker \epsilon = \sigma, \quad (27)$$

where σ is the stabilizer module and the kernel of ϵ represents the space of local Pauli operators commuting with all stabilizers. This TO condition requires that if a local operator commutes with stabilizers, this operator must be a product of stabilizers (a column vector in the stabilizer module). If the TO condition is satisfied, the ground state space is indistinguishable by any local operator. The ground state degeneracy on different manifolds is a part of the **topological order** of Pauli stabilizer codes. More precisely, the ground state degeneracy on a torus equals the number of anyon types, with each ground state labeled by an anyon string operator.

To obtain the possible anyons in this theory, for each $n \geq 1$, we solve the **anyon equation**

$$\begin{aligned} \epsilon(\alpha(x, y)\mathcal{X}_1 + \beta(x, y)\mathcal{X}_2 + \gamma(x, y)\mathcal{Z}_1 + \delta(x, y)\mathcal{Z}_2) \\ = (1 - x^n)[\dots, \dots] := (1 - x^n)v, \end{aligned} \quad (28)$$

where v is a length-2 row vector, referred to as an anyon. This anyon equation is previously sketched in Fig. 5, and here is the precise mathematical definition in the Laurent polynomial formalism. The physical interpretation of this equation is that when we apply Pauli matrices X_1, X_2, Z_1 , and Z_2 at locations $\alpha(x, y), \beta(x, y), \gamma(x, y)$, and $\delta(x, y)$, it violates the stabilizers around the origin $(0, 0)$ and the point $(n, 0)$ with patterns v and $-v$, respectively. This operator creates an anyon v at $(0, 0)$ and its antiparticle at $(n, 0)$. Note that if v is an anyon, $x^a y^b v$ is also an anyon for all $a, b \in \mathbb{Z}$. In addition, an anyon solved by a particular n can be solved from any multiple of n . The anyon equation (28) defines the string operator that moves an anyon in the x -direction. In principle, we should also write the anyon equation in y -direction.

To check whether two anyons are of the same type, we rely on the following equivalence relation:

$$v' \sim v \text{ (} v' \text{ is equivalent to } v \text{)}, \quad (29)$$

if and only if there exist finite-degree polynomials $p_1(x, y), p_2(x, y), p_3(x, y), p_4(x, y)$ such that

$$\begin{aligned} v' &= v + p_1(x, y)\epsilon(\mathcal{X}_1) + p_2(x, y)\epsilon(\mathcal{X}_2) \\ &\quad + p_3(x, y)\epsilon(\mathcal{Z}_1) + p_4(x, y)\epsilon(\mathcal{Z}_2). \end{aligned} \quad (30)$$

Physically, this can be understood as two anyons are of the same type if and only if they are differed by some local Pauli operators X_1, X_2, Z_1, Z_2 at locations specified by polynomials $p_1(x, y), p_2(x, y), p_3(x, y), p_4(x, y)$. Note that even if anyon v implies the existence of another anyon $x^a y^b v$, they do not need to be the same type. The Wen plaquette model is an example [73].

B. Examples

1. Trivial model $H_0 = -\sum_e X_e$

We first consider the trivial Hamiltonian Eq. (20). We can easily compute

$$\begin{aligned} \epsilon(\mathcal{X}_1) &= [0, 0], \quad \epsilon(\mathcal{X}_2) = [0, 0], \\ \epsilon(\mathcal{Z}_1) &= [1, 0], \quad \epsilon(\mathcal{Z}_2) = [0, 1]. \end{aligned} \quad (31)$$

Since linear combinations of $\{\epsilon(\mathcal{X}_1), \epsilon(\mathcal{X}_2), \epsilon(\mathcal{Z}_1), \epsilon(\mathcal{Z}_2)\}$ already generate all possible polynomials in each entry, all anyons are equivalent to the trivial anyon $v_0 = [0, 0]$. There is only one trivial anyon in this model.

2. Standard \mathbb{Z}_d toric code

We analyze the standard \mathbb{Z}_d toric code Eq. (22). The syndromes of single-qubit Pauli errors are

$$\begin{aligned} \epsilon(\mathcal{X}_1) &= [0, -1 + \bar{y}], \quad \epsilon(\mathcal{X}_2) = [0, 1 - \bar{x}], \\ \epsilon(\mathcal{Z}_1) &= [1 - x, 0], \quad \epsilon(\mathcal{Z}_2) = [1 - y, 0]. \end{aligned} \quad (32)$$

From the anyon equation (28), $\epsilon(\mathcal{X}_2)$ can generate a solution $v_m = [0, 1]$ and general solutions $[0, x^a y^b] \quad \forall a, b \in \mathbb{Z}$ (by choosing $n = 1$ and $\beta(x, y) = -x^{a+1} y^b$). Also, $\epsilon(\mathcal{Z}_1)$ can generate a solution $v_e = [1, 0]$ and general solutions $[x^c y^d, 0] \quad \forall c, d \in \mathbb{Z}$. Therefore, a generic anyon can be expressed as $[x^{a_1} y^{b_1} + x^{a_2} y^{b_2} + \dots, x^{c_1} y^{d_1} + x^{c_2} y^{d_2} + \dots]$.

Next, we want to check whether these anyons are equivalent or not. From the identity

$$(1-x)(1+x+x^2+\dots+x^{k-1}) = 1-x^k, \quad (33)$$

we have $[x^k p(y), \dots] \sim [p(y), \dots]$ since they are differed by the polynomial factor $(1+x+x^2+\dots+x^{k-1})p(y)$. Similarly, we have $\epsilon(\mathcal{Z}_2)$ for the y part. More precisely, we summarize the equivalence relation

$$\begin{aligned} [0, x^a y^b] &\sim [0, 1], \quad \forall a, b \in \mathbb{Z}, \\ [x^c y^d, 0] &\sim [1, 0], \quad \forall c, d \in \mathbb{Z}. \end{aligned} \quad (34)$$

Giving an anyon, adding polynomial factors of $\epsilon(\mathcal{X}_1), \epsilon(\mathcal{X}_2), \epsilon(\mathcal{Z}_1), \epsilon(\mathcal{Z}_2)$ can not change the parity of the sum of coefficients¹⁰ in each entry. We conclude that the following four anyons are inequivalent:

$$v_0 = [0, 0], \quad v_e = [1, 0], \quad v_m = [0, 1], \quad v_f = [1, 1]. \quad (35)$$

Note that we can choose v_e and v_m as the **basis anyons**, which generate the entire set of anyons. This choice is not canonical since another choice $\{v_e, v_f\}$ is also valid.

¹⁰ The sum of coefficients can be computed by substituting $x \rightarrow 1$ and $y \rightarrow 1$.

3. Two copies of \mathbb{Z}_d toric codes

Consider a new Hamiltonian modified from the toric code:

$$H_{\text{TC}} = - \sum_v \left[\begin{array}{c} | \\ X \\ \text{---} X^\dagger \text{---} \\ | \\ v \\ \text{---} X \\ | \\ X^\dagger \\ | \end{array} \right] - \sum_p \left[\begin{array}{c} \text{---} Z^\dagger \text{---} \\ \left[\begin{array}{c} Z^\dagger \\ p \\ Z \end{array} \right] \text{---} \\ \text{---} Z \text{---} \end{array} \right], \quad (36)$$

which stabilizers differ from Eq. (22):

$$S_1 = \begin{bmatrix} 1 - \bar{x}^2 \\ 1 - \bar{y} \\ 0 \\ 0 \end{bmatrix}, \quad S_2 = \begin{bmatrix} 0 \\ 0 \\ 1 - y \\ -1 + x^2 \end{bmatrix}. \quad (37)$$

The square lattice can be partitioned so the Hamiltonian is exactly two decoupled \mathbb{Z}_d toric codes. It has syndromes:

$$\begin{aligned} \epsilon(\mathcal{X}_1) &= [0, -1 + \bar{y}], \quad \epsilon(\mathcal{X}_2) = [0, 1 - \bar{x}^2], \\ \epsilon(\mathcal{Z}_1) &= [1 - x^2, 0], \quad \epsilon(\mathcal{Z}_2) = [1 - y, 0]. \end{aligned} \quad (38)$$

We focus on the Z part first and try to solve

$$\gamma(x, y) \epsilon(\mathcal{Z}_1) + \delta(x, y) \epsilon(\mathcal{Z}_2) = (1 - x^n)v, \quad (39)$$

For $n = 1$, we have

$$x^a y^b \epsilon(\mathcal{Z}_1) = x^a y^b [1 - x^2, 0] = (1-x)[x^a y^b + x^{a+1} y^b, 0]. \quad (40)$$

Therefore, we have anyons $v_{a,b}^{n=1} := [x^a y^b + x^{a+1} y^b, 0]$ for arbitrary $a, b \in \mathbb{Z}$. For $n = 2$, we have

$$x^c y^d \epsilon(\mathcal{Z}_1) = x^c y^d [1 - x^2, 0] = (1-x^2)[x^c y^d, 0], \quad (41)$$

which gives anyons $v_{c,d}^{n=2} := [x^c y^d, 0]$ for arbitrary $c, d \in \mathbb{Z}$. Notice that all $v_{a,b}^{n=1}$ can be generated by $v_{c,d}^{n=2}$ since

$$v_{a,b}^{n=1} = v_{a,b}^{n=2} + v_{a+1,b}^{n=2}. \quad (42)$$

In fact, $v_{c,d}^{n=2}$ has already generated all possible polynomials in the first entry. We do not need to look for $n \geq 3$ cases.

Next, we use $\epsilon(\mathcal{Z}_1)$ and $\epsilon(\mathcal{Z}_2)$ to find the equivalence classes of those anyons. By some algebraic argument, there are four inequivalent classes:

$$\begin{aligned} 1 &:= [0, 0], \\ e_1 &:= [1, 0], \\ e_2 &:= [x, 0], \\ e_1 e_2 &:= [1 + x, 0]. \end{aligned} \quad (43)$$

toric code stabilizer group, which commute with condensation terms $\mathcal{S}_3, \mathcal{S}_4$. The stabilizers of shifted double semion code be written as polynomials

$$\begin{aligned} \mathcal{S}_1 &= \begin{bmatrix} \bar{x} - 1 \\ \bar{y} - 1 \\ x^l(1 - y) \\ x^l(-1 + x) \end{bmatrix}, & \mathcal{S}_2 &= \begin{bmatrix} 0 \\ 0 \\ 2 + 2y \\ 2 + 2x \end{bmatrix}, \\ \mathcal{S}_3 &= \begin{bmatrix} 2x^l \\ 0 \\ 0 \\ 2\bar{y} \end{bmatrix}, & \mathcal{S}_4 &= \begin{bmatrix} 0 \\ 2x^l \\ 2\bar{x} \\ 0 \end{bmatrix}. \end{aligned} \quad (53)$$

If we set $l = 0$, Eq. (53) gives the stabilizers of the double semion code in Eq. (46). Given the stabilizers, the error syndromes are

$$\begin{aligned} \epsilon(\mathcal{X}_1) &= [\bar{x}^l(\bar{y} - 1), -2\bar{y} - 2, 0, -2x], \\ \epsilon(\mathcal{X}_2) &= [\bar{x}^l(1 - \bar{x}), -2\bar{x} - 2, -2y, 0], \\ \epsilon(\mathcal{Z}_1) &= [-1 + x, 0, 2\bar{x}^l, 0], \\ \epsilon(\mathcal{Z}_2) &= [-1 + y, 0, 0, 2\bar{x}^l]. \end{aligned} \quad (54)$$

Similar to the calculation in Eq. (48) and (50), we have

$$\begin{aligned} \epsilon(\mathcal{X}_2) + x^l y \epsilon(\mathcal{Z}_1) &= [-\bar{x}^{l+1} - x^l y, -2\bar{x}, 0, 0], \\ \epsilon(\mathcal{X}_1) - x^l \epsilon(\mathcal{Z}_2) &= (1 - y)[\bar{x}^l \bar{y} + x^l, -2\bar{y}, 0, 0], \\ 2\epsilon(\mathcal{Z}_1) &= (1 - x)[-2, 0, 0, 0], \\ 2\epsilon(\mathcal{Z}_2) &= (1 - y)[-2, 0, 0, 0]. \end{aligned} \quad (55)$$

This gives us the string operators for anyon s and b along the x - and y -directions in Eq. (56). They generate the

whole anyon theory of $\{e, s, b, \bar{s}\}$ where $\bar{s} = s \times b$.

$$\begin{aligned} W_e^s := & \begin{array}{c} \text{---} Z \text{---} \\ | \\ \cdots X_e \cdots \rightarrow \\ | \\ \xrightarrow{x^l} \\ | \\ \text{---} Z^\dagger \text{---} \\ | \\ \cdots X_e^\dagger \cdots \leftarrow \\ | \\ \xrightarrow{x^l} \\ | \\ \text{---} X_e \text{---} \text{---} Z^\dagger \\ | \\ \xrightarrow{x^l} \\ | \\ \text{---} X_e^\dagger \text{---} \text{---} Z \\ | \\ \xrightarrow{x^l} \\ | \\ \text{---} Z_e^2 \text{---}, \quad \begin{array}{c} | \\ Z_e^2 \\ | \end{array} \end{array} \end{array} \quad (56)$$

IV. COMPUTATIONAL METHOD

In this section, we describe how to transform the problem of finding anyon string operators in the previous section into implementing (modified) Gaussian elimination, which is closely related to the Hermite normal form. Computers can perform these algorithms efficiently in a polynomial time. Later, we show that the fusion rules of anyons can be derived from the Smith normal form of anyon relations, and the topological spins and braiding statistics of anyons can be computed from the string operators directly.

To numerically solve the anyon equation (28) to obtain anyons in a stabilizer code, the module over a polynomial ring is not straightforward to work with. As standard techniques in linear algebra, Gaussian elimination (GE) only works for a field, and Hermit normal form (HNF) and Smith normal form (SNF) are only applicable to a principal ideal domain (PID), which are reviewed in Appendix B. The polynomial ring $R = \mathbb{Z}_d[x, y, x^{-1}, y^{-1}]$ is

neither a field nor a PID. Therefore, instead of treating $\epsilon(P)$ as a row vector in the module over R , we truncate the degree of polynomials and store coefficients in the polynomial as a vector over \mathbb{Z}_d . For instance, a polynomial such as $f(x, y) = 1 + 2x + xy + 3y^2 \in R$ can be expressed as a **coefficient vector** over \mathbb{Z}_d

$$\tilde{f} = \begin{bmatrix} 1 & x & y & \bar{x} & \bar{y} & x^2 & xy & y^2 & x\bar{y} & \bar{x}y & \cdots \\ 1 & 2 & 0 & 0 & 0 & 0 & 1 & 3 & 0 & 0 & \cdots \end{bmatrix}, \quad (57)$$

where each entry represents the coefficient of the corresponding monomial $x^a y^b$ in the polynomial $f(x, y)$. In the rest of this paper, we denote \tilde{f} as the coefficient vector of the polynomial $f(x, y) \in R$. In practice, we choose the polynomial within $x^{\pm k}$ and $y^{\pm k}$, and the monomial $x^a y^b$ corresponds to the $((a+k) + (b+k)(2k+1) + 1)$ -th entry in the coefficient vector for all $-k \leq a, b \leq k$. The length of the coefficient vector is $(2k+1)^2$. In other words, we restrict ourselves to a finite region A that includes coordinates (i, j) with $-k \leq i, j \leq k$ in a plane, as shown in Fig. 8.

$(2k+1)^2-2k-1$ $x^k y^{-k}$	$(2k+1)^2-2k$ $x^k y^{-k+1}$...	$(2k+1)^2-1$ $x^k y^{k-1}$	$(2k+1)^2$ $x^k y^k$
$(2k+1)^2-4k-2$ $x^{k-1} y^{-k}$	$(2k+1)^2-4k-1$ $x^{k-1} y^{-k+1}$...	$(2k+1)^2-2k-3$ $x^{k-1} y^{k-1}$	$(2k+1)^2-2k-2$ $x^{k-1} y^k$
...
$2k+2$ $x^{-k+1} y^{-k}$	$2k+3$ $x^{-k+1} y^{-k+1}$...	$4k+1$ $x^{-k+1} y^{k-1}$	$4k+2$ $x^{-k+1} y^k$
1 $x^{-k} y^{-k}$	2 $x^{-k} y^{-k+1}$...	$2k$ $x^{-k} y^{k-1}$	$2k+1$ $x^{-k} y^k$

FIG. 8. The region A where the polynomials are truncated to. It contains all monomials with $x^{\pm k}$ and $y^{\pm k}$. The red numbers indicate the ordering in the coefficient vector. Any polynomial in $\mathbb{Z}_d[x, y, x^{-1}, y^{-1}]$ is truncated to a length- $(2k+1)^2$ row vector over \mathbb{Z}_d .

Given a fixed k , we define the **truncation map** as

$$f \in \mathbb{Z}_d[x, y, x^{-1}, y^{-1}] \rightarrow \tilde{f} \in \mathbb{Z}_d^{\otimes (2k+1)^2}. \quad (58)$$

We allow this truncation map to act on any $m \times n$ matrix M over $\mathbb{Z}_d[x, y, x^{-1}, y^{-1}]$ by acting on each entry to expand to a row vector with length $(2k+1)^2$, and by joining these row vectors to form an $m \times n(2k+1)^2$ matrix \tilde{M} over \mathbb{Z}_d . As argued in the previous section, sufficiently large A allows us to recover all topological data of a Pauli stabilizer code. To optimize running time, we can choose a rectangular region specified by the polynomial within $x^{\pm k_x}$ and $y^{\pm k_y}$. For example, when focusing on anyon string operators in the x -direction, a greater value of k_x compared to k_y is preferable. For convenience, our discussion will focus on the square area A and check the topological order condition, identify anyon string operators, and verify the fusion rules, topological spins, and braiding properties of anyons within A .

Also, we define the **translational duplicate map** TD_m that takes the input as a length- l row vector $F = [f_1, f_2, \dots, f_l]$ with each entry f_i in $\mathbb{Z}_d[x, y, x^{-1}, y^{-1}]$ and returns a $(2m+1)^2 \times l$ matrix formed by its translations within $x^{\pm m} y^{\pm m}$.¹¹

$$F \rightarrow \text{TD}_m(F) := \begin{bmatrix} x^{-m} y^{-m} F \\ x^{-m+1} y^{-m} F \\ \vdots \\ x^{m-1} y^{-m} F \\ x^m y^{-m} F \\ \hline x^{-m} y^{-m+1} F \\ x^{-m+1} y^{-m+1} F \\ \vdots \\ x^{m-1} y^{-m+1} F \\ x^m y^{-m+1} F \\ \hline \vdots \\ \vdots \\ \hline x^{-m} y^m F \\ x^{-m+1} y^m F \\ \vdots \\ x^{m-1} y^m F \\ x^m y^m F. \end{bmatrix}, \quad (59)$$

where $x^a y^b F$ is the row vector multiplying $x^a y^b$ to each entry of F , i.e., $x^a y^b F = [x^a y^b f_1, x^a y^b f_2, \dots, x^a y^b f_l]$.

A. Prime-dimensional qudit \mathbb{F}_p

As a warm-up, we assume that the qudit dimension d is a prime number to illustrate the method, and will later (in Sec. IV B) generalize to an arbitrary integer d . When $d = p$ is a prime, $\mathbb{Z}_p = \mathbb{F}_p$ is a finite field, greatly simplifying the computations.

1. Topological order condition

We check the TO condition (27) in the region A . Given the syndrome for a single Pauli operator, we find possible local combinations of Pauli operators such that all syndromes are canceled. We verify that these combined operators are in the stabilizer group.

First, we prepare a matrix consisting of error syn-

¹¹ We choose m to be smaller than k . For example, we set $m = k - 2r$, where r is the maximum range of each stabilizer.

dromes:

$$\widetilde{M}_1 := \begin{bmatrix} \widetilde{\text{TD}_m(\epsilon(\mathcal{X}_1))} \\ \widetilde{\text{TD}_m(\epsilon(\mathcal{X}_2))} \\ \widetilde{\text{TD}_m(\epsilon(\mathcal{Z}_1))} \\ \widetilde{\text{TD}_m(\epsilon(\mathcal{Z}_2))} \end{bmatrix}, \quad (60)$$

where the row space consists of the syndrome patterns of local Pauli operators. Next, we perform the Gaussian elimination to obtain a new matrix $\text{GE}(\widetilde{M}_1)$. Each zero row in $\text{GE}(\widetilde{M}_1)$ represents a relation:

$$\overline{\epsilon(p_1\mathcal{X}_1 + p_2\mathcal{X}_2 + p_3\mathcal{Z}_1 + p_4\mathcal{Z}_2)} = \widetilde{[0, 0]}, \quad (61)$$

for some polynomials $p_1, p_2, p_3, p_4 \in \mathbb{F}_p[x, y, x^{-1}, y^{-1}]$, restricted within $x^{\pm m}y^{\pm m}$. We denote the column vector $\mathcal{O} := \epsilon(p_1\mathcal{X}_1 + p_2\mathcal{X}_2 + p_3\mathcal{Z}_1 + p_4\mathcal{Z}_2)$ and compute the difference between the ranks of the following two matrices:

$$\widetilde{M}_2 := \begin{bmatrix} \widetilde{\text{TD}_{m'}(\mathcal{S}_1^\dagger)} \\ \widetilde{\text{TD}_{m'}(\mathcal{S}_2^\dagger)} \end{bmatrix}, \quad \text{and} \quad \widetilde{M}_2^\mathcal{O} := \begin{bmatrix} \widetilde{\mathcal{O}^\dagger} \\ \widetilde{\text{TD}_{m'}(\mathcal{S}_1^\dagger)} \\ \widetilde{\text{TD}_{m'}(\mathcal{S}_2^\dagger)} \end{bmatrix}. \quad (62)$$

Note that we choose $m' > m$ (and still $m' < k$) such that stabilizers can cover the support of \mathcal{O} . The rank difference is 0 if and only if the operator \mathcal{O} is spanned by $\mathcal{S}_1, \mathcal{S}_2$ and their translations. To check the TO condition, we verify that all zero rows in $\text{GE}(\widetilde{M}_1)$ correspond to a local operator \mathcal{O} with vanishing rank difference in Eq. (62).

2. Solving the anyon equation

To solve the anyon equation

$$\begin{aligned} \epsilon(\alpha(x, y)\mathcal{X}_1 + \beta(x, y)\mathcal{X}_2 + \gamma(x, y)\mathcal{Z}_1 + \delta(x, y)\mathcal{Z}_2) \\ = (1 - x^n)v, \end{aligned} \quad (63)$$

we perform Gaussian elimination on the following $6(2m+1)^2 \times 2(2k+1)^2$ matrix

$$\widetilde{M}_3 := \begin{bmatrix} \widetilde{\text{TD}_m(\epsilon(\mathcal{X}_1))} \\ \widetilde{\text{TD}_m(\epsilon(\mathcal{X}_2))} \\ \widetilde{\text{TD}_m(\epsilon(\mathcal{Z}_1))} \\ \widetilde{\text{TD}_m(\epsilon(\mathcal{Z}_2))} \\ \widetilde{\text{TD}_m([(1-x^n), 0])} \\ \widetilde{\text{TD}_m([0, (1-x^n)])} \end{bmatrix}. \quad (64)$$

After Gaussian elimination, each zero row in the matrix $\text{GE}(\widetilde{M}_3)$ gives an anyon v in this region:

$$\overline{\epsilon(p_1\mathcal{X}_1 + p_2\mathcal{X}_2 + p_3\mathcal{Z}_1 + p_4\mathcal{Z}_2)} = \overline{[p_5(1-x^n), p_6(1-x^n)]}, \quad (65)$$

where the anyon is $v := [p_5, p_6]$.

3. Equivalence relations between anyons

In this part, we provide an algorithm to categorize anyon types in a Pauli stabilizer model with \mathbb{Z}_p qudits. Two anyons v and v' are equivalent if

$$v' = v + p_1\epsilon(\mathcal{X}_1) + p_2\epsilon(\mathcal{X}_2) + p_3\epsilon(\mathcal{Z}_1) + p_4\epsilon(\mathcal{Z}_2). \quad (66)$$

where p_1, p_2, p_3 , and p_4 are polynomials within $x^{\pm m}y^{\pm m}$. In other words, we compute the quotient space of anyons using row vectors $\{\epsilon(\mathcal{X}_1), \epsilon(\mathcal{X}_2), \epsilon(\mathcal{Z}_1), \epsilon(\mathcal{Z}_2)\}$. To check this, we can compute the rank difference between the two matrices

$$\widetilde{M}_1 = \begin{bmatrix} \widetilde{\text{TD}_m(\epsilon(\mathcal{X}_1))} \\ \widetilde{\text{TD}_m(\epsilon(\mathcal{X}_2))} \\ \widetilde{\text{TD}_m(\epsilon(\mathcal{Z}_1))} \\ \widetilde{\text{TD}_m(\epsilon(\mathcal{Z}_2))} \end{bmatrix}, \quad \text{and} \quad \widetilde{M}_1^{v-v'} := \begin{bmatrix} \widetilde{v-v'} \\ \widetilde{\text{TD}_m(\epsilon(\mathcal{X}_1))} \\ \widetilde{\text{TD}_m(\epsilon(\mathcal{X}_2))} \\ \widetilde{\text{TD}_m(\epsilon(\mathcal{Z}_1))} \\ \widetilde{\text{TD}_m(\epsilon(\mathcal{Z}_2))} \end{bmatrix}. \quad (67)$$

Two matrices have equal rank if and only if the syndromes span $v - v'$, which is exactly the definition of equivalence $v \sim v'$ in Eq. (66).

Moreover, since each qudit has a prime dimension p , any topological Pauli stabilizer code is equivalent to finite copies of \mathbb{Z}_p toric codes. Therefore, we only need to count the number of basis anyons that generate all anyons, to obtain the topological order. Given the anyon set $V = \{v_1, v_2, \dots\}$ solved from the anyon equation (28), to count the number of basis anyons, we compute the rank difference between

$$\widetilde{M}_1 = \begin{bmatrix} \widetilde{\text{TD}_m(\epsilon(\mathcal{X}_1))} \\ \widetilde{\text{TD}_m(\epsilon(\mathcal{X}_2))} \\ \widetilde{\text{TD}_m(\epsilon(\mathcal{Z}_1))} \\ \widetilde{\text{TD}_m(\epsilon(\mathcal{Z}_2))} \end{bmatrix}, \quad \text{and} \quad \widetilde{M}_1^V := \begin{bmatrix} \widetilde{v_1} \\ \widetilde{v_2} \\ \widetilde{v_3} \\ \vdots \\ \widetilde{\text{TD}_m(\epsilon(\mathcal{X}_1))} \\ \widetilde{\text{TD}_m(\epsilon(\mathcal{X}_2))} \\ \widetilde{\text{TD}_m(\epsilon(\mathcal{Z}_1))} \\ \widetilde{\text{TD}_m(\epsilon(\mathcal{Z}_2))} \end{bmatrix}. \quad (68)$$

If the rank difference is $2k$, the topological Pauli stabilizer code corresponds to k copies of \mathbb{Z}_p toric codes.

B. Nonprime-dimensional qudit \mathbb{Z}_d

Over a ring \mathbb{Z}_d , Gaussian elimination does not work since the multiplication inverse of an element in \mathbb{Z}_d might not exist, e.g., the element 2 in \mathbb{Z}_4 . Moreover, \mathbb{Z}_d may contain zero divisors, i.e., a nonzero element a , such that there exists another nonzero element $x \in \mathbb{Z}_d$ satisfying $ax = 0$. The element 2 in \mathbb{Z}_4 is again an example since $2 \times 2 = 0$ in \mathbb{Z}_4 .

Therefore, we introduce the modified Gaussian elimination (MGE) algorithm over \mathbb{Z}_d , inspired by the Hermite normal form:

1. Given a $n \times m$ matrix A over \mathbb{Z}_d . We treat the entries in the first column $a_{i,1} \forall i \in \{1, 2, \dots, n\}$ as integers $\{0, 1, 2, 3, \dots, d-1\}$ in \mathbb{Z} . To recover the \mathbb{Z}_d periodicity, we insert a new row $[d, 0, 0, \dots, 0]$ below A , which becomes a $(n+1) \times m$ matrix A' . Next, we find the greatest common divisor of its first column $\{a_{1,1}, a_{2,1}, \dots, a_{n,1}, d\}$, denoted as $\gcd(a_{i,1})_d$.¹² From the extended Euclidean algorithm, there exists a linear combination:

$$\begin{aligned} r_1 a_{1,1} + r_2 a_{2,1} + \dots + r_n a_{n,1} + r_{n+1} d \\ = \gcd(a_{i,1})_d. \end{aligned} \quad (69)$$

Moreover, this linear combination can be obtained by subtracting one entry from another greater entry from the following list repetitively,

$$[a_{1,1}, a_{2,1}, a_{3,1}, \dots, a_{n,1}, d], \quad (70)$$

and the final entries are (up to reordering)

$$[\gcd(a_{i,1})_d, 0, 0, \dots, 0, 0]. \quad (71)$$

Subtracting one entry from another and reordering would correspond to row operations in the matrix A' . Therefore, we apply corresponding row operations in the matrix A' according to the extended Euclidean algorithm, which transforms the first column into

$$[\gcd(a_{i,1})_d, 0, 0, \dots, 0, 0]^T. \quad (72)$$

2. If $\gcd(a_{i,1})_d$ is a zero divisor, i.e., $\gcd(a_{i,1})_d > 0$ and

$$\gcd(a_{i,1})_d \times r^* \equiv 0 \pmod{d}$$

for some integer r^* with $0 < r^* \leq d-1$ (WLOG, we assume that r^* is the smallest one), we do not perform an operation in this row.¹³ If $\gcd(a_{i,1})_d$ is not a zero divisor, we multiply a proper number in this row to make it $+1$.

3. The first column and the first row are done. Repeat the above procedures on the submatrix without the first column and the first row.

¹² For the convenience, we choose $\gcd(a_{i,1})_d$ to be in the set $\{0, 1, 2, 3, \dots, d-1\}$.

¹³ Denote $\gcd(a_{i,1})_d \times r^* = kd$. We notice that r^* times this row has first entry $0 \pmod{d}$ and might affect the space spanned by other rows. In principle, we should insert a new row at the end of the matrix, which is r^* times the first row minus the row $[kd, 0, 0, \dots, 0]$, before we start to deal with the second column. However, this inserting is redundant since it is equivalent to inserting a new row $[-kd, 0, 0, \dots, 0]$ that is already covered by the insertion of $[d, 0, 0, \dots, 0]$ in step 1.

We provide a concrete example of how to implement this algorithm. Choose a matrix A over \mathbb{Z}_8 as

$$A = \begin{bmatrix} 4 & 2 & 0 \\ 6 & 0 & 3 \\ 0 & 7 & 4 \end{bmatrix}. \quad (73)$$

We insert a row $[8, 0, 0]$ in the beginning:

$$A' = \begin{bmatrix} 8 & 0 & 0 \\ 4 & 2 & 0 \\ 6 & 0 & 3 \\ 0 & 7 & 4 \end{bmatrix}. \quad (74)$$

The greatest common divisor of the first column is 2, which can be obtained from $(-1) \times 6 + 1 \times 8$:

$$A' = \begin{bmatrix} 2 & 0 & -3 \\ 4 & 2 & 0 \\ 6 & 0 & 3 \\ 0 & 7 & 4 \end{bmatrix} = \begin{bmatrix} 2 & 0 & 5 \\ 4 & 2 & 0 \\ 6 & 0 & 3 \\ 0 & 7 & 4 \end{bmatrix}, \quad (75)$$

since the second and third columns are still in \mathbb{Z}_8 . Then, we use the first row to cancel other rows

$$\begin{bmatrix} 2 & 0 & 5 \\ 0 & 2 & -10 \\ 0 & 0 & -12 \\ 0 & 7 & 4 \end{bmatrix} = \begin{bmatrix} 2 & 0 & 5 \\ 0 & 2 & 6 \\ 0 & 0 & 4 \\ 0 & 7 & 4 \end{bmatrix}. \quad (76)$$

The first row and column are done. We repeat the process by first inserting $[0, 8, 0]$:

$$\begin{bmatrix} 2 & 0 & 5 \\ 0 & 8 & 0 \\ 0 & 2 & 6 \\ 0 & 0 & 4 \\ 0 & 7 & 4 \end{bmatrix}. \quad (77)$$

The gcd of the second column is 1, obtained from $8 - 7$:

$$\begin{bmatrix} 2 & 0 & 5 \\ 0 & 1 & -4 \\ 0 & 2 & 6 \\ 0 & 0 & 4 \\ 0 & 7 & 4 \end{bmatrix} = \begin{bmatrix} 2 & 0 & 5 \\ 0 & 1 & 4 \\ 0 & 2 & 6 \\ 0 & 0 & 4 \\ 0 & 7 & 4 \end{bmatrix}. \quad (78)$$

Next, we use the second row to cancel the rows below

$$\begin{bmatrix} 2 & 0 & 5 \\ 0 & 1 & 4 \\ 0 & 0 & -2 \\ 0 & 0 & 4 \\ 0 & 0 & -24 \end{bmatrix} = \begin{bmatrix} 2 & 0 & 5 \\ 0 & 1 & 4 \\ 0 & 0 & 6 \\ 0 & 0 & 4 \\ 0 & 0 & 0 \end{bmatrix}. \quad (79)$$

Finally, we insert $[0, 0, 8]$

$$\begin{bmatrix} 2 & 0 & 5 \\ 0 & 1 & 4 \\ 0 & 0 & 8 \\ 0 & 0 & 6 \\ 0 & 0 & 4 \\ 0 & 0 & 0 \end{bmatrix}, \quad (80)$$

and find the gcd of the third column is 2, which can be used to cancel out the remaining part:

$$\begin{bmatrix} 2 & 0 & 5 \\ 0 & 1 & 4 \\ 0 & 0 & 2 \\ 0 & 0 & 0 \\ 0 & 0 & 0 \\ 0 & 0 & 0 \end{bmatrix}. \quad (81)$$

We will prove the following four theorems about the modified Gaussian elimination.

Theorem 1. *The nonzero rows in the final matrix span the same space as the initial matrix.*

Proof. Each procedure is reversible, and the matrix does not lose any information. \square

Theorem 2. *All relations between the original rows are contained in the zero rows at the end.*

Proof. Consider a relation between the original rows $r = \sum_i (c_i a_{i,1}) = 0$. Because each row $a_{a,i}$ is spanned by the rows in the final rows A' (according to Theorem 1), $r = \sum_i (c_i a_{i,1})$ is spanned by rows in A' . We need to show that the zero rows in A' span it. This is trivial since A' is in the row echelon form, and if the linear combination involves any nonzero row, the combined row will also be nonzero. \square

Next, to check whether a row vector v is spanned by the matrix A , we first apply the modified Gaussian elimination algorithm to reduce the matrix A to its final triangular form A' . Define $v^{(0)} = v$. Given $v^{(k-1)}$, if $a'_{k,k} | v_k^{(k-1)}$, where $a'_{k,k}$ is the k -th diagonal entry of A' and $v_k^{(k-1)}$ is the k -th entry of $v^{(k-1)}$, define

$$v^{(k)} = v^{(k-1)} - \frac{v_k^{(k-1)}}{a'_{k,k}} A'[k, -], \quad (82)$$

where $A'[k, -]$ is the k -th row of A' . Otherwise, we could not define $v^{(k)}$ and stop this process. Note that the first k entries of $v^{(k)}$ are 0.

Theorem 3. *A row vector v of length n is spanned by row vectors of the matrix A iff the process defined above achieves $v^{(n)}$.*

Proof. Since, by Thm. 1, the row span of A' is the same as the row span of A , we must prove that v is spanned by the rows of A' iff the process achieves $v^{(n)}$. We begin with the \Rightarrow direction. We assume that v is spanned by the rows of A' , so that $v = v^{(0)} = \sum_{i=1}^n \alpha_i A'[i, -]$ for some coefficients α_i . Since A' is upper triangular, it must be that $v_k = \sum_{i=1}^k \alpha_i a'_{i,k}$. Therefore,

$$\alpha_k a'_{k,k} = v_k - \sum_{i=1}^{k-1} \alpha_i a'_{i,k}. \quad (83)$$

We claim that $v^{(k)} = v - \sum_{i=1}^k \alpha_i A'[i, -]$, so that the process indeed achieves $v^{(n)}$. We prove this by induction. For the base case, we use that $a'_{1,1} | v_1$ by Eq. (83), so that by Eq. (82) $v^{(1)} = v - \frac{v_1}{a'_{1,1}} A'[1, -] = v - \alpha_1 A'[1, -]$. Now for the inductive step, we assume that $v^{(k-1)} = v - \sum_{i=1}^{k-1} \alpha_i A'[i, -]$. Hence, $v_k^{(k-1)} = \alpha_k a'_{k,k}$ by (83). Then by Eq. (82) $v^{(k)} = v^{(k-1)} - \alpha_k A'[k, -]$, which proves the inductive step.

We now prove the \Leftarrow direction. We assume that $a'_{k,k} | v_k^{(k-1)}$ for every k , and we thus define α_k by $v_k^{(k-1)} = \alpha_k a'_{k,k}$. Then, reversing Eq. (82), we find that $v^{(k-1)} = v^{(k)} + \alpha_k A'[k, -]$. Noticing that $v^{(n)}$ must be $(0, \dots, 0)$, we find that $v = v^{(0)} = \sum_{i=1}^n \alpha_i A'[i, -]$. \square

Theorem 4. *The modified Gaussian elimination algorithm on the matrix A over \mathbb{Z}_d is equivalent to applying the standard Gaussian elimination algorithm over a PID on the following matrix over \mathbb{Z} :*

$$\tilde{A} = \begin{bmatrix} A_{11} & A_{12} & \cdots & A_{1m} \\ A_{21} & A_{22} & \cdots & A_{2m} \\ \vdots & \vdots & \ddots & \vdots \\ A_{n1} & A_{n2} & \cdots & A_{nm} \\ d & 0 & \cdots & 0 \\ 0 & d & \cdots & 0 \\ \vdots & \vdots & \ddots & \vdots \\ 0 & 0 & \cdots & d \end{bmatrix} \quad (84)$$

Proof. A linear system $xA = b \pmod{d}$, for x a $1 \times n$ row vector and b a $1 \times m$ row vector, is encoded by the linear equation $x\tilde{A} = b$ over \mathbb{Z} , where y is a $1 \times m$ row vector of additional variables. The latter system is exactly $\tilde{x}\tilde{A} = b$ over \mathbb{Z} , where \tilde{x} is the $1 \times (n+m)$ row vector (x, y) . It follows that if x is the solution to $xA = b \pmod{d}$ and \tilde{x} is the solution to $\tilde{x}\tilde{A} = b$, then $\tilde{x}_i = x_i \pmod{d}$ for $i = 1, \dots, n$. \square

1. Topological order condition

We check the TO condition (27) in the region A . Similar to Sec. IV A 1, we prepare a matrix consisting of

syndrome pattern of local Pauli operators:

$$\widetilde{M}_1 := \begin{bmatrix} \overline{\text{TD}_m(\epsilon(\mathcal{X}_1))} \\ \overline{\text{TD}_m(\epsilon(\mathcal{X}_2))} \\ \overline{\text{TD}_m(\epsilon(\mathcal{Z}_1))} \\ \overline{\text{TD}_m(\epsilon(\mathcal{Z}_2))} \end{bmatrix}. \quad (85)$$

Next, we perform the modified Gaussian elimination to obtain a new matrix $\text{MGE}(\widetilde{M}_1)$, and each zero row in $\text{MGE}(\widetilde{M}_1)$ corresponds to a relation:

$$\overline{\epsilon(p_1\mathcal{X}_1 + p_2\mathcal{X}_2 + p_3\mathcal{Z}_1 + p_4\mathcal{Z}_2)} = \widetilde{[0, 0]}, \quad (86)$$

for some polynomials p_1, p_2, p_3 , and p_4 restricted within $x^{\pm m}y^{\pm m}$. We denote the column vector $\mathcal{O} := \epsilon(p_1\mathcal{X}_1 + p_2\mathcal{X}_2 + p_3\mathcal{Z}_1 + p_4\mathcal{Z}_2)$. However, the rank over a non-free module is not well-defined, so the previous method of computing rank difference in Sec. IV A 1 does not apply. Instead, we use Theorem 3 to check whether $\widetilde{\mathcal{O}}^\dagger$ is spanned by $\text{MGE}(\widetilde{M}_2)$, where \widetilde{M}_2 is defined the same as previous Eq. (62):

$$\widetilde{M}_2 := \begin{bmatrix} \overline{\text{TD}_{m'}(\mathcal{S}_1^\dagger)} \\ \overline{\text{TD}_{m'}(\mathcal{S}_2^\dagger)} \end{bmatrix}. \quad (87)$$

If all local operators \mathcal{O} obtained from the zero rows of $\text{MGE}(\widetilde{M}_1)$ are spanned by $\text{MGE}(\widetilde{M}_2)$, the TO condition is satisfied.

2. Solving the anyon equation

Gaussian elimination in Sec. IV A 2 is replaced by the modified Gaussian elimination in this section. To solve the anyon equation (63), we perform the modified Gaussian elimination on \widetilde{M}_3 :

$$\widetilde{M}_3 = \begin{bmatrix} \overline{\text{TD}_m(\epsilon(\mathcal{X}_1))} \\ \overline{\text{TD}_m(\epsilon(\mathcal{X}_2))} \\ \overline{\text{TD}_m(\epsilon(\mathcal{Z}_1))} \\ \overline{\text{TD}_m(\epsilon(\mathcal{Z}_2))} \\ \overline{\text{TD}_m([(1-x^n), 0])} \\ \overline{\text{TD}_m([0, (1-x^n)])} \end{bmatrix}. \quad (88)$$

Each zero row in the matrix $\text{MGE}(\widetilde{M}_3)$ gives an anyon v in this region:

$$\overline{\epsilon(p_1\mathcal{X}_1 + p_2\mathcal{X}_2 + p_3\mathcal{Z}_1 + p_4\mathcal{Z}_2)} = \overline{[p_5(1-x^n), p_6(1-x^n)]}, \quad (89)$$

where the anyon is $v := [p_5, p_6]$.

3. Equivalence relations between anyons

In this part, we provide an algorithm to categorize anyon types in a Pauli stabilizer model with \mathbb{Z}_d qudits. The equivalence relation of two anyons is defined in Eq. (66). We can use Theorem 3 to check whether $\widetilde{v' - v}$ can be spanned by $\text{MGE}(\widetilde{M}_1)$, with \widetilde{M}_1 defined in Eq. (85). This determines whether v is equivalent to v' .

C. Fusion rules from the Smith normal form

In this section, we discuss how to derive fusion rules of anyons. Assume that we have solved the anyon equation and obtain a list of anyon $V = \{v_1, v_2, v_3, \dots\}$. Many are redundant, and we are looking for the basis anyons.

We consider the following procedure:

1. Start with $M^{(0)} := \text{MGE}(\widetilde{M}_1)$ and $V_{\text{gen}} = \{\}$.
2. Given $M^{(i-1)}$, we use Theorem 3 to check whether v_i is spanned by $M^{(i-1)}$. If v_i is not spanned by $M^{(i-1)}$, we add v_i into V_{gen} and define $M^{(i)}$ as $M^{(i-1)}$ with an extra row v_i joined below. Otherwise, $M^{(i)} := M^{(i-1)}$.
3. Repeat the previous step until running over all anyons in V .

From the construction, it is straightforward to prove that V_{gen} generates all anyons in V . However, V_{gen} can still be redundant. For example, consider the \mathbb{Z}_{12} toric code stabilizer, and assume that we have solved anyons

$$V = \{v_{m^2}, v_{m^4}, v_{e^2m^4}, v_{e^2m^3}, v_e, v_m, v_{e^3}, v_{m^6}\}, \quad (90)$$

where e and m are the basis anyons (still unknown). According to the procedure above, the anyon set V_{gen} is

$$V_{\text{gen}} = \{v_{m^2}, v_{e^2m^4}, v_{m^3}, v_e\}. \quad (91)$$

These anyons are still redundant since we have

$$3v_{m^2} + 2v_{m^3} \sim \mathbf{0}, \quad (92)$$

while both $3v_{m^2}$ and $2v_{m^3}$ are not the trivial anyon $\mathbf{0}$. To completely remove this redundancy, we slightly modify the procedure above. When we add v_i into V_{gen} , we also compute the least multiple of v_i such that it can be spanned by $M^{(i-1)}$ and record this relation. In the example above, we obtain

$$\begin{aligned} 6v_{m^2} &\sim \mathbf{0}, \\ 0v_{m^2} + 6v_{e^2m^4} &\sim \mathbf{0}, \\ 3v_{m^2} + 0v_{e^2m^4} + 2v_{m^3} &\sim \mathbf{0}, \\ 2v_{m^2} - 1v_{e^2m^4} + 0v_{m^3} + 2v_e &\sim \mathbf{0}, \end{aligned} \quad (93)$$

which can be represented as the **relation matrix**

$$M = \begin{array}{c} \begin{array}{cccc} v_{m^2} & v_{e^2m^2} & v_{m^3} & v_e \\ \begin{bmatrix} 6 & 0 & 0 & 0 \\ 0 & 6 & 0 & 0 \\ 3 & 0 & 2 & 0 \\ 2 & -1 & 0 & 2 \end{bmatrix} \end{array} \end{array}. \quad (94)$$

Note that row operations on M do not affect the labels of anyons in the relation matrix, but the column operations on M require the rearrangement of anyon labels on each column. More precisely, adding column k to j in the relation M requires the redefinition of anyons as $v'_j = v_j$ and $v'_k = (-v_j + v_k)$:

$$M_{i,j}v_j + M_{i,k}v_k = (M_{i,j} + M_{i,k})v'_j + M_{i,k}v'_k \quad \forall i. \quad (95)$$

Then, we calculate the Smith normal form (SNF) of M , obtaining the matrices P , Q , and A satisfying $PMQ = A$. For M in Eq. (94), its A and Q are

$$A = \begin{bmatrix} 1 & 0 & 0 & 0 \\ 0 & 1 & 0 & 0 \\ 0 & 0 & 12 & 0 \\ 0 & 0 & 0 & 12 \end{bmatrix}, \quad Q = \begin{bmatrix} 1 & -11 & 42 & -8 \\ 0 & -1 & 4 & -2 \\ 0 & 1 & -3 & 0 \\ 0 & 1 & -4 & 1 \end{bmatrix}, \quad (96)$$

where Q is unimodular, i.e., $\det Q = \pm 1$, and can be used to determine the basis anyons after the rearrangement, following the redefinition of anyons in Eq. (95). The orders of basis anyons correspond to the diagonal elements of matrix A . In this example, we conclude that the fusion rules are $\mathbb{Z}_{12} \times \mathbb{Z}_{12}$ by omitting the trivial anyons of order 1.

D. Topological spins from the T-junction process

Given the polynomial formulation of stabilizers and anyons. The topological spin of anyons can also be determined from the polynomial description of anyons [23]. Given the operators P_x^v and P_y^v that move anyon v along the x - and y -directions, respectively, we can define longer string operators u_1, u_2, u_3 that move anyon v along the x - and y -directions as

$$\begin{aligned} u_1 &= -x^{-n_x}(1 - x^{-n_x} + \dots - x^{-qn_x})P_x^v, \\ u_2 &= (1 - y^{-n_y} + y^{-2n_y} + \dots + y^{-qn_y})P_y^v, \\ u_3 &= (1 - x^{n_x} - x^{2n_x} - \dots - x^{qn_x})P_x^v, \end{aligned} \quad (97)$$

where u_1 and u_3 are the left and right-moving string operators along the x -direction, and u_2 is the string operator that moves anyon v downward along the y -direction. Here n_x, n_y are the minimum stepsizes that move anyon v along the x - and y -directions. Hence, the topological spin of anyon v can be written as

$$\begin{aligned} \theta(v) &= \lim_{q \rightarrow \infty} [u_1, u_2, u_3] \\ &= \lim_{q \rightarrow \infty} ([u_1, u_2] + [u_2, u_3] + [u_3, u_1]), \end{aligned} \quad (98)$$

where $[A, B]$ is the coefficient of x^0y^0 in $A^\dagger \Lambda B$. This process can be regarded as computing the exchange statistics (topological spin) of anyon v by a T-junction [24, 65–68]. Although anyon v is a point-like particle, it still has a finite size. We take the limit $q \rightarrow \infty$ to ensure that the T-junction process gives us the correct statistics.

V. ALGORITHM FOR EXTRACTING TOPOLOGICAL DATA

In previous sections, we discuss how to obtain string operators by solving linear equations and how to obtain linearly-independent anyon set by the (modified) Gaussian elimination over fields or non-PID rings. Armed with those techniques, we can develop an algorithm that extracts topological data from a translation invariant Pauli stabilizer model.

In this section, we describe the algorithm that diagnoses and extracts anyonic statistics from the input translation invariant Pauli stabilizer model, which is written as vectors of polynomials over a $R = \mathbb{Z}_d[x, y, x^{-1}, y^{-1}]$. The output of this algorithm includes the string operators of anyon excitations, their fusion rules, topological spins, and braiding statistics. Note that this algorithm is applicable to nonprime qudit dimensions such as \mathbb{Z}_8 or \mathbb{Z}_9 qudits. This algorithm involves two parts:

1. Solve string operators for all anyon types.
2. Obtain fusion rules and topological spins of anyons from given string operators.

It has four adjustable parameters: the truncation degree k for polynomials (in Eq. (58)), range of the translation duplicate map m (in Eq. (59)), range of the longest string N_x, N_y (will be discussed in this section), the length of extended string operators q (in Eq. (97)).

In Sec. V A, we provide a detailed description of obtaining anyon string operators by solving linear equations. In Sec. V B, we discuss the second part of this algorithm to extract topological spins and braiding statistics.

A. Extracting string operators from translation invariant Pauli stabilizers

A prior step of this algorithm is to check whether the translation invariant Pauli stabilizer code has topological order; if so, this algorithm calculates the anyon string operators. The following steps describe the routine of obtaining anyon string operators and their fusion rules.

- Step 1: Given input $\mathcal{S}_i, i = 1, \dots, t$, a generating set of stabilizers. Error syndromes $\epsilon(\mathcal{X}), \epsilon(\mathcal{Z})$ can be obtained by Eq. (26) for a given set of stabilizers \mathcal{S}_i .
- Step 2: Step 2: Follow the procedure described in Sec. IV B 1.

- Step 3: Repeat the following steps 3-1 to 3-3 for $n_x = 1, \dots, N_x$, $n_y = 1, \dots, N_y$ where N_x, N_y are adjustable parameters that determine the longest string we search. After we sweep from $n_x, n_y = 1$ to $n_x = N_x, n_y = N_y$, we will obtain the numbers of anyons for different choices of n_x, n_y . We will choose the smallest values of n_x, n_y that reach the maximum number of anyons.

- Step 3-1: Use the error syndromes $\epsilon(\mathcal{X}), \epsilon(\mathcal{Z})$ and $(1 - x^{n_x})$ to construct a matrix \widetilde{M}_3 in the form of Eq. (64).
- Step 3-2: Depending on prime or nonprime d , we perform Gaussian elimination or the modified Gaussian elimination in Sec. IV B on the matrix \widetilde{M}_3 . We obtain the relationship between its rows. Hence, we get the coefficients $(\alpha, \beta, \gamma, \delta)$ and anyon v in Eq. (28).
- Step 3-3: We have a set of anyons with redundancy. For example, it includes an anyon spanned by others (up to syndromes of local Pauli operators.). To obtain the most compact form of anyons, we would like to keep the basis anyons and exclude others, following the procedure in Sec. IV C. We first use the matrix \widetilde{M}_1 formed by the error syndromes. For the matrix \widetilde{M}_1 over \mathbb{Z}_d , when d is prime, we sequentially insert anyon row vectors into the matrix one by one and check the rank of the matrix after insertion (or use Theorem 3 for nonprime d). If the rank of the matrix is unchanged after adding the new anyon (or the anyon is spanned by the matrix), then this newly added anyon is generated by the existing anyons. We do not keep this anyon and continue with the next one. Finally, we compute the Smith normal form of the anyon relation matrix to obtain the basis anyons and their fusion rules.¹⁴

- Step 4: Using the coefficients of the error syndrome polynomials in Eq. (28), we can obtain the string operators in the x -direction. More explicitly, from a solution of the equation

$$(1 - x^{n_x})v = p_1(x, y)\epsilon(\mathcal{X}_1) + p_2(x, y)\epsilon(\mathcal{X}_2) + p_3(x, y)\epsilon(\mathcal{Z}_1) + p_4(x, y)\epsilon(\mathcal{Z}_2), \quad (99)$$

the string operator P_x is obtained as

$$P_x = \begin{bmatrix} p_1(x, y) \\ p_2(x, y) \\ p_3(x, y) \\ p_4(x, y) \end{bmatrix}. \quad (100)$$

- Step 5: From anyon v solved in the x -direction, we utilize the matrix MGE(\widetilde{M}_1) (modified Gaussian elimination of \widetilde{M}_1 in Eq. (85)) and Theorem 3 to solve the anyon equation in the $-y$ -direction:

$$(1 - y^{-n_y})v = p_5(x, y)\epsilon(\mathcal{X}_1) + p_6(x, y)\epsilon(\mathcal{X}_2) + p_7(x, y)\epsilon(\mathcal{Z}_1) + p_8(x, y)\epsilon(\mathcal{Z}_2). \quad (101)$$

From this solution, we obtain the string operator P_y in the $-y$ -direction

$$P_y = \begin{bmatrix} p_5(x, y) \\ p_6(x, y) \\ p_7(x, y) \\ p_8(x, y) \end{bmatrix}. \quad (102)$$

The P_x and P_y are shown in the part (a) of Fig. 9.

Now, we have obtained the string operators of the basis anyons.

B. Extracting topological spins of anyons

In Sec. V A, we have demonstrated how to extract anyon string operators by solving the anyon equation (28), we can obtain the string operators of all anyons, labeled P_x^i and P_y^i , which represent the string operator of the i -th anyon in the x -direction and $-y$ -direction, respectively. To obtain the topological spin between all anyons, we perform the following steps:

1. Obtain the topological spin θ for each basis anyon by using the T-junction process in Sec. IV D.
2. Construct the string operator for anyon $v_i \times v_j$ where v_i and v_j are basis anyons. For example, for anyon v_1 and anyon v_2 , we first construct string operators that move $v_1 \times v_2$ in the x - and $-y$ -directions of anyon $v_1 \times v_2$ as $P_x^{v_1 \times v_2} = P_x^{v_2} P_x^{v_1}$ and $P_y^{v_1 \times v_2} = P_y^{v_2} P_y^{v_1}$. Then, we substitute $P_x^{v_1 \times v_2}$ and $P_y^{v_1 \times v_2}$ in Eq. (97) to obtain long string operators U_1, U_2, U_3 . Because anyon $v_1 \times v_2$ may have non-negligible size, we use the extended string operators U_1, U_2, U_3 as shown in Fig. 9 such that the braiding process is unaffected by the size of anyons. We have extended the length of string operators in x - and y -directions to q -times of the original length.
3. Finally, we can calculate the topological spin of anyon $v_1 \times v_2$

$$\begin{aligned} \theta(v_1 v_2) &= [U_1, U_2, U_3] \\ &= [U_1, U_2] + [U_2, U_3] + [U_3, U_1]. \end{aligned} \quad (103)$$

Using the fact that $B(v_1, v_2) = \frac{\theta(v_1 \times v_2)}{\theta(v_1)\theta(v_2)}$ (see Appendix A), we can obtain the mutual braiding $B(v_1, v_2)$ between v_1 and v_2 .

¹⁴ Since calculating the Smith normal form for a large matrix is challenging, in practice, we can first repeat the procedure for prime-dimensional qudits to refine the anyons, and further calculate the Smith normal form.

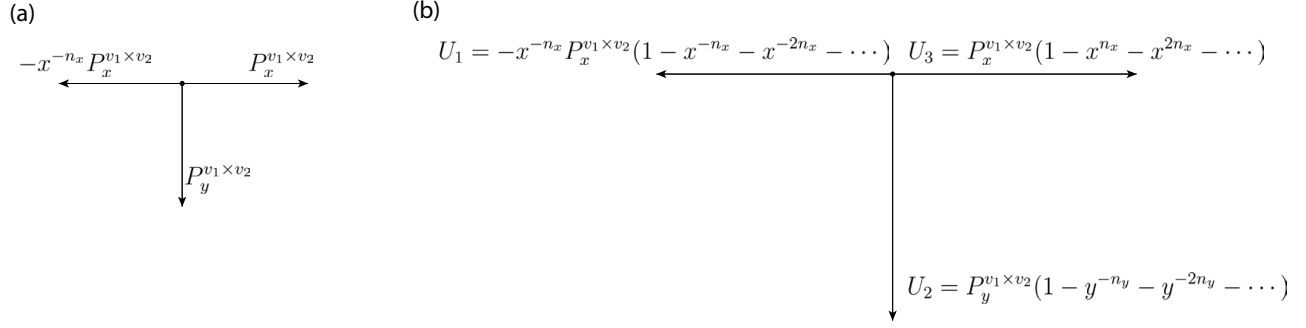


FIG. 9. (a) The T-junction process for short string operators. Anyon $v_1 \times v_2$ is the composite of two anyons v_1 and v_2 , which might have a finite size larger than the short string, so the process might fail to detect the correct statistics of $v_1 \times v_2$. (b) To avoid the size effect of anyon $v_1 \times v_2$, we extend P_x and P_y to the long string operators U_1, U_2, U_3 , which is q times longer.

	v_1	v_2	v_3	v_4	\dots
v_1	$\theta(v_1)$	$B(v_1, v_2)$	$B(v_1, v_3)$	$B(v_1, v_4)$	\dots
v_2	$B(v_2, v_1)$	$\theta(v_2)$	$B(v_2, v_3)$	$B(v_2, v_4)$	\dots
v_3	$B(v_3, v_1)$	$B(v_3, v_2)$	$\theta(v_3)$	$B(v_3, v_4)$	\dots
v_4	$B(v_4, v_1)$	$B(v_4, v_2)$	$B(v_4, v_3)$	$\theta(v_4)$	\dots
\vdots	\vdots	\vdots	\vdots	\vdots	\ddots

TABLE I. Topological spins and braiding statistics of basis anyons $\{v_1, v_2, v_3, v_4, \dots\}$.

C. Rearranging the basis anyons

This section demonstrates a method that rearranges the basis anyons of a \mathbb{Z}_p (prime p) Pauli stabilizer code to decoupled $\{e, m\}$ pairs in finite copies of \mathbb{Z}_p toric codes. For example, the regular color code is two copies of \mathbb{Z}_2 toric codes, and we aim to find the decoupled pairs $\{e_1, m_1\}$ and $\{e_2, m_2\}$ from the basis anyons we found. The procedure is as follows

1. Start from the entire anyon set \mathcal{V} and compute all topological spins. We search for a nontrivial boson b , where the existence of a nontrivial boson is proved in Ref. [24]. The order of b must be p .
2. We find another anyon c such that

$$B(b, c) = \exp\left(\frac{2\pi i}{p}\right). \quad (104)$$

The existence of such c is proved in Ref. [75]. WLOG, we can assume c to be a boson. If c is not a boson, we can always find a $c' = c \times b^\#$ to be a boson that has the same braiding with b .

3. Start from $\{b, c\}$ and follow the procedure in Sec. IV C to obtain the basis anyons set:

$$V_{\text{basis}} = \{b, c, v_1, v_2, v_3, \dots\}. \quad (105)$$

WLOG, we can assume that all v_j has no braiding with b since we can always redefine $v_j \rightarrow v_j \times c^\#$. Similarly, we can assume that all v_j has no braiding

with c by redefining $v_j \rightarrow v_j \times b^\#$. Therefore, $\{b, c\}$ are completely decoupled from the remaining basis anyons, denoted as $\{e_1, m_1\}$.

4. Consider a new set of anyons generated by $\{v_1, v_2, v_3, \dots\}$. Repeat the above steps to obtain $\{e_1, m_1\}$ decoupled from the remaining basis anyons. Continue until all $\{e, m\}$ pairs are found.

After the rearrangement of the basis anyons, the table of topological spins and braiding statistics, defined in Table I, has the specific form:

	e_1	m_1	e_2	m_2	e_3	m_3	\dots
e_1	1	-1	1	1	1	1	\dots
m_1	-1	1	1	1	1	1	\dots
e_2	1	1	1	-1	1	1	\dots
m_2	1	1	-1	1	1	1	\dots
e_3	1	1	1	1	1	-1	\dots
m_3	1	1	1	1	-1	1	\dots
\vdots	\ddots						

(106)

VI. APPLICATIONS ON VARIOUS QUANTUM CODES

In this section, we apply the algorithm to various quantum codes to test the TO condition and extract their topological data (if there exist). We start from the modified color codes in Sec. VIA, which are self-dual CSS codes on \mathbb{Z}_2 qubits. According to Ref. [23], they can be decomposed into finite copies of \mathbb{Z}_2 toric codes. Our algorithm confirms this and finds the $\{e, m\}$ pairs in the decoupled copies of the \mathbb{Z}_2 toric codes. In Sec. VIB, we investigate anyons of CSS codes on \mathbb{Z}_4 qudits mapped from the double semion code [76]. We confirm the conjecture in Ref. [76] that this code is two copies of \mathbb{Z}_2 toric code and find the decoupled $\{e, m\}$ pairs. In Sec. VIC, we investigate a model called the six-semion code defined on $\mathbb{Z}_4 \times \mathbb{Z}_4$ qudits whose basis anyons are v_1 and v_2 with topological spin $-i$ that indicates that v_1 and v_2 are (anti-)semions. The mutual braiding between them

gives the i phase. The topological orders detected for these examples are summarized in Table. II.

A. Modified color code

We construct six examples of self-dual CSS codes on the 2d honeycomb lattice, denoted as modified color codes. Their stabilizer terms are shown in Fig. 1. Al-

though Ref. [23] has shown that all the 2d translation invariant Pauli stabilizer models for prime-dimensional qudits can be decomposed into finite copies of toric codes, we do not have prior knowledge about the number of copies of toric codes that these modified color codes can be decomposed to. We use these modified color codes as a showcase to demonstrate the effectiveness of our algorithm in determining the topological data. For examples that satisfy the TO condition, the algorithm finds string operators, fusion rules, topological spins, and braiding statistics of anyons.

The stabilizers and syndromes of those six examples are

$$\mathcal{S}_1^{\textcircled{1}} = \begin{bmatrix} 1 + \bar{x} + y \\ 1 + \bar{y} + x \\ 0 \\ 0 \end{bmatrix}, \quad \mathcal{S}_2^{\textcircled{1}} = \begin{bmatrix} 0 \\ 0 \\ 1 + \bar{x} + y \\ 1 + \bar{y} + x \end{bmatrix}, \quad (107)$$

$$\begin{aligned} \epsilon(\mathcal{X}_1)^{\textcircled{1}} &= [0, 1 + x + \bar{y}], & \epsilon(\mathcal{X}_2)^{\textcircled{1}} &= [0, 1 + y + \bar{x}], \\ \epsilon(\mathcal{Z}_1)^{\textcircled{1}} &= [1 + x + \bar{y}, 0], & \epsilon(\mathcal{Z}_2)^{\textcircled{1}} &= [1 + y + \bar{x}, 0], \end{aligned} \quad (108)$$

$$\mathcal{S}_1^{\textcircled{2}} = \begin{bmatrix} 1 + \bar{x} + y + \bar{x}\bar{y} \\ 1 + \bar{y} + x + x\bar{y} \\ 0 \\ 0 \end{bmatrix}, \quad \mathcal{S}_2^{\textcircled{2}} = \begin{bmatrix} 0 \\ 0 \\ 1 + \bar{x} + y + \bar{x}\bar{y} \\ 1 + \bar{y} + x + x\bar{y} \end{bmatrix}, \quad (109)$$

$$\begin{aligned} \epsilon(\mathcal{X}_1)^{\textcircled{2}} &= [0, 1 + x + \bar{y} + x\bar{y}], & \epsilon(\mathcal{X}_2)^{\textcircled{2}} &= [0, 1 + y + \bar{x} + \bar{x}\bar{y}], \\ \epsilon(\mathcal{Z}_1)^{\textcircled{2}} &= [1 + x + \bar{y} + x\bar{y}, 0], & \epsilon(\mathcal{Z}_2)^{\textcircled{2}} &= [1 + y + \bar{x} + \bar{x}\bar{y}, 0], \end{aligned} \quad (110)$$

$$\mathcal{S}_1^{\textcircled{3}} = \begin{bmatrix} 1 + \bar{x} + y + \bar{x}\bar{y} + xy \\ 1 + \bar{y} + x + \bar{x}\bar{y} + xy \\ 0 \\ 0 \end{bmatrix}, \quad \mathcal{S}_2^{\textcircled{3}} = \begin{bmatrix} 0 \\ 0 \\ 1 + \bar{x} + y + \bar{x}\bar{y} + xy \\ 1 + \bar{y} + x + \bar{x}\bar{y} + xy \end{bmatrix}, \quad (111)$$

$$\begin{aligned} \epsilon(\mathcal{X}_1)^{\textcircled{3}} &= [0, 1 + x + \bar{y} + xy + \bar{x}\bar{y}], & \epsilon(\mathcal{X}_2)^{\textcircled{3}} &= [0, 1 + y + \bar{x} + xy + \bar{x}\bar{y}], \\ \epsilon(\mathcal{Z}_1)^{\textcircled{3}} &= [1 + x + \bar{y} + xy + \bar{x}\bar{y}, 0], & \epsilon(\mathcal{Z}_2)^{\textcircled{3}} &= [1 + y + \bar{x} + xy + \bar{x}\bar{y}, 0], \end{aligned} \quad (112)$$

$$\mathcal{S}_1^{\textcircled{4}} = \begin{bmatrix} 1 + \bar{x} + y + \bar{x}\bar{y} + xy + \bar{x}\bar{y} \\ 1 + \bar{y} + x + \bar{x}\bar{y} + xy + \bar{x}\bar{y} \\ 0 \\ 0 \end{bmatrix}, \quad \mathcal{S}_2^{\textcircled{4}} = \begin{bmatrix} 0 \\ 0 \\ 1 + \bar{x} + y + \bar{x}\bar{y} + xy + \bar{x}\bar{y} \\ 1 + \bar{y} + x + \bar{x}\bar{y} + xy + \bar{x}\bar{y} \end{bmatrix}, \quad (113)$$

$$\begin{aligned} \epsilon(\mathcal{X}_1)^{\textcircled{4}} &= [0, 1 + x + \bar{y} + xy + \bar{x}\bar{y} + \bar{x}\bar{y}], & \epsilon(\mathcal{X}_2)^{\textcircled{4}} &= [0, 1 + y + \bar{x} + xy + \bar{x}\bar{y} + \bar{x}\bar{y}], \\ \epsilon(\mathcal{Z}_1)^{\textcircled{4}} &= [1 + x + \bar{y} + xy + \bar{x}\bar{y} + \bar{x}\bar{y}, 0], & \epsilon(\mathcal{Z}_2)^{\textcircled{4}} &= [1 + y + \bar{x} + xy + \bar{x}\bar{y} + \bar{x}\bar{y}, 0], \end{aligned} \quad (114)$$

model	Topological order
Regular color code (example ①)	Two copies of \mathbb{Z}_2 toric codes
Example ②	TO condition failed
Modified color code A (example ③)	Four copies of \mathbb{Z}_2 toric codes
Modified color code B (example ④)	Eight copies of \mathbb{Z}_2 toric codes
Modified color code C (example ⑤)	Four copies of \mathbb{Z}_2 toric codes
Modified color code D (example ⑥)	Six copies of \mathbb{Z}_2 toric codes
\mathbb{Z}_4 CSS code induced from double semion	Two copies of \mathbb{Z}_2 toric codes
Double semion code with \mathbb{Z}_4 qudits	Double semion topological order
Six-semion code with $\mathbb{Z}_4 \times \mathbb{Z}_4$ qudits	Six-semion topological order

TABLE II. The topological orders of various examples in Fig. 1 and, obtained from the algorithm described in Sec. V. Here, we check the regular color code and double semion code with \mathbb{Z}_4 qudits (details in Appendix. C), which serve as sanity checks.

$$\mathcal{S}_1^{⑤} = \begin{bmatrix} 1 + \bar{x} + y + y^2 \\ 1 + \bar{y} + x + \bar{y}^2 \\ 0 \\ 0 \end{bmatrix}, \quad \mathcal{S}_2^{⑤} = \begin{bmatrix} 0 \\ 0 \\ 1 + \bar{x} + y + y^2 \\ 1 + \bar{y} + x + \bar{y}^2 \end{bmatrix}, \quad (115)$$

$$\begin{aligned} \epsilon(\mathcal{X}_1)^{⑤} &= [0, 1 + x + \bar{y} + \bar{y}^2], & \epsilon(\mathcal{X}_2)^{⑤} &= [0, 1 + y + \bar{x} + y^2], \\ \epsilon(\mathcal{Z}_1)^{⑤} &= [1 + x + \bar{y} + \bar{y}^2, 0], & \epsilon(\mathcal{Z}_2)^{⑤} &= [1 + y + \bar{x} + y^2, 0], \end{aligned} \quad (116)$$

$$\mathcal{S}_1^{⑥} = \begin{bmatrix} 1 + \bar{x} + y + xy^3 \\ 1 + \bar{y} + x + \bar{xy}^3 \\ 0 \\ 0 \end{bmatrix}, \quad \mathcal{S}_2^{⑥} = \begin{bmatrix} 0 \\ 0 \\ 1 + \bar{x} + y + xy^3 \\ 1 + \bar{y} + x + \bar{xy}^3 \end{bmatrix}, \quad (117)$$

$$\begin{aligned} \epsilon(\mathcal{X}_1)^{⑥} &= [0, 1 + x + \bar{y} + \bar{xy}^3], & \epsilon(\mathcal{X}_2)^{⑥} &= [0, 1 + y + \bar{x} + xy^3], \\ \epsilon(\mathcal{Z}_1)^{⑥} &= [1 + x + \bar{y} + \bar{xy}^3, 0], & \epsilon(\mathcal{Z}_2)^{⑥} &= [1 + y + \bar{x} + xy^3, 0]. \end{aligned} \quad (118)$$

Input above stabilizer and syndrome polynomials into the algorithm, we found that example ② is not a topological order while the rest of the examples are topological orders. For examples that satisfy topological order conditions, the algorithm provides the string operators of basis anyons, with pictorial descriptions shown in Appendix. C. The algorithm then performs the T-junction calculation and obtains the topological spins and braiding statistics for the examples ①, ③, ④, ⑤, ⑥ that are shown in Table. III, IV, V, VI, VII, respectively.

These tables show that basis anyons can be decomposed into $\{e, m\}$ pairs in finite copies of \mathbb{Z}_2 toric codes for the modified color codes with topological orders. This matches the theorem that 2d \mathbb{Z}_2 topological Pauli stabilizer codes can always be decomposed to copies of \mathbb{Z}_2 toric codes.

	v_1	v_2	v_3	v_4
v_1	1	-1	1	1
v_2	-1	1	1	1
v_3	1	1	1	-1
v_4	1	1	-1	1

TABLE III. Topological spins and braiding statistics of anyons for the regular color code (example ①). We can see this table is formed by two decoupled copies of toric code, where $\{v_1, v_2\}$ and $\{v_3, v_4\}$ correspond to $\{e_1, m_1\}$ and $\{e_2, m_2\}$ of two copies of toric code.

B. CSS codes induced from double semion

In Sec. VI A, we have shown that our algorithm gives us the expected result for 2d \mathbb{Z}_2 topological codes whose local dimension is a prime integer. In this subsection, we investigate a more challenging case that is a topological

	v_1	v_2	v_3	v_4	v_5	v_6	v_7	v_8
v_1	1	1	1	1	1	1	1	-1
v_2	1	1	1	-1	1	1	1	1
v_3	1	1	1	1	1	-1	1	1
v_4	1	-1	1	1	1	1	1	1
v_5	1	1	1	1	1	1	-1	1
v_6	1	1	-1	1	1	1	1	1
v_7	1	1	1	1	-1	1	1	1
v_8	-1	1	1	1	1	1	1	1

TABLE IV. Topological spins and braiding statistics of anyons for the modified color code A (example ③). We can see this table is formed by four copies of decoupled toric code, where $\{v_1, v_8\}, \{v_2, v_4\}, \{v_3, v_6\}, \{v_5, v_7\}$ correspond to the $\{e, m\}$ pairs in the four copies of toric codes.

	v_1	v_2	v_3	v_4	v_5	v_6	v_7	v_8
v_1	1	1	1	-1	1	1	1	1
v_2	1	1	1	1	1	-1	1	1
v_3	1	1	1	1	1	1	-1	1
v_4	-1	1	1	1	1	1	1	1
v_5	1	1	1	1	1	1	1	-1
v_6	1	-1	1	1	1	1	1	1
v_7	1	1	-1	1	1	1	1	1
v_8	1	1	1	1	-1	1	1	1

TABLE VI. Topological spins and braiding statistics of anyons for the modified color code C (example ⑤). We can see this table is formed by four copies of decoupled toric code, where $\{v_1, v_4\}, \{v_2, v_6\}, \{v_3, v_7\}, \{v_5, v_8\}$ correspond to the $\{e, m\}$ pairs in the four copies of toric codes.

	v_1	v_2	v_3	v_4	v_5	v_6	v_7	v_8	v_9	v_{10}	v_{11}	v_{12}	v_{13}	v_{14}	v_{15}	v_{16}
v_1	1	1	1	1	1	1	1	1	-1	1	1	1	1	1	1	1
v_2	1	1	1	1	1	1	1	1	1	1	-1	1	1	1	1	1
v_3	1	1	1	1	1	1	1	1	1	1	1	1	-1	1	1	1
v_4	1	1	1	1	1	1	1	1	1	1	1	-1	1	1	1	1
v_5	1	1	1	1	1	1	1	1	1	1	1	1	1	-1	1	1
v_6	1	1	1	1	1	1	1	1	1	-1	1	1	1	1	1	1
v_7	1	1	1	1	1	1	1	1	1	1	1	1	1	1	-1	1
v_8	1	1	1	1	1	1	1	1	1	1	1	1	1	1	1	-1
v_9	-1	1	1	1	1	1	1	1	1	1	1	1	1	1	1	1
v_{10}	1	1	1	1	1	-1	1	1	1	1	1	1	1	1	1	1
v_{11}	1	-1	1	1	1	1	1	1	1	1	1	1	1	1	1	1
v_{12}	1	1	1	-1	1	1	1	1	1	1	1	1	1	1	1	1
v_{13}	1	1	-1	1	1	1	1	1	1	1	1	1	1	1	1	1
v_{14}	1	1	1	1	-1	1	1	1	1	1	1	1	1	1	1	1
v_{15}	1	1	1	1	1	1	-1	1	1	1	1	1	1	1	1	1
v_{16}	1	1	1	1	1	1	1	-1	1	1	1	1	1	1	1	1

TABLE V. Topological spins and braiding statistics of anyons for the modified color code B (example ④). We can see this table is formed by four copies of decoupled toric code, where $\{v_1, v_9\}, \{v_2, v_{11}\}, \{v_3, v_{13}\}, \{v_4, v_{12}\}, \{v_5, v_{14}\}, \{v_6, v_{10}\}, \{v_7, v_{15}\}, \{v_8, v_{16}\}$ correspond to the $\{e, m\}$ pairs in the eight copies of toric codes.

Pauli stabilizer code defined on nonprime-dimensional qudits and show their capability of finding the anyons for a topological Pauli stabilizer code with nonprime qudits.

There is a recent paper [76] discussing the mapping between qudit Pauli stabilizer codes to CSS codes. The authors map the double-semion Pauli stabilizer code that is a non-CSS code on \mathbb{Z}_4 qudits to a CSS code by doubling the number of qudits. This code was conjectured to be equivalent to two copies of \mathbb{Z}_2 toric codes. Our algorithm confirms the conjecture.

	v_1	v_2	v_3	v_4	v_5	v_6	v_7	v_8	v_9	v_{10}	v_{11}	v_{12}
v_1	1	1	1	-1	1	1	1	1	1	1	1	1
v_2	1	1	1	1	1	1	1	1	-1	1	1	1
v_3	1	1	1	1	1	1	-1	1	1	1	1	1
v_4	-1	1	1	1	1	1	1	1	1	1	1	1
v_5	1	1	1	1	1	1	1	1	1	-1	1	1
v_6	1	1	1	1	1	1	1	1	1	1	-1	1
v_7	1	1	-1	1	1	1	1	1	1	1	1	1
v_8	1	1	1	1	1	1	1	1	1	1	1	-1
v_9	1	-1	1	1	1	1	1	1	1	1	1	1
v_{10}	1	1	1	1	-1	1	1	1	1	1	1	1
v_{11}	1	1	1	1	1	-1	1	1	1	1	1	1
v_{12}	1	1	1	1	1	1	1	-1	1	1	1	1

TABLE VII. Topological spins and braiding statistics of anyons for the modified color code D (example ⑥). We can see this table is formed by four copies of decoupled toric code, where $\{v_1, v_4\}, \{v_2, v_9\}, \{v_3, v_7\}, \{v_5, v_{10}\}, \{v_6, v_{11}\}, \{v_8, v_{12}\}$ correspond to the $\{e, m\}$ pairs in the six copies of toric codes.

The stabilizers of this CSS code are

$$\begin{aligned}
\mathcal{S}_1 &= - \begin{array}{c} \begin{array}{|c|} \hline X \\ \hline \end{array} \\ \begin{array}{|c|} \hline X_1 X_2 \\ \hline \end{array} \\ \begin{array}{|c|} \hline v \\ \hline \end{array} \\ \begin{array}{|c|} \hline X_1^\dagger X_2^\dagger \\ \hline \end{array} \\ \begin{array}{|c|} \hline X_2^\dagger \\ \hline \end{array} \end{array}, \quad \mathcal{S}_2 = \begin{array}{|c|} \hline X_1^2 \\ \hline p \\ \hline X_1^2 \\ \hline \end{array}, \\
\mathcal{S}_3 &= \begin{array}{|c|} \hline X_2^2 \\ \hline -X_1^2 \\ \hline \end{array}, \quad \mathcal{S}_4 = \begin{array}{|c|} \hline X_2^2 \\ \hline X_1^2 \\ \hline \end{array}. \\
\mathcal{S}_5 &= - \begin{array}{c} \begin{array}{|c|} \hline Z_2 \\ \hline \end{array} \\ \begin{array}{|c|} \hline Z_1^\dagger Z_2^\dagger \\ \hline \end{array} \\ \begin{array}{|c|} \hline v \\ \hline \end{array} \\ \begin{array}{|c|} \hline Z_1^\dagger Z_2^\dagger \\ \hline \end{array} \\ \begin{array}{|c|} \hline Z_1 \\ \hline \end{array} \end{array}, \quad \mathcal{S}_6 = \begin{array}{|c|} \hline Z_2^2 \\ \hline p \\ \hline Z_2^2 \\ \hline \end{array}, \\
\mathcal{S}_7 &= \begin{array}{|c|} \hline Z_1^2 \\ \hline -Z_2^2 \\ \hline \end{array}, \quad \mathcal{S}_8 = \begin{array}{|c|} \hline Z_1^2 \\ \hline Z_2^2 \\ \hline \end{array}.
\end{aligned} \tag{119}$$

In Eq. (119), we assign two \mathbb{Z}_4 qudits on each edge whose Pauli matrices are colored blue and red, respectively.

We utilize our algorithm to investigate the anyons in the CSS code and find anyon string operators, fusion rules, topological spins, and braiding statistics. The topological spins and braiding statistics of the basis anyons are shown in Table. VIII, which shows there are two decoupled $\{e, m\}$ pairs: $\{v_1, v_3\}$ and $\{v_2, v_4\}$. Moreover, $2v_1 \sim 2v_2 \sim 2v_3 \sim 2v_4 \sim \mathbf{0}$ indicates that all basis anyons have order 2. Hence, this model is two copies of \mathbb{Z}_2 toric codes.

	v_1	v_2	v_3	v_4
v_1	1	1	-1	1
v_2	1	1	1	-1
v_3	-1	1	1	1
v_4	1	-1	1	1

TABLE VIII. Topological spins and braiding statistics of anyons for the CSS codes induced from double semion code. We can see this table is formed by two decoupled copies of toric code, where $\{v_1, v_3\}$ and $\{v_2, v_4\}$ correspond to $\{e_1, m_1\}$ and $\{e_2, m_2\}$ in the two copies of toric codes.

C. Six-semion stabilizer code

The six-semion stabilizer code has stabilizers

$$\begin{aligned}
\mathcal{S}_1 &= - \begin{array}{c} \begin{array}{|c|} \hline Z_1^\dagger \\ \hline \end{array} \\ \begin{array}{|c|} \hline X_1^\dagger Z_1^\dagger X_2^\dagger \\ \hline \end{array} \\ \begin{array}{|c|} \hline v \\ \hline \end{array} \\ \begin{array}{|c|} \hline X_1^\dagger Z_1^\dagger X_2^\dagger \\ \hline \end{array} \\ \begin{array}{|c|} \hline X_1 X_2 \\ \hline \end{array} \end{array}, \quad \mathcal{S}_2 = \begin{array}{|c|} \hline Z_1^2 \\ \hline p \\ \hline Z_1^2 \\ \hline \end{array}, \\
\mathcal{S}_3 &= - \begin{array}{c} \begin{array}{|c|} \hline Z_2^\dagger \\ \hline \end{array} \\ \begin{array}{|c|} \hline X_2^\dagger Z_2^\dagger \\ \hline \end{array} \\ \begin{array}{|c|} \hline v \\ \hline \end{array} \\ \begin{array}{|c|} \hline X_2^\dagger Z_2^\dagger \\ \hline \end{array} \\ \begin{array}{|c|} \hline X_2 \\ \hline \end{array} \end{array}, \quad \mathcal{S}_4 = \begin{array}{|c|} \hline Z_2^2 \\ \hline p \\ \hline Z_2^2 \\ \hline \end{array}, \\
\mathcal{S}_5 &= \begin{array}{|c|} \hline X_1^2 \\ \hline -Z_1^2 \\ \hline \end{array}, \quad \mathcal{S}_6 = \begin{array}{|c|} \hline X_1^2 \\ \hline Z_1^2 \\ \hline \end{array}, \\
\mathcal{S}_7 &= \begin{array}{|c|} \hline X_2^2 \\ \hline -Z_1^2 Z_2^2 \\ \hline \end{array}, \quad \mathcal{S}_8 = \begin{array}{|c|} \hline X_2^2 \\ \hline Z_1^2 Z_2^2 \\ \hline \end{array}.
\end{aligned} \tag{120}$$

This model can be regarded as condensing $e_1^2 m_1^2$ and $e_1^2 e_2^2 m_2^2$ anyons in two copies of \mathbb{Z}_4 toric codes [19]. The $\mathcal{S}_5, \mathcal{S}_6, \mathcal{S}_7, \mathcal{S}_8$ are the condensing terms. The first four terms of Eq. (120) come from the stabilizer group of two copies of \mathbb{Z}_4 toric code. The anyon theory of this model includes four bosons, six semions, and six anti-semions.

We use the algorithm discussed in Sec. V to analyze this model and find the basis anyons v_1 and v_2 . The topological spins and braiding statistics of them are shown in Table. IX. The fusion rules are $4v_1 \sim 4v_2 \sim \mathbf{0}$, indicating that both have order 4.

	v_1	v_2
v_1	-i	i
v_2	i	-i

TABLE IX. Topological spins and braiding statistics of basis anyons in the six-semion code. The mutual braiding between v_1 and v_2 gives the i phase, indicating that v_1 and v_2 are semions.

ACKNOWLEDGMENT

We thank Nathanan Tantivasadakarn and Victor V. Albert for their helpful discussions and for providing the CSS code example. YC thanks Tyler Ellison, Nathanan Tantivasadakarn, and Bowen Yang for teaching the polynomial method, for useful feedback on this manuscript, and for clarifying anyons in stabilizer/subsystem codes.

YC thanks Hsin-Po Wang for pointing out the truncation of the Laurent polynomials. YC thanks Yun-Ting Cheng for technical support. Y.X. thanks the organizers and participants of the YIPQS long-term workshop YITP-T-23-01 “Quantum Information, Quantum Matter and Quantum Gravity (2023),” held at Yukawa Institute for Theoretical Physics in Kyoto University, where part of this work was completed. Y.X. was partially supported by ARO Grant No. W911NF-15-1-0397, National

Science Foundation QLCI Grant No. OMA2120757, AFOSR-MURI Grant No. FA9550-19-1-0399, and Department of Energy QSA program. JTI thanks the Joint Quantum Institute at the University of Maryland for support through a JQI fellowship. Y.X. thanks Yujie Zhang and Shan-Ming Ruan for their hospitality in Tokyo and Kyoto. Y.X. thanks Zhiwei Zhang, Honggeng Zhang, Xuan Su, Qionsi Yan, and Bo He for their mental support.

-
- [1] Xie Chen, Zheng-Cheng Gu, and Xiao-Gang Wen, “Complete classification of one-dimensional gapped quantum phases in interacting spin systems,” *Phys. Rev. B* **84**, 235128 (2011).
- [2] Michael Levin and Zheng-Cheng Gu, “Braiding statistics approach to symmetry-protected topological phases,” *Phys. Rev. B* **86**, 115109 (2012).
- [3] Xie Chen, Zheng-Cheng Gu, Zheng-Xin Liu, and Xiao-Gang Wen, “Symmetry-protected topological orders in interacting bosonic systems,” *Science* **338**, 1604–1606 (2012).
- [4] Zheng-Cheng Gu and Michael Levin, “Effect of interactions on two-dimensional fermionic symmetry-protected topological phases with $z=2$ symmetry,” *Physical Review B* **89**, 201113 (2014).
- [5] Beni Yoshida, “Topological phases with generalized global symmetries,” *Physical Review B* **93**, 155131 (2016).
- [6] Anton Kapustin and Ryan Thorngren, “Higher symmetry and gapped phases of gauge theories,” in *Algebra, Geometry, and Physics in the 21st Century: Kontsevich Festschrift*, edited by Denis Auroux, Ludmil Katzarkov, Tony Pantev, Yan Soibelman, and Yuri Tschinkel (Springer International Publishing, Cham, 2017) pp. 177–202.
- [7] Tian Lan, Liang Kong, and Xiao-Gang Wen, “Classification of $(3+1)$ D bosonic topological orders: The case when pointlike excitations are all bosons,” *Phys. Rev. X* **8**, 021074 (2018).
- [8] Tian Lan and Xiao-Gang Wen, “Classification of $3+1$ D bosonic topological orders (ii): The case when some pointlike excitations are fermions,” *Phys. Rev. X* **9**, 021005 (2019).
- [9] Theo Johnson-Freyd, “On the classification of topological orders,” *Communications in Mathematical Physics* **393**, 989–1033 (2022).
- [10] Yu-An Chen and Po-Shen Hsin, “Exactly solvable lattice hamiltonians and gravitational anomalies,” *SciPost Physics* **14**, 089 (2023).
- [11] Sergey B Bravyi and A Yu Kitaev, “Quantum codes on a lattice with boundary,” arXiv preprint quant-ph/9811052 (1998).
- [12] Eric Dennis, Alexei Kitaev, Andrew Landahl, and John Preskill, “Topological quantum memory,” *Journal of Mathematical Physics* **43**, 4452–4505 (2002).
- [13] A Yu Kitaev, “Fault-tolerant quantum computation by anyons,” *Annals of physics* **303**, 2–30 (2003).
- [14] Alexei Kitaev, “Anyons in an exactly solved model and beyond,” *Annals of Physics* **321**, 2–111 (2006).
- [15] Hector Bombin and Miguel Angel Martin-Delgado, “Topological quantum distillation,” *Physical review letters* **97**, 180501 (2006).
- [16] Héctor Bombín, “Gauge color codes: optimal transversal gates and gauge fixing in topological stabilizer codes,” *New Journal of Physics* **17**, 083002 (2015).
- [17] Sergey Bravyi, Barbara M Terhal, and Bernhard Leemhuis, “Majorana fermion codes,” *New Journal of Physics* **12**, 083039 (2010).
- [18] Sagar Vijay, Timothy H Hsieh, and Liang Fu, “Majorana fermion surface code for universal quantum computation,” *Physical Review X* **5**, 041038 (2015).
- [19] Tyler D. Ellison, Yu-An Chen, Arpit Dua, Wilbur Shirley, Nathanan Tantivasadakarn, and Dominic J. Williamson, “Pauli stabilizer models of twisted quantum doubles,” *PRX Quantum* **3**, 010353 (2022).
- [20] Héctor Bombín, “Structure of 2d topological stabilizer codes,” *Communications in Mathematical Physics* **327**, 387–432 (2014).
- [21] Jürg Fröhlich and Fabrizio Gabbiani, “Braid statistics in local quantum theory,” *Reviews in Mathematical Physics* **2**, 251–353 (1990).
- [22] Karl-Henning Rehren, “Braid group statistics and their superselection rules,” *The algebraic theory of superselection sectors*. Palermo , 333–355 (1989).
- [23] Jeongwan Haah, “Classification of translation invariant topological pauli stabilizer codes for prime dimensional qudits on two-dimensional lattices,” *Journal of Mathematical Physics* **62** (2021).
- [24] Jeongwan Haah, Lukasz Fidkowski, and Matthew B. Hastings, “Nontrivial quantum cellular automata in higher dimensions,” *Communications in Mathematical Physics* **398**, 469–540 (2023).
- [25] Dolev Bluvstein, Harry Levine, Giulia Semeghini, Tout T Wang, Sepehr Ebadi, Marcin Kalinowski, Alexander Keesling, Nishad Maskara, Hannes Pichler, Markus Greiner, *et al.*, “A quantum processor based on coherent transport of entangled atom arrays,” *Nature* **604**, 451–456 (2022).
- [26] Dolev Bluvstein, Simon J Evered, Alexandra A Geim, Sophie H Li, Hengyun Zhou, Tom Manovitz, Sepehr Ebadi, Madelyn Cain, Marcin Kalinowski, Dominik Hangleiter, *et al.*, “Logical quantum processor based on reconfigurable atom arrays,” *Nature* , 1–3 (2023).
- [27] “Suppressing quantum errors by scaling a surface code logical qubit,” *Nature* **614**, 676–681 (2023).
- [28] Sebastian Krinner, Nathan Lacroix, Ants Remm, Agustin Di Paolo, Elie Genois, Catherine Leroux, Christoph Hellings, Stefania Lazar, Francois Swiadek, Johannes Herrmann, *et al.*, “Realizing repeated quantum error correction in a distance-three surface code,” *Nature* **605**, 669–674 (2022).

- [29] KJ Satzinger, Y-J Liu, A Smith, C Knapp, M Newman, C Jones, Z Chen, C Quintana, X Mi, A Dunsworth, *et al.*, “Realizing topologically ordered states on a quantum processor,” *Science* **374**, 1237–1241 (2021).
- [30] “Non-abelian braiding of graph vertices in a superconducting processor,” *Nature*, 1–6 (2023).
- [31] Giulia Semeghini, Harry Levine, Alexander Keesling, Sepehr Ebadi, Tout T Wang, Dolev Bluvstein, Ruben Verresen, Hannes Pichler, Marcin Kalinowski, Rhine Samajdar, *et al.*, “Probing topological spin liquids on a programmable quantum simulator,” *Science* **374**, 1242–1247 (2021).
- [32] Mohsin Iqbal, Nathanan Tantivasadakarn, Ruben Verresen, Sara L Campbell, Joan M Dreiling, Caroline Figgatt, John P Gaebler, Jacob Johansen, Michael Mills, Steven A Moses, *et al.*, “Creation of non-abelian topological order and anyons on a trapped-ion processor,” arXiv preprint arXiv:2305.03766 (2023).
- [33] Michael Foss-Feig, Arkin Tikku, Tsung-Cheng Lu, Karl Mayer, Mohsin Iqbal, Thomas M Gatterman, Justin A Gerber, Kevin Gilmore, Dan Gresh, Aaron Hankin, *et al.*, “Experimental demonstration of the advantage of adaptive quantum circuits,” arXiv preprint arXiv:2302.03029 (2023).
- [34] Dominic V. Else and Chetan Nayak, “Classifying symmetry-protected topological phases through the anomalous action of the symmetry on the edge,” *Phys. Rev. B* **90**, 235137 (2014).
- [35] Ken Shiozaki, Hassan Shapourian, and Shinsei Ryu, “Many-body topological invariants in fermionic symmetry-protected topological phases: Cases of point group symmetries,” *Physical Review B* **95**, 205139 (2017).
- [36] Ken Shiozaki, Hassan Shapourian, Kiyonori Gomi, and Shinsei Ryu, “Many-body topological invariants for fermionic short-range entangled topological phases protected by antiunitary symmetries,” *Physical Review B* **98**, 035151 (2018).
- [37] Hassan Shapourian, Ken Shiozaki, and Shinsei Ryu, “Partial time-reversal transformation and entanglement negativity in fermionic systems,” *Physical Review B* **95**, 165101 (2017).
- [38] Kyle Kawagoe and Michael Levin, “Microscopic definitions of anyon data,” *Phys. Rev. B* **101**, 115113 (2020).
- [39] Ze-Pei Cian, Hossein Dehghani, Andreas Elben, Benoît Vermersch, Guanyu Zhu, Maissam Barkeshli, Peter Zoller, and Mohammad Hafezi, “Many-body chern number from statistical correlations of randomized measurements,” *Physical Review Letters* **126**, 050501 (2021).
- [40] Hossein Dehghani, Ze-Pei Cian, Mohammad Hafezi, and Maissam Barkeshli, “Extraction of the many-body chern number from a single wave function,” *Physical Review B* **103**, 075102 (2021).
- [41] Kyle Kawagoe and Michael Levin, “Anomalies in bosonic symmetry-protected topological edge theories: Connection to f symbols and a method of calculation,” *Phys. Rev. B* **104**, 115156 (2021).
- [42] Ze-Pei Cian, Mohammad Hafezi, and Maissam Barkeshli, “Extracting wilson loop operators and fractional statistics from a single bulk ground state,” arXiv preprint arXiv:2209.14302 (2022).
- [43] Bowen Shi, Kohtaro Kato, and Isaac H Kim, “Fusion rules from entanglement,” *Annals of Physics* **418**, 168164 (2020).
- [44] Isaac H Kim, Bowen Shi, Kohtaro Kato, and Victor V Albert, “Chiral central charge from a single bulk wave function,” *Physical Review Letters* **128**, 176402 (2022).
- [45] Isaac H Kim, Bowen Shi, Kohtaro Kato, and Victor V Albert, “Modular commutator in gapped quantum many-body systems,” *Physical Review B* **106**, 075147 (2022).
- [46] Ryohei Kobayashi, Taige Wang, Tomohiro Soejima, Roger SK Mong, and Shinsei Ryu, “Extracting higher central charge from a single wave function,” arXiv preprint arXiv:2303.04822 (2023).
- [47] Iris Cong, Soonwon Choi, and Mikhail D Lukin, “Quantum convolutional neural networks,” *Nature Physics* **15**, 1273–1278 (2019).
- [48] Iris Cong, Nishad Maskara, Minh C Tran, Hannes Pichler, Giulia Semeghini, Susanne F Yelin, Soonwon Choi, and Mikhail D Lukin, “Enhancing detection of topological order by local error correction,” arXiv preprint arXiv:2209.12428 (2022).
- [49] Minh C Tran, Daniel K Mark, Wen Wei Ho, and Soonwon Choi, “Measuring arbitrary physical properties in analog quantum simulation,” *Physical Review X* **13**, 011049 (2023).
- [50] Xiao Xiao, JK Freericks, and AF Kemper, “Robust measurement of wave function topology on nisq quantum computers,” *Quantum* **7**, 987 (2023).
- [51] Carolyn Zhang, “Topological invariants for symmetry-protected topological phase entanglers,” *Phys. Rev. B* **107**, 235104 (2023).
- [52] Aleksander Kubica, Beni Yoshida, and Fernando Pastawski, “Unfolding the color code,” *New Journal of Physics* **17**, 083026 (2015).
- [53] Sergey Bravyi, Matthew B. Hastings, and Spyridon Michalakis, “Topological quantum order: Stability under local perturbations,” *Journal of Mathematical Physics* **51**, 093512 (2010).
- [54] Jeongwan Haah, “Commuting pauli hamiltonians as maps between free modules,” *Communications in Mathematical Physics* **324**, 351–399 (2013).
- [55] Eric C Rowell, “From quantum groups to unitary modular tensor categories,” *Contemporary Mathematics* **413**, 215–230 (2006).
- [56] Eric Rowell, Richard Stong, and Zhenghan Wang, “On classification of modular tensor categories,” *Communications in Mathematical Physics* **292**, 343–389 (2009).
- [57] Zhenghan Wang, *Topological quantum computation*, 112 (American Mathematical Soc., 2010).
- [58] Liang Wang and Zhenghan Wang, “In and around abelian anyon models,” *Journal of Physics A: Mathematical and Theoretical* **53**, 505203 (2020).
- [59] Julia Plavnik, Andrew Schopieray, Zhiqiang Yu, and Qing Zhang, “Modular tensor categories, subcategories, and galois orbits,” *Transformation Groups* (2023), 10.1007/s00031-022-09787-9.
- [60] Claudio Chamon, “Quantum glassiness in strongly correlated clean systems: An example of topological over-protection,” *Physical review letters* **94**, 040402 (2005).
- [61] Jeongwan Haah, “Local stabilizer codes in three dimensions without string logical operators,” *Physical Review A* **83**, 042330 (2011).
- [62] Sagar Vijay, Jeongwan Haah, and Liang Fu, “Fracton topological order, generalized lattice gauge theory, and duality,” *Physical Review B* **94**, 235157 (2016).
- [63] Wilbur Shirley, Kevin Slagle, Zhenghan Wang, and Xie Chen, “Fracton models on general three-dimensional

- manifolds,” *Physical Review X* **8**, 031051 (2018).
- [64] Michael Pretko, Xie Chen, and Yizhi You, “Fraction phases of matter,” *International Journal of Modern Physics A* **35**, 2030003 (2020).
- [65] Michael Levin and Xiao-Gang Wen, “Quantum ether: Photons and electrons from a rotor model,” *Phys. Rev. B* **73**, 035122 (2006).
- [66] Jason Alicea, Yuval Oreg, Gil Refael, Felix Von Oppen, and Matthew PA Fisher, “Non-abelian statistics and topological quantum information processing in 1d wire networks,” *Nature Physics* **7**, 412–417 (2011).
- [67] Kyle Kawagoe and Michael Levin, “Microscopic definitions of anyon data,” *Phys. Rev. B* **101**, 115113 (2020).
- [68] Lukasz Fidkowski, Jeongwan Haah, and Matthew B. Hastings, “Gravitational anomaly of (3+1)-dimensional F_2 toric code with fermionic charges and fermionic loop self-statistics,” *Phys. Rev. B* **106**, 165135 (2022).
- [69] Haruki Watanabe, Meng Cheng, and Yohei Fuji, “Ground state degeneracy on torus in a family of zn toric code,” *Journal of Mathematical Physics* **64** (2023).
- [70] Arpit Dua, Isaac H Kim, Meng Cheng, and Dominic J Williamson, “Sorting topological stabilizer models in three dimensions,” *Physical Review B* **100**, 155137 (2019).
- [71] Yu-An Chen, Alexey V Gorshkov, and Yijia Xu, “Error-correcting codes for fermionic quantum simulation,” arXiv preprint arXiv:2210.08411 (2022).
- [72] Riley W Chien and Joel Klassen, “Optimizing fermionic encodings for both hamiltonian and hardware,” arXiv preprint arXiv:2210.05652 (2022).
- [73] Xiao-Gang Wen, “Quantum orders in an exact soluble model,” *Physical review letters* **90**, 016803 (2003).
- [74] Robbert Dijkgraaf and Edward Witten, “Topological gauge theories and group cohomology,” *Communications in Mathematical Physics* **129**, 393–429 (1990).
- [75] Tyler D. Ellison, Yu-An Chen, Arpit Dua, Wilbur Shirley, Nathanan Tantivasadakarn, and Dominic J. Williamson, “Pauli topological subsystem codes from Abelian anyon theories,” *Quantum* **7**, 1137 (2023).
- [76] Michael Liaofan Liu, Nathanan Tantivasadakarn, and Victor V Albert, “Subsystem css codes, a tighter stabilizer-to-css mapping, and goursat’s lemma,” arXiv preprint arXiv:2311.18003 (2023).
- [77] R.K. Martin, *Large Scale Linear and Integer Optimization: A Unified Approach* (Springer US, 2012).

Appendix A: Relation between braiding statistics and topological spins

In this appendix, we review how the topological spins in abelian anyon theories completely determine the braiding statistics. Specifically, from the topological spin given in Eq. (6), we derive Eq. (7). We again consider the T-junction setup as shown in Fig. 4. Using the T-junction, braiding anyon a counterclockwise around anyon b is seen to be given by

$$B_\theta(a, b) = (W_3^b)^\dagger W_2^b (W_1^a)^\dagger W_3^a (W_2^b)^\dagger W_1^b \times (W_3^a)^\dagger W_2^a (W_1^b)^\dagger W_3^b (W_2^a)^\dagger W_1^a. \quad (\text{A1})$$

Suppose that a starts at $\bar{\gamma}_1(0)$ and b at $\bar{\gamma}_3(0)$. Then this corresponds to moving a and b in the following order:

1. $a: \bar{\gamma}_1(0) \rightarrow p \rightarrow \bar{\gamma}_2(0)$,
2. $b: \bar{\gamma}_3(0) \rightarrow p \rightarrow \bar{\gamma}_1(0)$,
3. $a: \bar{\gamma}_2(0) \rightarrow p \rightarrow \bar{\gamma}_3(0)$,
4. $b: \bar{\gamma}_1(0) \rightarrow p \rightarrow \bar{\gamma}_2(0)$,
5. $a: \bar{\gamma}_3(0) \rightarrow p \rightarrow \bar{\gamma}_1(0)$,
6. $b: \bar{\gamma}_2(0) \rightarrow p \rightarrow \bar{\gamma}_3(0)$,

thus performing the braid as desired. Using from Eq. (6) that

$$\theta(a) = (W_3^a)^\dagger W_2^a (W_1^a)^\dagger W_3^a (W_2^a)^\dagger W_1^a, \quad (\text{A2})$$

we will show that

$$B_\theta(a, b) = \frac{\theta(a \times b)}{\theta(a)\theta(b)}. \quad (\text{A3})$$

Ultimately, this follows from the definition $W_i^{a \times b} := W_i^b W_i^a$; that is, moving the composite anyon $a \times b$ is equivalent to moving each anyon separately along the same path.

Since each W_i^a is a Pauli, we have that

$$\begin{aligned} W_i^a W_j^b &= z_{i,j}^{a,b} W_j^b W_i^a \\ (W_i^a)^\dagger (W_j^b)^\dagger &= z_{i,j}^{a,b} (W_j^b)^\dagger (W_i^a)^\dagger \\ W_i^a (W_j^b)^\dagger &= (z_{i,j}^{a,b})^{-1} (W_j^b)^\dagger W_i^a, \end{aligned} \quad (\text{A4})$$

for some complex numbers $z_{i,j}^{a,b}$. Starting from Eq. (A2), we have that

$$\begin{aligned} \theta(a \times b)^{-1} &= (W_1^{a \times b})^\dagger W_2^{a \times b} (W_3^{a \times b})^\dagger W_1^{a \times b} (W_2^{a \times b})^\dagger W_3^{a \times b} \end{aligned} \quad (\text{A5})$$

$$\begin{aligned} &= (W_1^a)^\dagger (W_1^b)^\dagger W_2^b W_2^a (W_3^a)^\dagger (W_3^b)^\dagger \\ &\quad \times W_1^b W_1^a (W_2^a)^\dagger (W_2^b)^\dagger W_3^b W_3^a \end{aligned} \quad (\text{A6})$$

$$\begin{aligned} &= (z_{2,3}^{a,b})^{-1} z_{3,3}^{a,b} \\ &\quad \times (W_1^a)^\dagger (W_1^b)^\dagger W_2^b (W_3^b)^\dagger W_2^a (W_3^a)^\dagger \\ &\quad \times z_{2,2}^{a,b} (z_{1,2}^{a,b})^{-1} \end{aligned} \quad (\text{A7})$$

$$\begin{aligned} &\quad \times W_1^b (W_2^b)^\dagger W_1^a (W_2^a)^\dagger W_3^b W_3^a \\ &= (z_{2,3}^{a,b})^{-1} z_{3,3}^{a,b} z_{1,1}^{a,b} (z_{1,2}^{a,b})^{-1} z_{1,3}^{a,b} \\ &\quad \times (W_1^b)^\dagger W_2^b (W_3^b)^\dagger (W_1^a)^\dagger W_2^a (W_3^a)^\dagger \end{aligned} \quad (\text{A8})$$

$$\begin{aligned} &\quad \times z_{2,2}^{a,b} (z_{1,2}^{a,b})^{-1} (z_{2,3}^{a,b})^{-1} z_{1,3}^{a,b} \\ &\quad \times W_1^b (W_2^b)^\dagger W_3^b W_1^a (W_2^a)^\dagger W_3^a \\ &= (z_{2,3}^{a,b})^{-1} z_{3,3}^{a,b} z_{1,1}^{a,b} (z_{1,2}^{a,b})^{-1} z_{1,3}^{a,b} \\ &\quad \times (W_1^b)^\dagger W_2^b (W_3^b)^\dagger (W_1^a)^\dagger W_2^a (W_3^a)^\dagger \\ &\quad \times z_{2,2}^{a,b} (z_{1,2}^{a,b})^{-1} (z_{2,3}^{a,b})^{-1} z_{1,3}^{a,b} \\ &\quad \times W_1^b (W_2^b)^\dagger W_3^b W_1^a (W_2^a)^\dagger W_3^a \end{aligned} \quad (\text{A9})$$

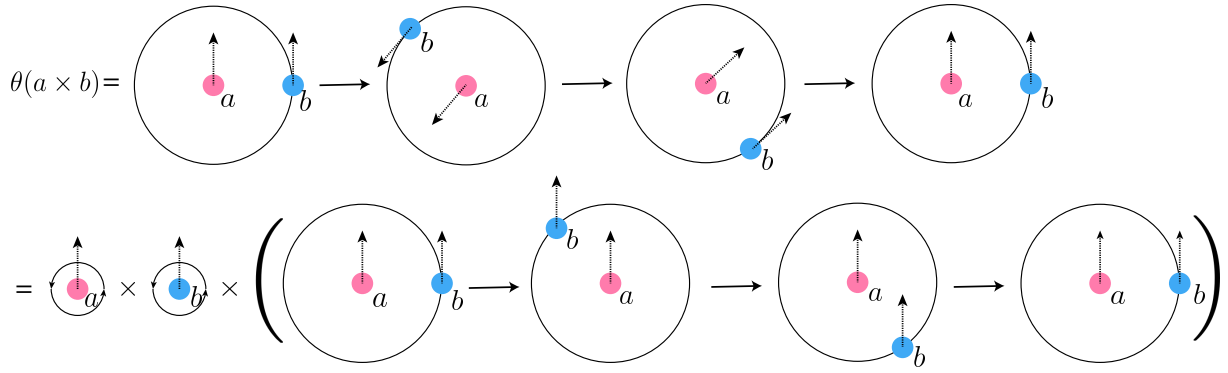


FIG. 10. Relation between $\theta(a \times b)$, $\theta(a)$, $\theta(b)$ and the mutual braiding $B(a, b)$. This equality indicates $\theta(a \times b) = \theta(a) \times \theta(b) \times B(a, b)$.

$$\begin{aligned}
&= (z_{2,3}^{a,b})^{-1} z_{3,3}^{a,b} z_{1,1}^{a,b} (z_{1,2}^{a,b})^{-1} z_{1,3}^{a,b} \\
&\quad \times z_{2,2}^{a,b} (z_{1,2}^{a,b})^{-1} (z_{2,3}^{a,b})^{-1} z_{1,3}^{a,b} \\
&\quad \times (z_{3,1}^{a,b})^{-1} z_{2,1}^{a,b} (z_{1,1}^{a,b})^{-1} \\
&\quad \times z_{3,2}^{a,b} (z_{2,2}^{a,b})^{-1} z_{1,2}^{a,b} \\
&\quad \times (z_{3,3}^{a,b})^{-1} z_{2,3}^{a,b} (z_{1,3}^{a,b})^{-1} \\
&\quad \times (W_1^b)^\dagger W_2^b (W_3^b)^\dagger W_1^b (W_2^b)^\dagger W_3^b \\
&\quad \times (W_1^a)^\dagger W_2^a (W_3^a)^\dagger W_1^a (W_2^a)^\dagger W_3^a \\
&= z_{3,2}^{a,b} (z_{1,2}^{a,b})^{-1} z_{2,1}^{a,b} (z_{3,1}^{a,b})^{-1} (z_{2,3}^{a,b})^{-1} z_{1,3}^{a,b} \\
&\quad \times \theta(b)^{-1} \theta(a)^{-1}.
\end{aligned} \tag{A10}$$

$$\begin{aligned}
&= z_{3,2}^{a,b} (z_{1,2}^{a,b})^{-1} z_{2,1}^{a,b} (z_{3,1}^{a,b})^{-1} (z_{2,3}^{a,b})^{-1} z_{1,3}^{a,b} \\
&\quad \times \theta(b)^{-1} \theta(a)^{-1}.
\end{aligned} \tag{A11}$$

Thus,

$$\frac{\theta(a \times b)}{\theta(a)\theta(b)} = (z_{3,2}^{a,b})^{-1} z_{1,2}^{a,b} (z_{2,1}^{a,b})^{-1} z_{3,1}^{a,b} z_{2,3}^{a,b} (z_{1,3}^{a,b})^{-1}. \tag{A12}$$

Meanwhile, from Eq. (A1),

$$\begin{aligned}
B_\theta(a, b) &= (W_3^b)^\dagger W_2^b (W_1^a)^\dagger W_3^a (W_2^b)^\dagger W_1^b \\
&\quad \times (W_3^a)^\dagger W_2^a (W_1^b)^\dagger W_3^b (W_2^a)^\dagger W_1^a \\
&= (z_{3,2}^{a,b})^{-1} z_{1,2}^{a,b} \\
&\quad \times (W_3^b)^\dagger (W_1^a)^\dagger W_3^a W_1^b \\
&\quad \times (W_3^a)^\dagger W_2^a (W_1^b)^\dagger W_3^b (W_2^a)^\dagger W_1^a \\
&= (z_{3,2}^{a,b})^{-1} z_{1,2}^{a,b} (z_{2,1}^{a,b})^{-1} z_{3,1}^{a,b} \\
&\quad \times (W_3^b)^\dagger (W_1^a)^\dagger W_2^a W_3^b (W_2^a)^\dagger W_1^a \\
&= (z_{3,2}^{a,b})^{-1} z_{1,2}^{a,b} (z_{2,1}^{a,b})^{-1} z_{3,1}^{a,b} z_{2,3}^{a,b} (z_{1,3}^{a,b})^{-1}.
\end{aligned} \tag{A13}$$

$$\begin{aligned}
&= (z_{3,2}^{a,b})^{-1} z_{1,2}^{a,b} \\
&\quad \times (W_3^b)^\dagger (W_1^a)^\dagger W_3^a W_1^b \\
&\quad \times (W_3^a)^\dagger W_2^a (W_1^b)^\dagger W_3^b (W_2^a)^\dagger W_1^a \\
&= (z_{3,2}^{a,b})^{-1} z_{1,2}^{a,b} (z_{2,1}^{a,b})^{-1} z_{3,1}^{a,b} \\
&\quad \times (W_3^b)^\dagger (W_1^a)^\dagger W_2^a W_3^b (W_2^a)^\dagger W_1^a \\
&= (z_{3,2}^{a,b})^{-1} z_{1,2}^{a,b} (z_{2,1}^{a,b})^{-1} z_{3,1}^{a,b} z_{2,3}^{a,b} (z_{1,3}^{a,b})^{-1}.
\end{aligned} \tag{A14}$$

$$\begin{aligned}
&= (z_{3,2}^{a,b})^{-1} z_{1,2}^{a,b} (z_{2,1}^{a,b})^{-1} z_{3,1}^{a,b} \\
&\quad \times (W_3^b)^\dagger (W_1^a)^\dagger W_2^a W_3^b (W_2^a)^\dagger W_1^a \\
&= (z_{3,2}^{a,b})^{-1} z_{1,2}^{a,b} (z_{2,1}^{a,b})^{-1} z_{3,1}^{a,b} z_{2,3}^{a,b} (z_{1,3}^{a,b})^{-1}.
\end{aligned} \tag{A15}$$

$$\begin{aligned}
&= (z_{3,2}^{a,b})^{-1} z_{1,2}^{a,b} (z_{2,1}^{a,b})^{-1} z_{3,1}^{a,b} z_{2,3}^{a,b} (z_{1,3}^{a,b})^{-1}.
\end{aligned} \tag{A16}$$

Comparing to Eq. (A12), we see that

$$B_\theta(a, b) = \frac{\theta(a \times b)}{\theta(a)\theta(b)}. \tag{A17}$$

Another way to interpret this equation is to treat the topological spin $\theta(a)$ as a 2π rotation of an anyon a , according to the spin-statistics theorem. As depicted in Fig. 10, the 2π rotation of anyon $a \times b$ can be decomposed into three pieces: the 2π rotation of anyon a , the 2π rotation of anyon b , and the mutual braiding between

anyons a and b . However, we emphasize that this is a physical picture instead of a rigorous proof derived by Eqs. (A12) and (A16).

Appendix B: The Hermite normal form and the Smith normal form

Throughout this work, we have been broadly interested in solving linear systems of equations over a ring R . Specifically, suppose we have an $r \times c$ matrix A with entries $A_{ij} \in R$ and a vector $b \in R^c$ represented by a column $b_i \in R$. To solve the system defined by A and b , we must find a vector $x \in R^r$ such that $Ax = b$, where $=$ denotes equality within R . We will denote the linear system by $(A, b)_R$.

When R is a field \mathbb{K} , such as \mathbb{R} or a finite field \mathbb{F}_{p^n} , $(A, b)_\mathbb{K}$ can be solved efficiently using standard Gaussian elimination. By performing row operations, we effectively transform the system $Ax = b$ into $C Ax = C b$, where $C \in \text{GL}(r, \mathbb{K})$ with GL denoting the general linear group. One can efficiently find C such that CA is in reduced echelon form, making x easy to find.

When R is not a field but instead only a principal ideal domain (PID), an analogous procedure finds $C \in \text{GL}(r, R)$ such that CA is the *Hermite normal form* (HNF) of A [77]. The HNF of A can be efficiently found. The most important property of the HNF is that it is upper triangular. When $R = \mathbb{Z}$, C is called a *unimodular* matrix. Using the HNF, linear systems $(A, b)_\mathbb{Z}$ over \mathbb{Z} can be efficiently solved. The ring of modular integers $\mathbb{Z}_n = \mathbb{Z}/n\mathbb{Z}$ is not a PID, but linear systems can still be solved using the HNF by turning the system over \mathbb{Z}_n into a system over \mathbb{Z} . Specifically, we transform the system $Ax = b \pmod{n}$ into $Ax - ny = b$, where $y \in \mathbb{Z}^c$ is an additional set of variables. We define the new $(r+c) \times 1$ variable vector $\tilde{x} = x \oplus y$ and the new $r \times (r+c)$ matrix $\tilde{A} = \begin{pmatrix} A & -n\mathbf{1}_{r \times c} \end{pmatrix}$. The value of x in the solution \tilde{x} to the system $(\tilde{A}, b)_\mathbb{Z}$ over \mathbb{Z} is the solution to the system $(A, b)_{\mathbb{Z}_n}$ over \mathbb{Z}_n .

In this work, we are most interested in solving linear systems $(A, b)_R$ over the polynomial ring $R = \mathbb{Z}_n[x, y]$.

Using the same procedure above, we can reduce this to solving linear systems $(A, b)_R$ over the polynomial ring $R = \mathbb{Z}[x, y]$. By truncating the polynomials coming from $\mathbb{Z}[x, y]$ to some maximum degree d , we obtain a new (larger) linear system over simply \mathbb{Z} .

One natural question is: can we solve the linear system over $\mathbb{Z}[x, y]$ *directly*, without truncating the degree of the polynomials? Unfortunately, $\mathbb{Z}[x, y]$ is not a PID, and thus the HNF cannot be used. We cannot, in general, get around degree truncation. Specifically, we can effectively solve linear systems over $\mathbb{Z}[x, y]$ if and only if we can construct an algorithm that outputs an upper bound on the polynomial degrees that occur during the solving algorithm. The \Rightarrow direction is obvious, and the \Leftarrow direction follows from our discussion above, where we reduced a general linear system over $\mathbb{Z}[x, y]$ to a linear system over \mathbb{Z} once we picked a degree at which to truncate. In Eq. (28), for example, there is no general way of bounding the degree since v can be arbitrary. Hence, the best we can do is pick a degree to truncate.

Finally, we recall the *Smith normal form* (SNF). The HNF of a matrix over a PID is analogous to the reduced echelon form of a matrix over a field. In a similar way, the SNF of a matrix over a PID is analogous to the diagonalization of a matrix over a field. Specifically, one can efficiently use row and column operations amounting to matrices $C \in \text{GL}(r, R)$ and $D \in \text{GL}(c, R)$ such that CAD is diagonal. CAD is called the SNF of A , and it further satisfies that its nonzero diagonal elements d_1, \dots, d_ℓ satisfy $d_1 \mid d_2 \mid \dots \mid d_\ell$. d_1, \dots, d_ℓ are unique and are called the *elementary divisors* of A .

Appendix C: String operators of various examples

This appendix presents the pictorial description of anyon string operators we solved for the regular color code, the modified color codes, the double semion code, the CSS code from the doubled semion code, and the six-semion code.

As we discussed in Sec. V A, we need to solve Eq. (28) for different choices of n_x, n_y and choose the smallest n_x, n_y that maximize the number of anyon solutions. Here, we report the number of independent anyon solutions of the different models with different choices of n_x, n_y in Table. X.

1. Color code and modified color codes

In this section, we use our algorithm to investigate five models satisfying topological order conditions shown in Fig. 1 except example ②, and the resulting string operator is shown in the following figure:

Since all five models are self-dual, we omit whether each qubit represents X or Z. Here, the blue dots represent

the string operator in the x -direction, and the red dots represent the string operator in the y -direction. When the string operator in the x -direction coincides with the string operator in the y -direction, we use purple dots to represent the overlapping qubits. The black dot represents the origin and distinguishes between different stabilizer positions.

The result is summarized as follows:

- For the regular color code (example ①), we obtain four independent anyon solutions at $(1 - x^3)$ and $(1 - y^{-3})$. The string operators are shown in Fig. 11
- The second model does not satisfy the topological condition.
- For the modified color code A (example ③), we can obtain maximally eight independent anyon solutions at $(1 - x^5)$ and $(1 - y^{-5})$. The string operators are shown in Fig. 12
- For the modified color code B (example ④), we can obtain maximally sixteen independent anyon solutions at $(1 - x^{12})$ and $(1 - y^{-12})$. The string operators are shown in Figs. 13, 14, 15, 16, 17, 18, 19, 20.
- For the modified color code C (example ⑤), we can obtain maximally eight independent anyon solutions at $(1 - x^4)$ and $(1 - y^{-4})$. The string operators are shown in Fig. 21.
- For the modified color code D (example ⑥), we can obtain maximally twelve independent anyon solutions at $(1 - x^4)$ and $(1 - y^{-4})$. The string operators are shown in Figs. 22 and 23.

2. CSS code induced from double semion code

For the CSS code induced from double semion code, we obtain four basis anyons at $(1 - x^1)$ and $(1 - y^{-1})$ (also for greater n_x, n_y). The string operators for $n_x, n_y = 5$ are shown in Fig. 24 and 25.

3. Double semion code

For the six-semion code, we obtain two basis anyons at $(1 - x^1)$ and $(1 - y^{-1})$ (also for greater n_x, n_y). The string operators for $n_x, n_y = 5$ are shown in Fig. 26.

4. Six-semion code

For the six-semion code, we obtain 2 basis anyons at $(1 - x^1)$ and $(1 - y^{-1})$ (also for greater n_x, n_y). The string operators for $n_x, n_y = 5$ are shown in Fig. 27.

number of anyons	$n = 1$	$n = 2$	$n = 3$	$n = 4$	$n = 5$	$n = 6$	$n = 7$	$n = 8$
Regular color code (example ①) x -direction	0	0	4	0	0	4	0	0
Regular color code (example ①) y -direction	0	0	4	0	0	4	0	0
Modified color code A (example ③) x -direction	0	0	0	0	8	0	0	0
Modified color code A (example ③) y -direction	0	0	0	0	8	0	0	0
Modified color code B (example ④) x -direction	4	8	8	12	4	12	4	12
Modified color code B (example ④) y -direction	4	8	8	12	4	12	4	12
Modified color code C (example ⑤) x -direction	2	4	2	8	2	4	2	8
Modified color code C (example ⑤) y -direction	2	4	2	8	2	4	2	8
Modified color code D (example ⑥) x -direction	4	8	4	12	4	8	4	12
Modified color code D (example ⑥) y -direction	4	8	4	12	4	8	4	12
CSS code from double semion code x -direction	4	4	4	4	4	4	4	4
CSS code from double semion code y -direction	4	4	4	4	4	4	4	4
six-semion code x -direction	2	2	2	2	2	2	2	2
six-semion code y -direction	2	2	2	2	2	2	2	2
Double semion code	2	2	2	2	2	2	2	2
Double semion code	2	2	2	2	2	2	2	2

TABLE X. The number of independent anyon solutions of Eq. (28) with different choices of n_x, n_y for different examples. We can see that the number of independent anyon solutions has a periodic pattern when we change n_x, n_y . Moreover, if $n_x = n_y$, we find that the number of independent anyon solutions along the x - and y -directions are the same for a given model. The algorithm shows that the modified color code B has 16 independent anyon solutions when $n_x = n_y = 12$. We have checked their periodicity up to $n_x, n_y = 16$, while only showing n_x, n_y up to 8 in this table.

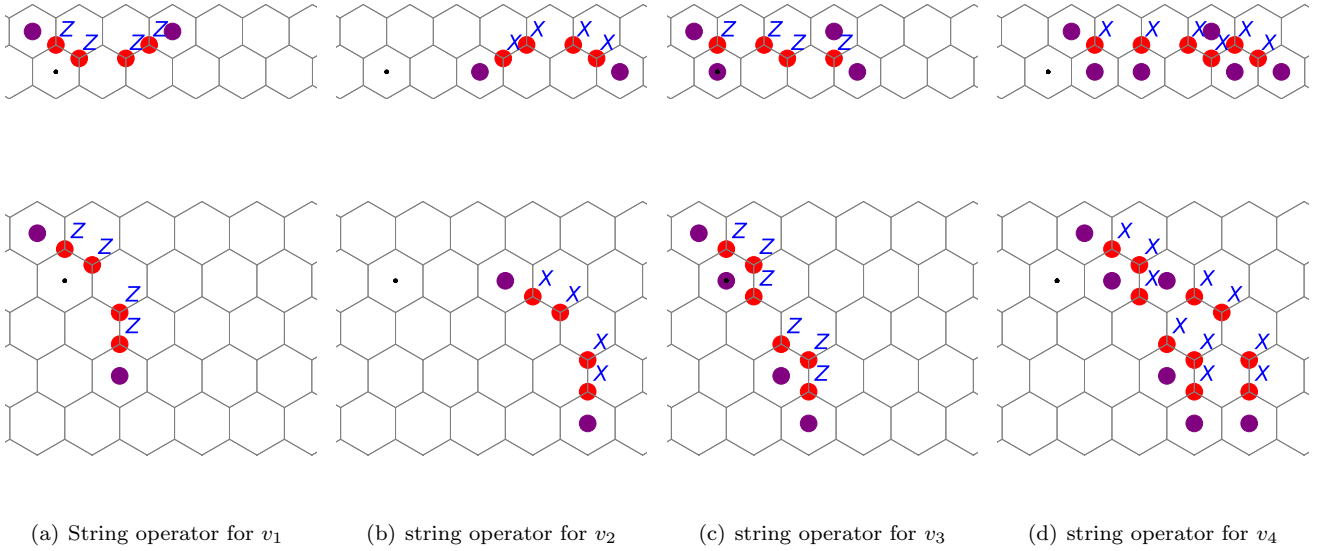


FIG. 11. The string operators in the regular color code (example ①). Subfigures (a)~(d) represent the string operators for anyons v_1, \dots, v_4 . For each subfigure, the first row represents the anyon string operators that move an anyon along the x -direction, and the second row represents the anyon string operators that move an anyon along the y -direction.

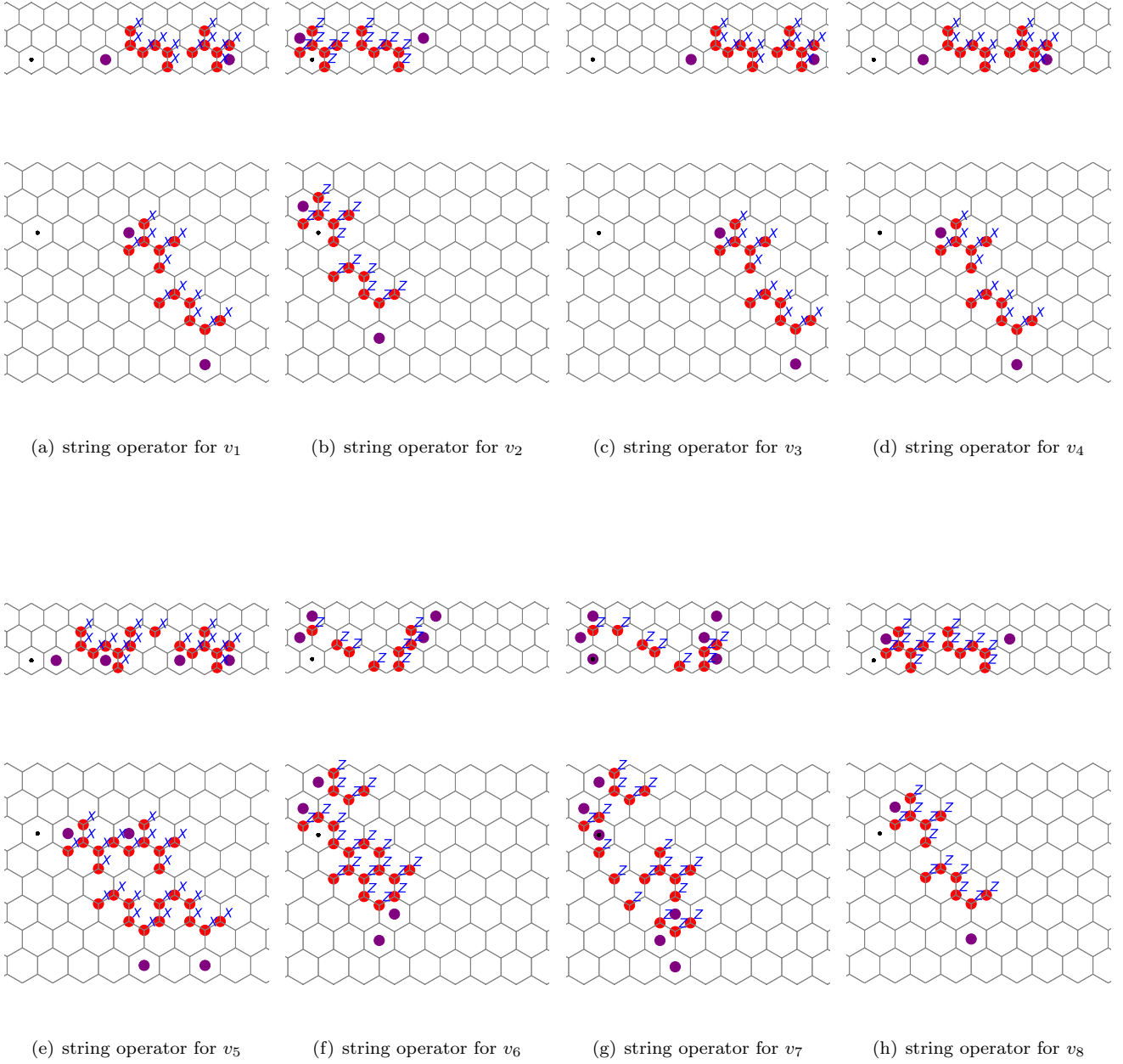


FIG. 12. The string operators in the modified color code A (example ③). Subfigures (a)~ (h) represent the string operators for anyons v_1, \dots, v_8 . For each subfigure, the first row represents the anyon string operators that move an anyon along the x -direction, and the second row represents the anyon string operators that move an anyon along the y -direction.

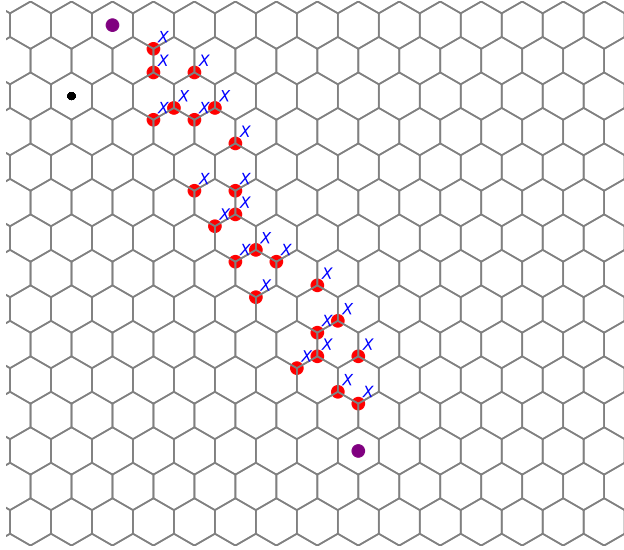
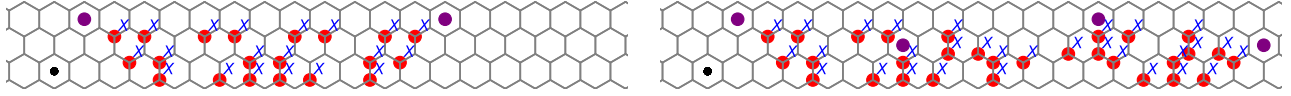
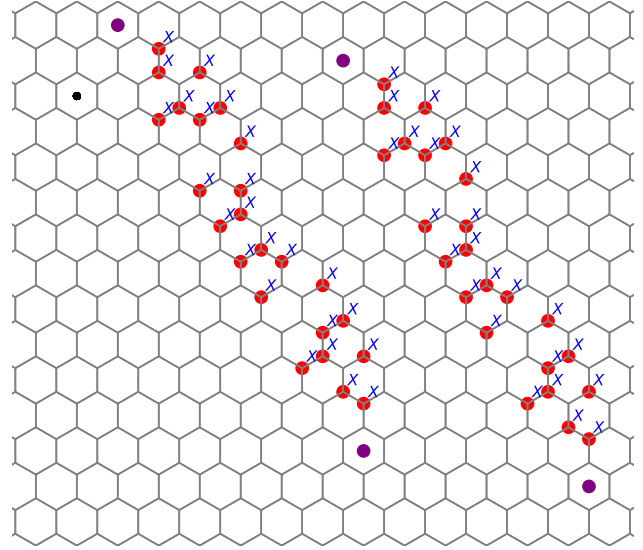
(a) string operator for v_1 (b) string operator for v_2

FIG. 13. The string operators in the modified color code B (example ④). Subfigures (a) and (b) represent the string operators for anyons v_1 and v_2 . For each subfigure, the first row represents the anyon string operators that move an anyon along the x -direction, and the second row represents the anyon string operators that move an anyon along the y -direction.

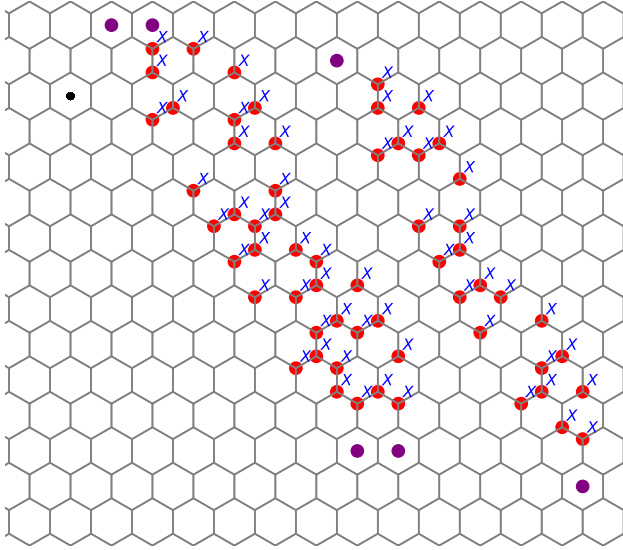
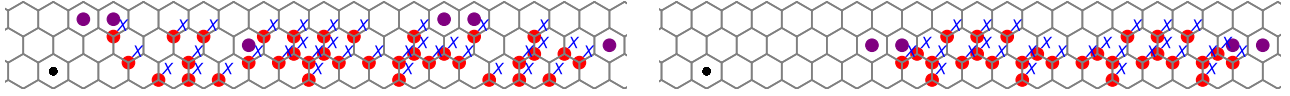
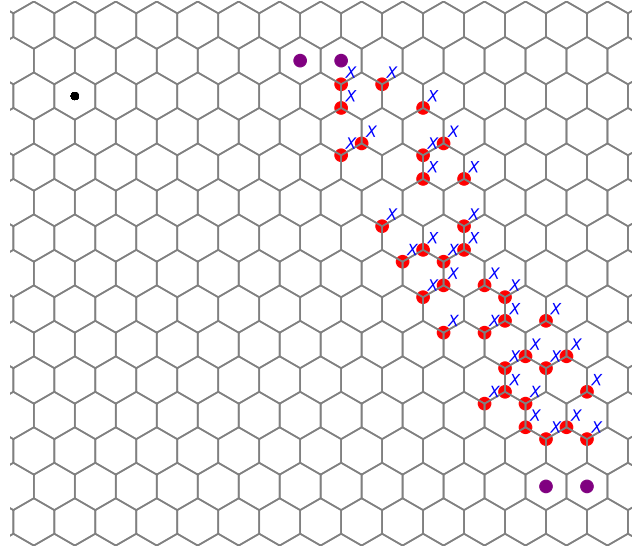
(a) string operator for v_3 (b) string operator for v_4

FIG. 14. (Continued) The string operators in the modified color code B (example ④). Subfigures (a) and (b) represent the string operators for anyons v_3 and v_4 . For each subfigure, the first row represents the anyon string operators that move an anyon along the x -direction, and the second row represents the anyon string operators that move an anyon along the y -direction.

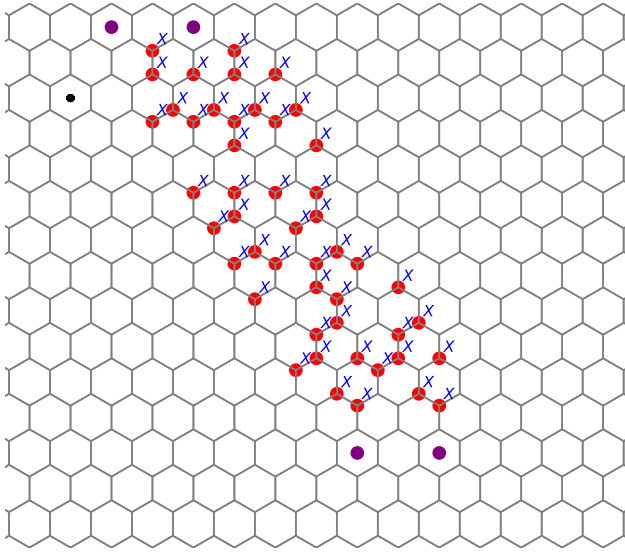
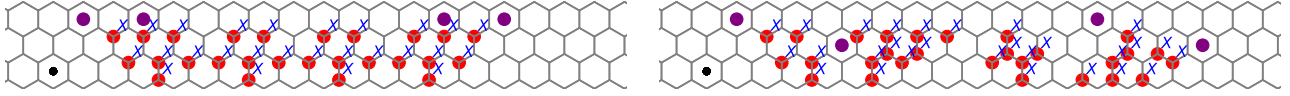
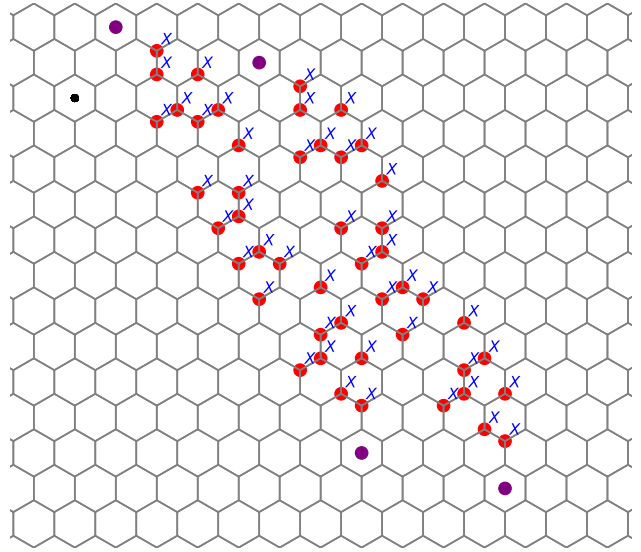
(a) string operator for v_5 (b) string operator for v_6

FIG. 15. (Continued) The string operators in the modified color code B (example ④). Subfigure (a) and (b) represent the string operators for anyons v_5 and v_6 . For each subfigure, the first row represents the anyon string operators that move an anyon along the x -direction, and the second row represents the anyon string operators that move an anyon along the y -direction.

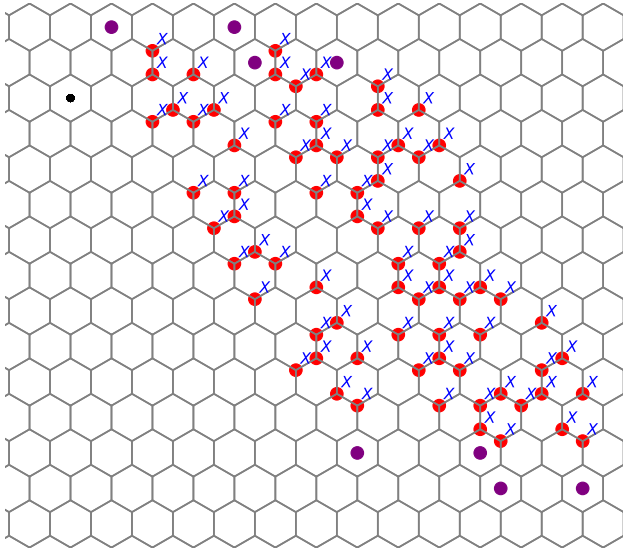
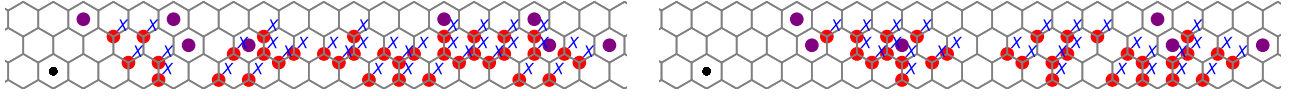
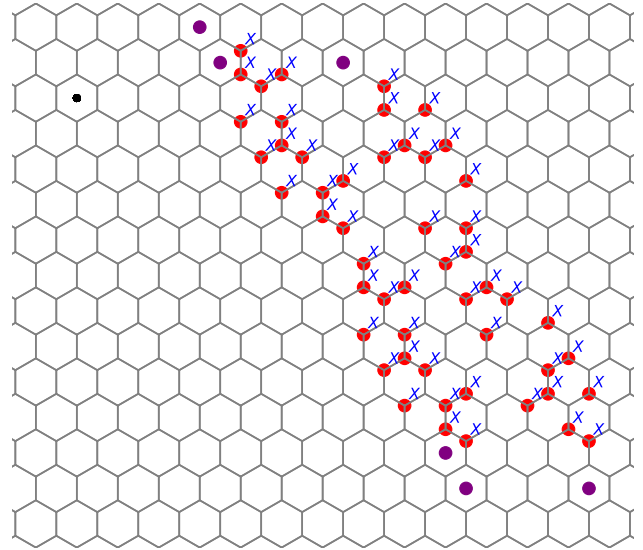
(a) string operator for v_7 (b) string operator for v_8

FIG. 16. (Continued) The string operators in the modified color code B (example ④). Subfigures (a) and (b) represent the string operators for anyons v_7 and v_8 . For each subfigure, the first row represents the anyon string operators that move an anyon along the x -direction, and the second row represents the anyon string operators that move an anyon along the y -direction.

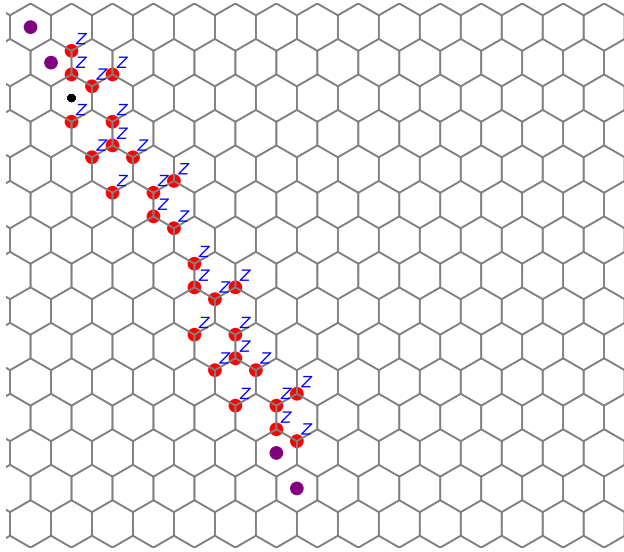
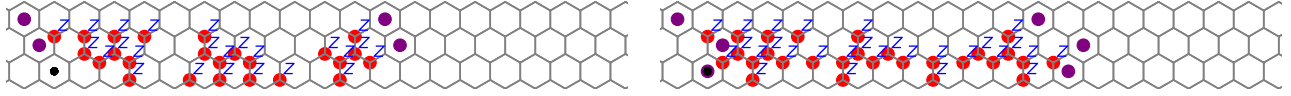
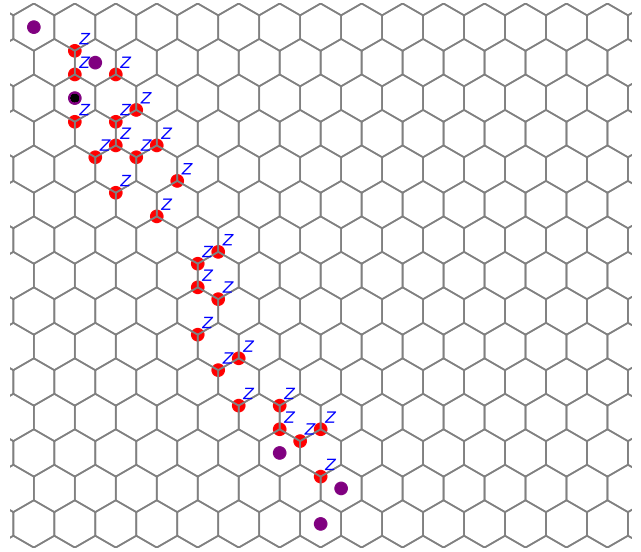
(a) string operator for v_9 (b) string operator for v_{10}

FIG. 17. (Continued) The string operators in of the modified color code B (example ④). Subfigure (a) and (b) represent the string operators for anyons v_9 and v_{10} . For each subfigure, the first row represents the anyon string operators that move an anyon along the x -direction, and the second row represents the anyon string operators that move an anyon along the y -direction.

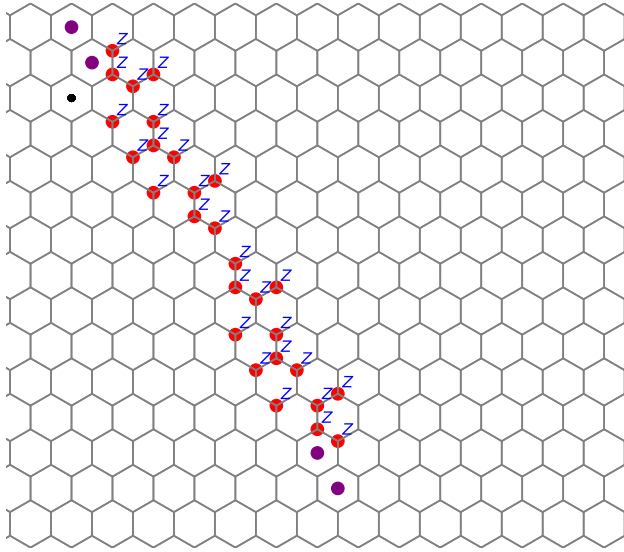
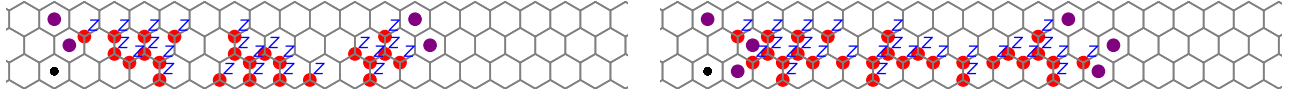
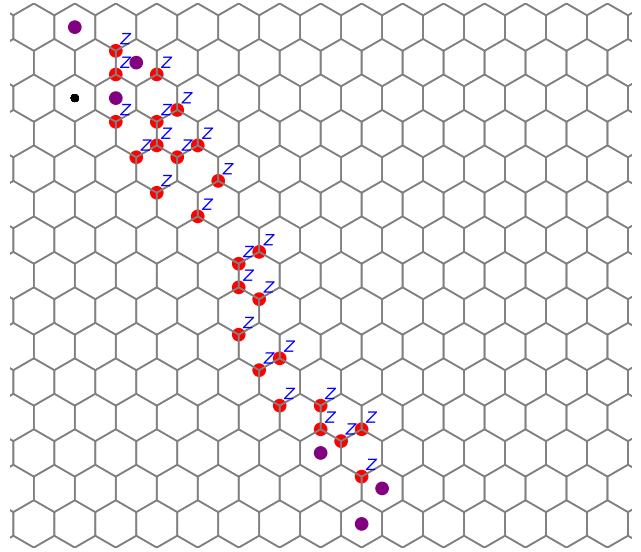
(a) string operator for v_{11} (b) string operator for v_{12}

FIG. 18. (Continued) The string operators in the modified color code B (example ④). Subfigure (a) and (b) represent the string operators for anyons v_{11} and v_{12} . For each subfigure, the first row represents the anyon string operators that move an anyon along the x -direction, and the second row represents the anyon string operators that move an anyon along the y -direction.

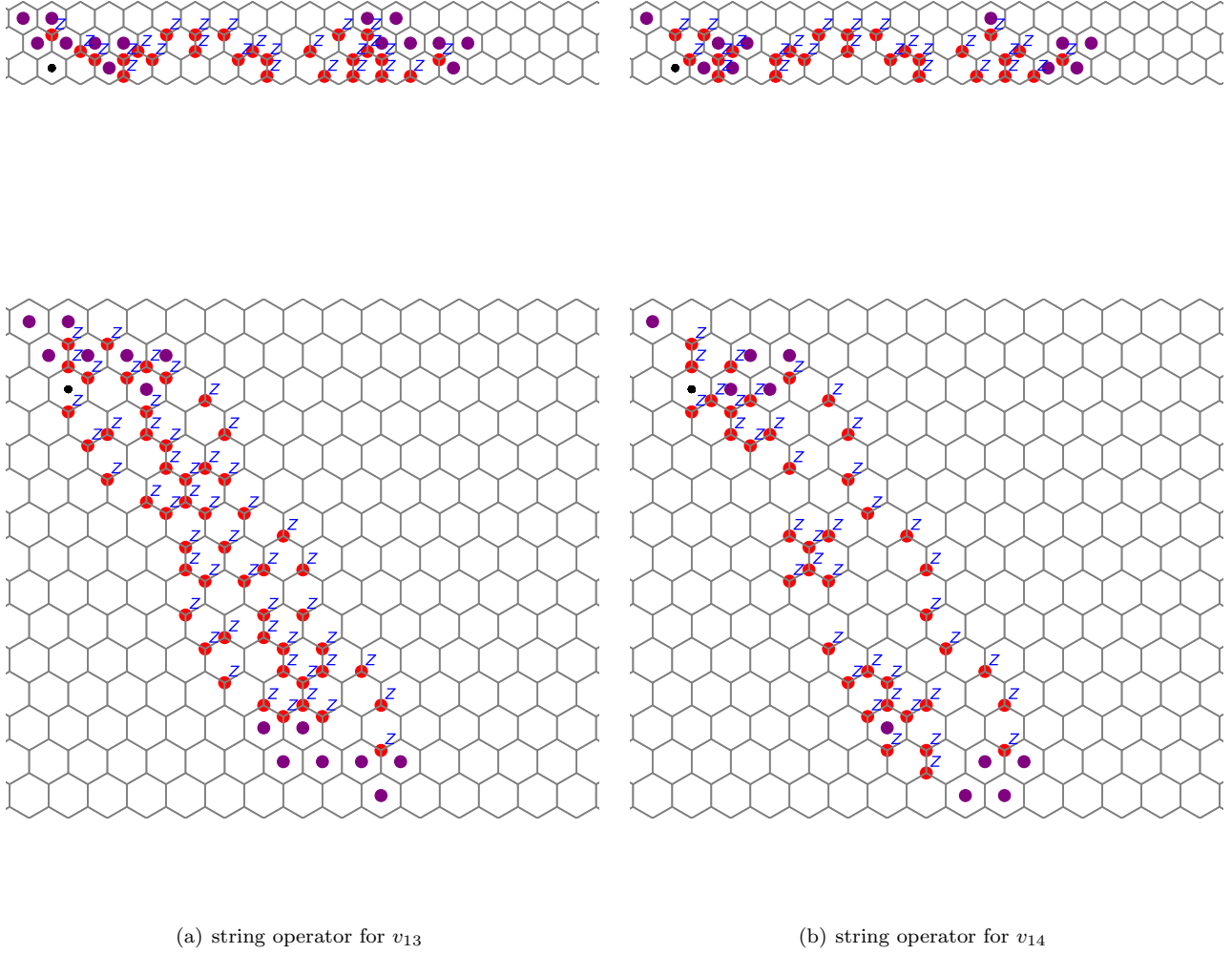


FIG. 19. (Continued) The string operators in the modified color code B (example ④). Subfigures (a) and (b) represent the string operators for anyons v_{13} and v_{14} . For each subfigure, the first row represents the anyon string operators that move an anyon along the x -direction, and the second row represents the anyon string operators that move an anyon along the y -direction.

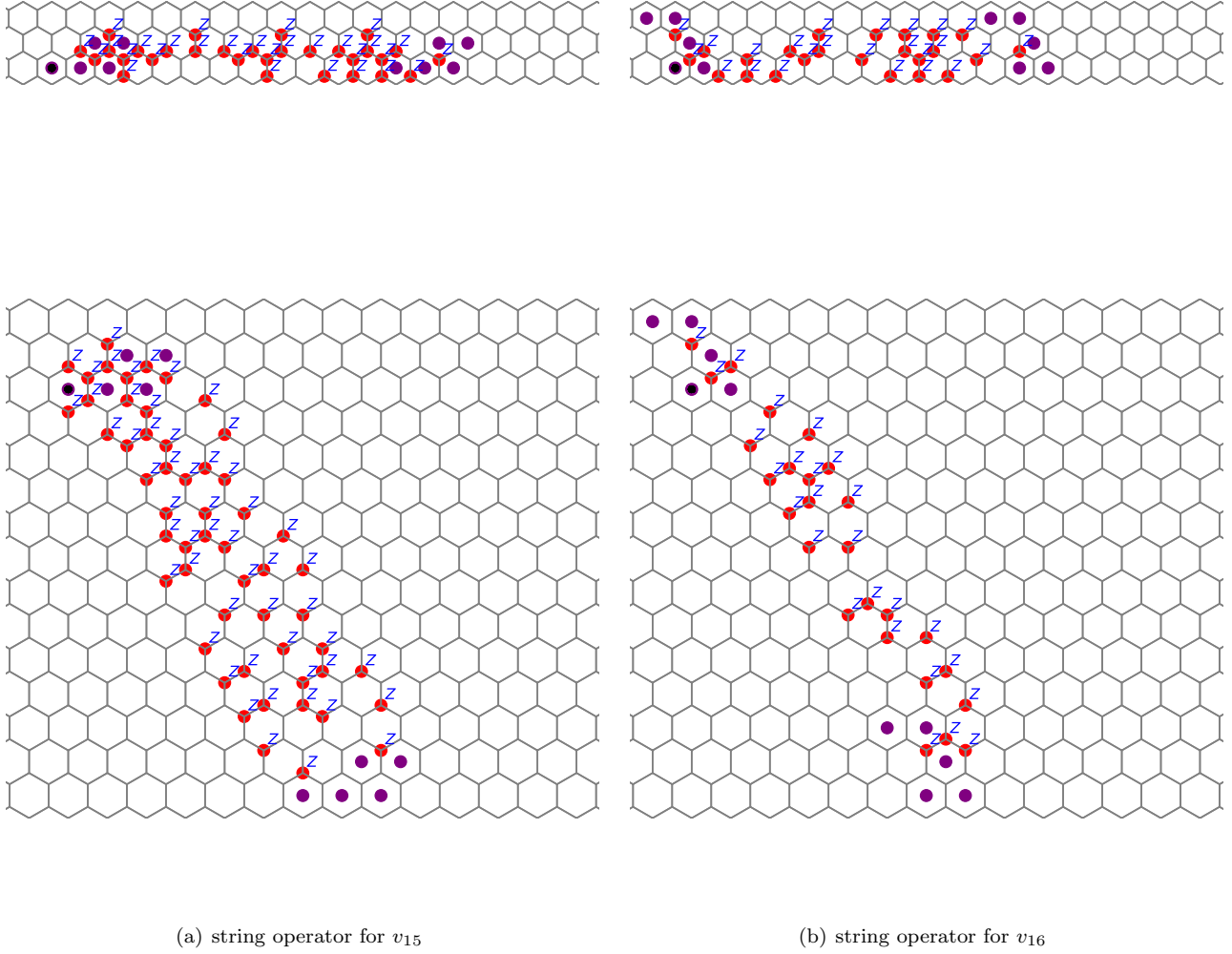


FIG. 20. (Continued) The string operators in the modified color code B (example ④). Subfigure (a) and (b) represent the string operators for anyons v_{15} and v_{16} . For each subfigure, the first row represents the anyon string operators that move an anyon along the x -direction, and the second row represents the anyon string operators that move an anyon along the y -direction.

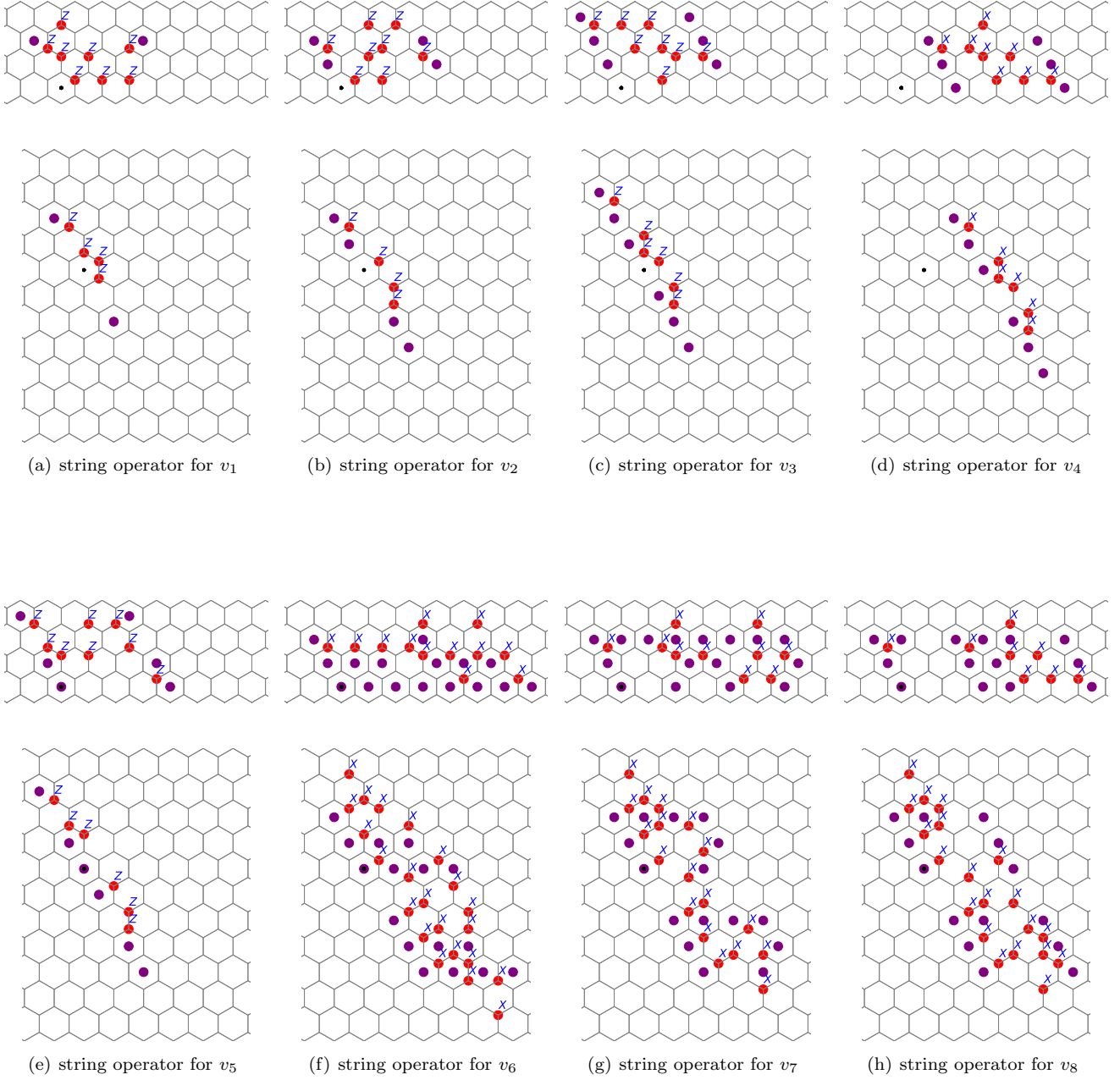


FIG. 21. The string operators in the modified color code C (example ⑤). Subfigures (a)~ (h) represent the string operators for anyons v_1, \dots, v_8 . For each subfigure, the first row represents the anyon string operators that move an anyon along the x -direction, and the second row represents the anyon string operators that move an anyon along the y -direction.

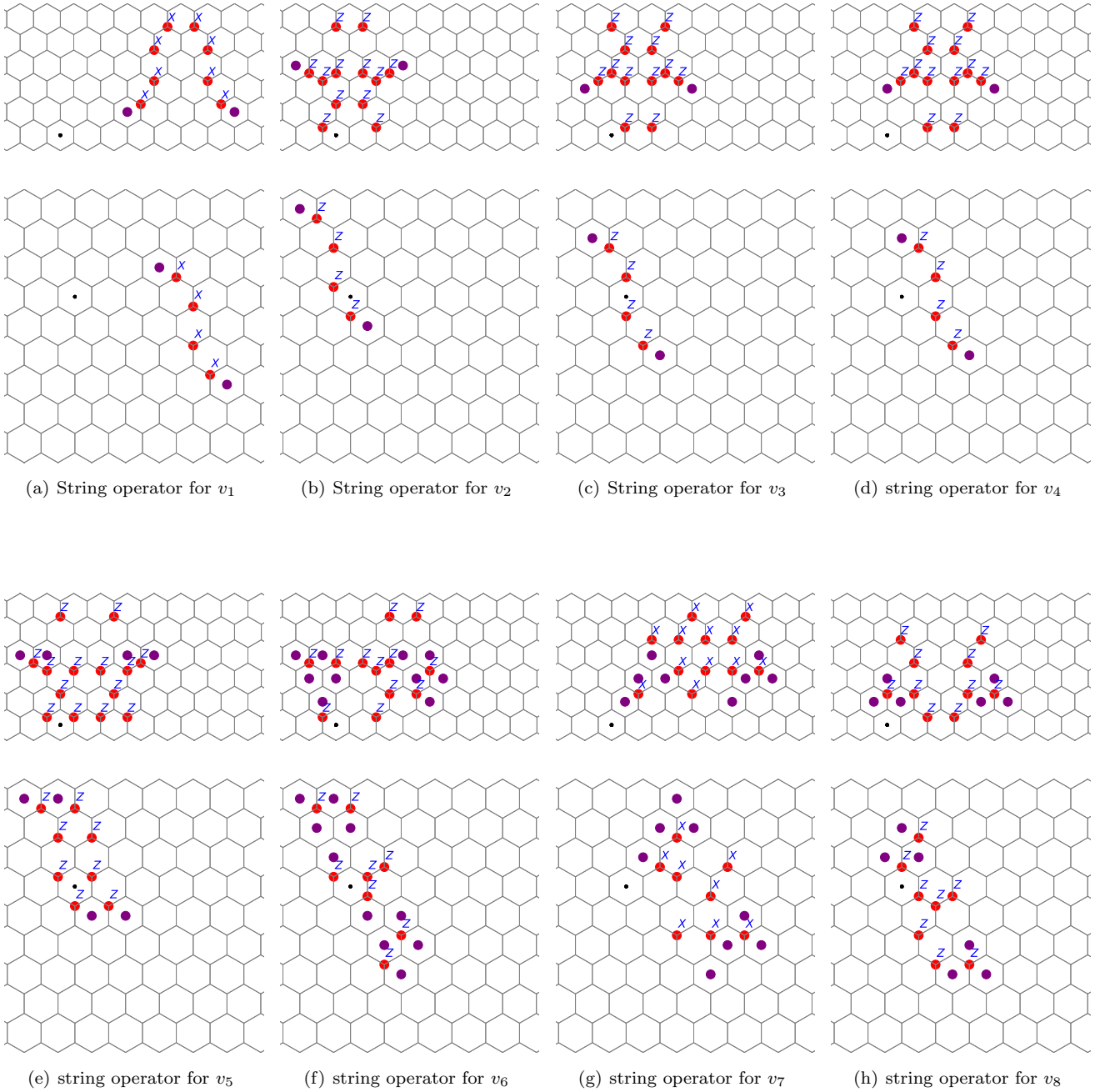


FIG. 22. The string operators in the modified color code D (example ⑥). Subfigures (a)~ (h) represent the string operators for anyons v_1, \dots, v_8 . For each subfigure, the first row represents the anyon string operators that move an anyon along the x -direction, and the second row represents the anyon string operators that move an anyon along the y -direction.

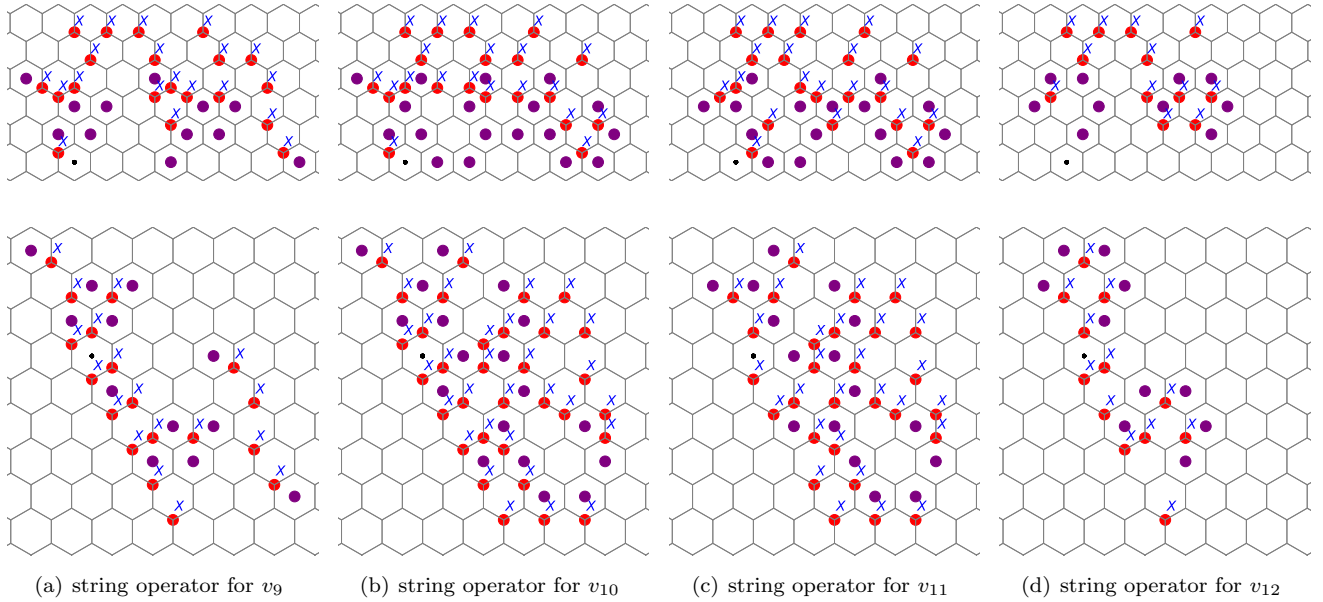
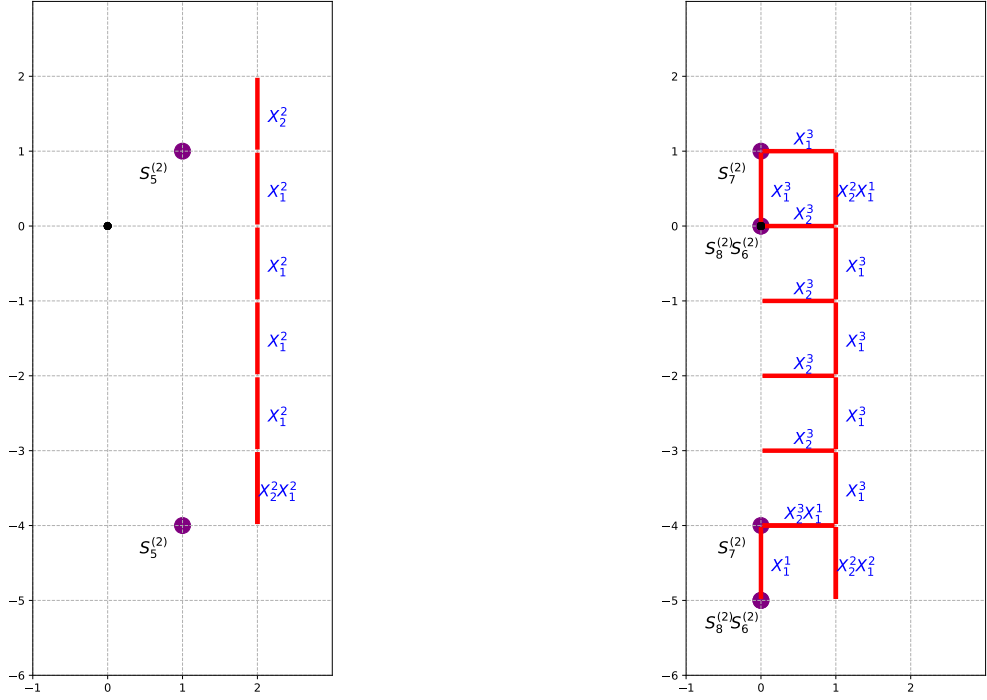
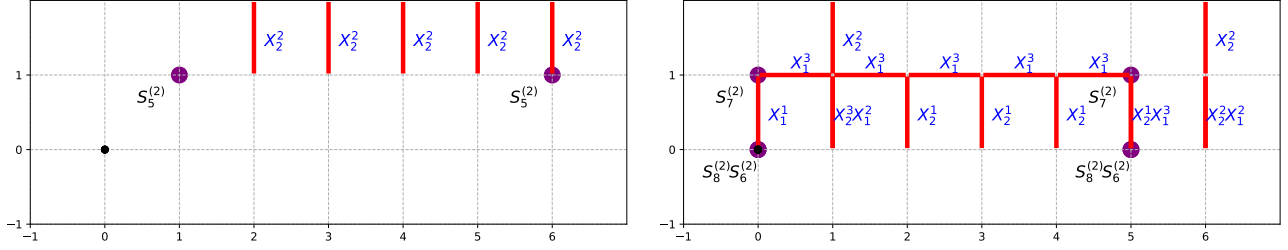


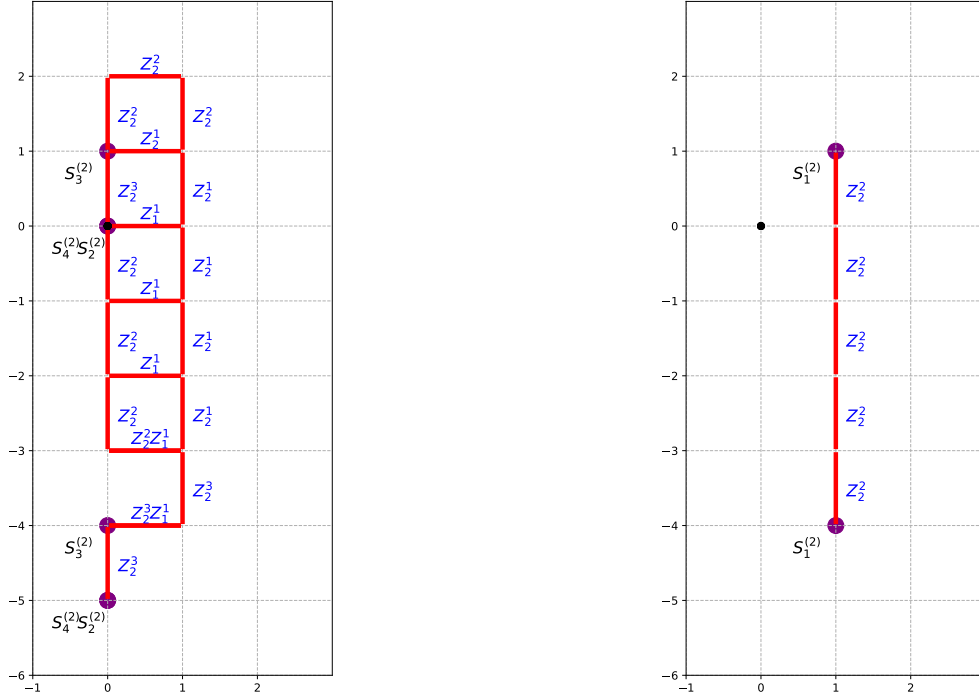
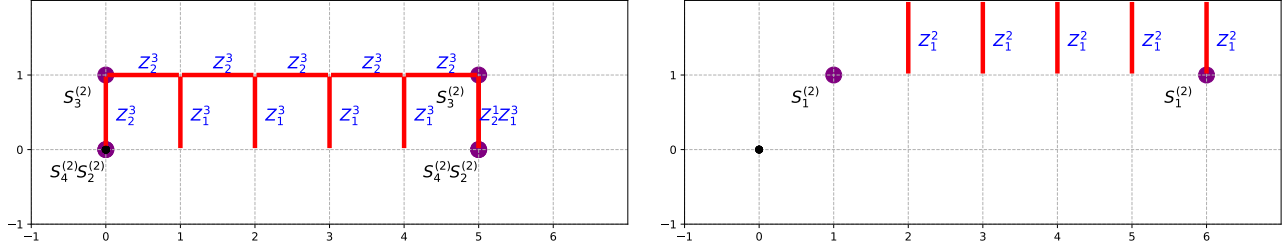
FIG. 23. (Continued) The string operators in the modified color code D (example ⑥). Subfigures (a)~(d) represent the string operators for anyons v_9, \dots, v_{12} . For each subfigure, the first row represents the anyon string operators that move an anyon along the x -direction, and the second row represents the anyon string operators that move an anyon along the y -direction.



(a) The string operator of anyons v_1 in the CSS code induced from double semion code.

(b) The string operator of anyons v_2 in the CSS code induced from double semion code.

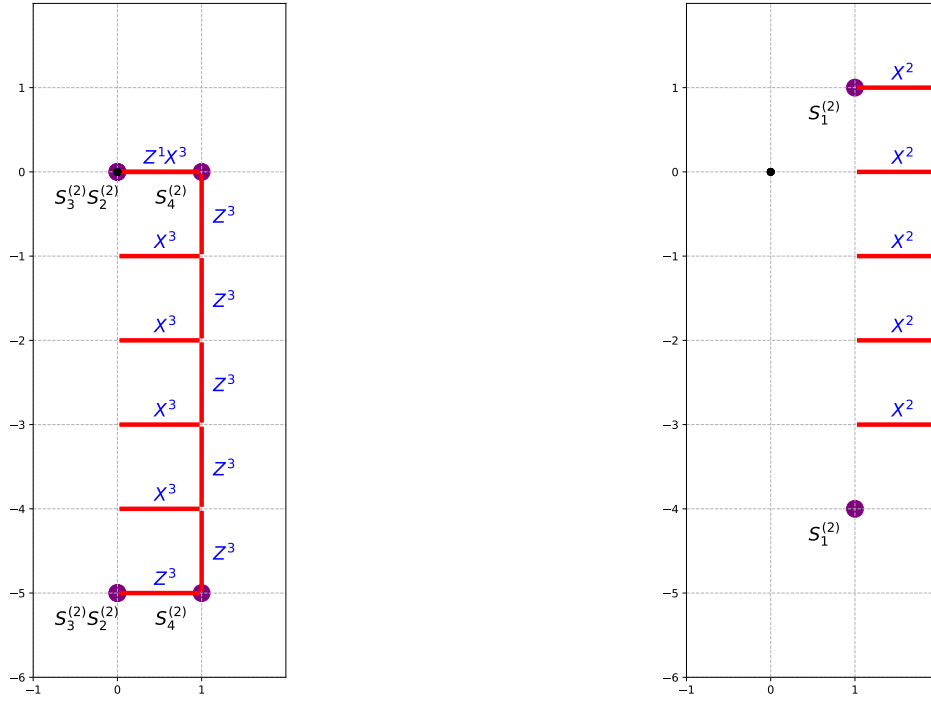
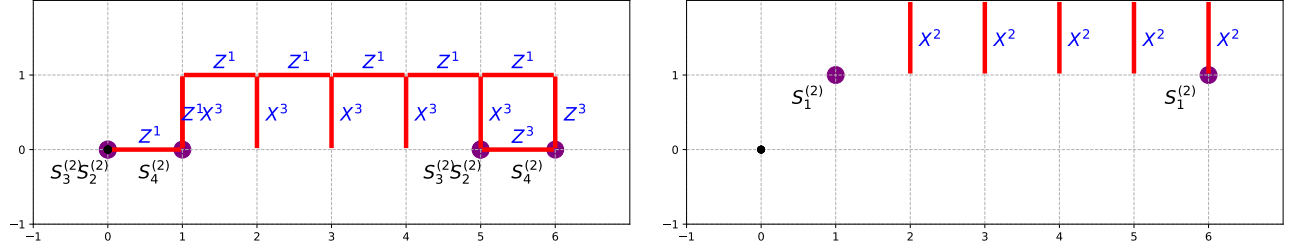
FIG. 24. The string operators of anyons v_1 and v_2 in the CSS code induced from double semion codes. For each subfigure, the first row represents the anyon string operators that move an anyon along the x -direction, and the second row represents the anyon string operators that move an anyon along the y -direction. Purple dots label the syndrome patterns at the endpoints of each string. Here, we denote the violation of plaquette terms S_2 and S_6 by purple dots on their bottom-left vertex. For S_3, S_7 , we denote the violation of them by purple dots on the top vertex above the vertical edge. For S_4, S_8 , we denote the violation of them by purple dots at the vertex below the vertical edge. Since this code is defined over \mathbb{Z}_4 qudits, we put superscript on S to indicate the violation of the stabilizer with a phase, for example, $S_5^{(2)}$ indicates that violations of S_5 up to a phase $\omega^2 = -1$ where $\omega = e^{i2\pi/4}$. We use this convention in all the following figures.



(a) The string operator of anyon v_3 in the CSS code induced from double semion code.

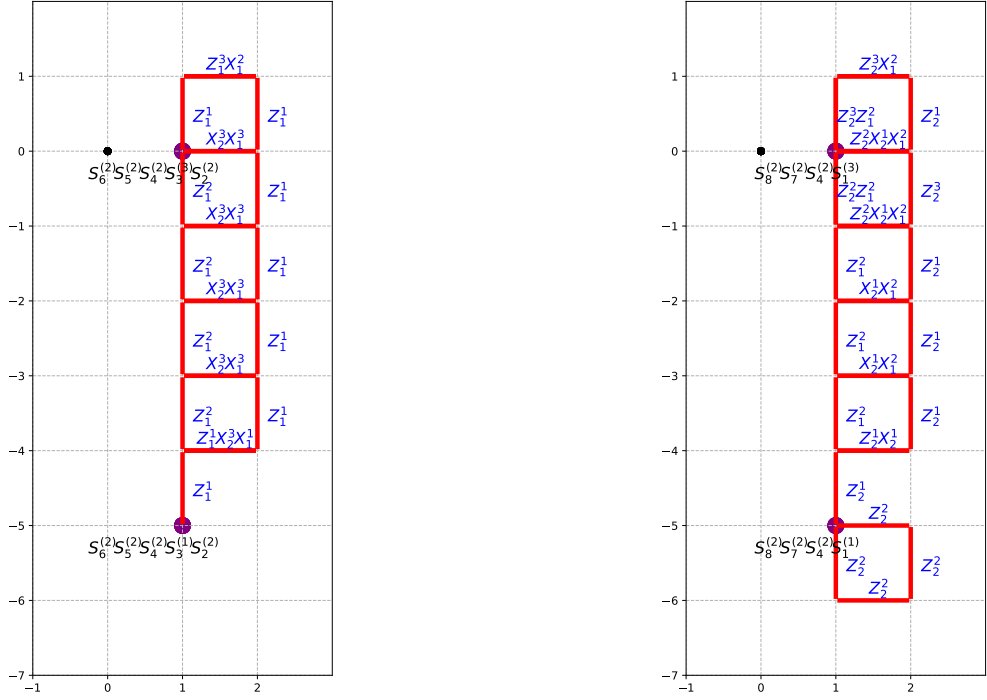
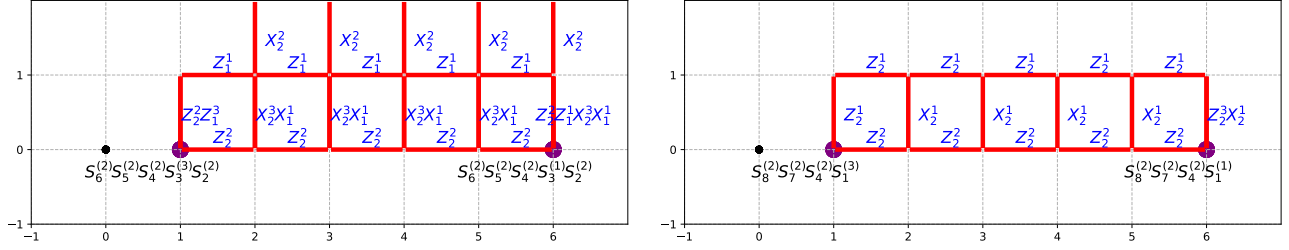
(b) The string operator of anyon v_4 in the CSS code induced from double semion code.

FIG. 25. (Continued) The string operators of anyons v_3 and v_4 in the CSS code induced from double semion codes. For each subfigure, the first row represents the anyon string operators that move an anyon along the x -direction, and the second row represents the anyon string operators that move an anyon along the y -direction. Purple dots label the syndrome patterns at the endpoints of each string.



(a) The string operator of anyon v_1 in the double semion code. (b) The string operator of anyon v_2 for the double semion code.

FIG. 26. The string operators of anyons v_1 and v_2 in the double semion code. For each subfigure, the first row represents the anyon string operators that move an anyon along the x -direction, the second row represents the anyon string operators that move an anyon along the y -direction. Purple dots label the syndrome patterns at the endpoints of each string.



(a) The string operator of anyon v_1 in the six-semion code.

(b) The string operator of anyon v_2 in the six-semion code.

FIG. 27. The string operators of anyons v_1 and v_2 in the six-semion code. For each subfigure, the first row represents the anyon string operators that move an anyon along the x -direction, the second row represents the anyon string operators that move an anyon along the y -direction. The syndrome pattern of end points of each strings are labeled by purple dots.